

# UNIVERSITÀ DEGLI STUDI DI PADOVA

Dipartimento di Fisica e Astronomia “Galileo Galilei”

Master Degree in Astrophysics and Cosmology

Final Dissertation

## A semi-empirical model to constrain the growth of supermassive black holes

**Thesis supervisor**

Prof.ssa Giulia Rodighiero

**Thesis co-supervisor**

Prof. Francesco Shankar

**Candidate**

Agnese Cherubini

Academic Year 2021/2022

## Abstract

*State-of-the-art.* The presence of supermassive black holes (SMBHs) at the center of galaxies has been proved by the most recent observations. The mass of these SMBHs is found to correlate with a number of properties of the host galaxies. Such relations have been extensively studied from a theoretical and observational point of view to acquire clues about the evolution of SMBHs within their hosts. SMBHs are thought to grow their mass through at least two mechanisms: 1) they are fuelled by the cold gas in the surroundings falling into the central region because of gravitational forces; 2) they build a certain amount of mass through BH-BH mergers as a consequence of the merging of their hosts. The relative role of these two scenarios has not been completely understood yet. There are predictions based on models and/or hydrodynamic simulations, but they are necessarily characterized by many input assumptions and related parameters that can induce strong degeneracies or divergences. A step forward to unveil the evolution and merger histories of massive black holes will be achieved in the next future thanks to advances in Gravitational Waves detections and in observations at high redshifts.

*This project.* In the present thesis project I present a novel *semi-empirical methodology* that avoids the modelling of galaxy and SMBH growth and assembly within dark matter halos from first principles. The approach here defined starts by assuming the empirical scaling relations between stellar mass and halo mass (SMHM), that at  $z < 4$  are computed from the equivalence between the cumulative number of galaxies and the halo mass function. Thanks to this relation it will be possible to convert dark matter halo assembly history into respective *galaxy* growth histories. These are characterized by a total mean mass accretion,  $\langle M_{\star, \text{tot}} \rangle$ , and a mean rate of galaxy mergers,  $\langle M_{\star, \text{merg}} \rangle$ . By subtracting the two quantities the average mass acquired through the only star formation processes is obtained. A similar procedure is applied, for the first time, to black holes by starting from black hole mass - galaxy properties relations, such as  $M_{\text{BH}} - M_{\star}$  (with galactic mass) and  $M_{\text{BH}} - \sigma$  (with velocity dispersion) relations. They are used to infer, from the dark matter and then the stellar accretion tracks, the total growth  $\langle M_{\text{BH}, \text{tot}} \rangle$  and mean black hole merger contribution  $\langle M_{\text{BH}, \text{merg}} \rangle$ , and finally to extract the black holes growth via gas accretion through the equation  $\langle M_{\text{BH}, \text{tot}} \rangle - \langle M_{\text{BH}, \text{merg}} \rangle$ . This method will allow to predict in a fast and robust way i) the black hole accretion curves (i.e. 'light curves'), ii) the amount of the contribution of black hole mergers in the assembly process across cosmic time.

The methodology introduced adopts as input just a series of N-body simulations and/or analytic dark matter merger trees and it is designed to work on minimal assumptions. Some risks still persist and mainly reside in the choices of SMHM and BH-host galaxies relations. Also the rate of galaxy/black hole mergers strongly depends on the shape and redshift dependence of the input relations. About these some valid priors can be extracted from the low redshift Universe ( $z \sim 0$ ), where direct constraints on BH/AGN-galaxy scaling relations are available. Moreover, precious information can be derived from the comparison of the mean black hole accretion tracks obtained from the outlined calculation with those extracted from *continuity equation* models. The latter is a technique

that, from bolometric AGN luminosity functions depending on  $z$  and for given mean radiative efficiency and Eddington ratio, allows to evaluate the average growth rate of black holes. Through this comparison it is ultimately possible to acquire a general understanding of the types of relations that are more efficient in reproducing the evolutionary paths of SMBHs and the expected contribution of BH – BH mergers in the whole process.

# Contents

<b>1</b>	<b>Introduction</b>	5
1.1	Formation of SMBHs	5
1.2	Evolution of SMBHs	8
1.2.1	X-ray background	9
1.2.2	Growth of SMBHs	11
1.2.3	Downsizing evolution	14
1.3	SMBHs and host galaxies	14
1.3.1	Detection of SMBHs	15
1.3.2	Scaling relations: hints of co-evolution?	16
1.4	This thesis	19
<b>2</b>	<b>Description of DECODE</b>	21
2.1	Semi-empirical models	21
2.2	DECODE implementation	23
2.2.1	Catalogue of parent halos	25
2.2.2	Population of subhalos	25
2.2.3	Time of infall	26
2.2.4	Merging timescale	28
2.3	Stellar Mass - Halo Mass (SMHM) relation	30
2.3.1	Stellar Mass Function	30
<b>3</b>	<b>Output of DECODE</b>	35
3.1	Dark-matter halos growth	36
3.1.1	Input parameters	36
3.1.2	Running the code	38
3.2	From halo mass to stellar mass	40
<b>4</b>	<b>Main: SMBH application I</b>	45
4.1	SMBH evolutionary model	46
4.1.1	AGN bolometric luminosity function	47
4.1.2	Local black hole mass function	48
4.1.3	Evolved black hole mass function	49
4.2	Building accretion curves: $M_{\text{BH}} - M_{\star}$ relation	51
4.2.1	Data sample and Chosen relations	53

4.2.2	SMBH growing curves: first results . . . . .	55
4.2.3	Broken power law relation . . . . .	57
4.2.4	Contribution of mergers . . . . .	60
<b>5</b>	<b>Main: SMBH application II</b>	<b>65</b>
5.1	Velocity dispersion from $M_*$ . . . . .	66
5.2	Data sample and Chosen relations . . . . .	68
5.3	First results . . . . .	70
5.4	Alternative relations . . . . .	73
5.4.1	Broken power law $M_{\text{BH}} - \sigma$ relation . . . . .	74
5.4.2	Log-quadratic $M_{\text{BH}} - \sigma$ relation . . . . .	74
5.5	Contribution of mergers . . . . .	76
<b>6</b>	<b>Results</b>	<b>81</b>
6.1	SMBH growth: scaling relations . . . . .	81
6.1.1	Discussion: $M_{\text{BH}} - M_*$ relation . . . . .	82
6.1.2	$M_{\text{BH}} - M_{*,\text{bulge}}$ Scaling relation . . . . .	87
6.1.3	Discussion: $M_{\text{BH}} - \sigma_*$ relation . . . . .	93
6.2	Mergers . . . . .	94
6.2.1	Global merger contribution: percentages . . . . .	95
6.2.2	High mass end: merging timescale . . . . .	98
6.3	Conclusions . . . . .	100
<b>7</b>	<b>Future</b>	<b>105</b>
7.1	Modification of DECODE . . . . .	105
7.2	Diffmah: Differentiable Model of Halo Assembly . . . . .	107
7.3	Question of mergers . . . . .	109
7.4	Future observations and applications . . . . .	110

# Chapter 1

## Introduction

When astronomers refer to black holes, at least two categories can be distinguished: from one side there are the so called stellar black holes, with masses reaching few tens times the mass of the Sun (Fender & Belloni (2012)); to the other side supermassive black holes (SMBHs) that are characterized by masses up to billions of times the mass of the Sun and that are the protagonist of this thesis project. Most of the best studied SMBHs have masses in the range between  $\gtrsim 10^6 M_{\odot}$  and few  $10^{9-10} M_{\odot}$  (Gultekin et al. (2009)). The population of supermassive black holes may be extended to lower masses, down to few  $10^5 M_{\odot}$  (Peterson et al. (2005)), even though this range is much harder to probe. From an observational point of view these two types of black holes seem to be separated by a gap, hence it is probable that there are intrinsic differences between stellar black holes and SMBHs. The former are found in large numbers throughout galaxies, while the latter tend to be located at the center of their host galaxies and usually there is only one SMBH observed per galaxy. Very distant are also the processes which lead to the formation of these two. For what concerns stellar mass black holes, they are believed to be the remnants of the collapse of massive stars, with masses  $\gtrsim 10 M_{\odot}$ . Supermassive black holes instead form a scenario much complex and still not completely understood. There are various hypothesis that are being investigated through theoretical and observational points of view. In the following Section I am going to summarize some of the work done in this direction.

### 1.1 Formation of SMBHs

Supermassive black holes must have formed from the same material that constitutes galaxies and the rest of the universe. The most accredited cosmological model is the so-called  $\Lambda$ CDM model, according to which the mass content of the universe is dominated by a non-baryonic dark matter that does not interact electromagnetically, but only gravitationally with its environment. The remaining part is represented by the baryonic matter in the form of diffuse gas or condensed in stars, and its contribution is at most of 15 %. Current cosmological theories attribute the birth and growth of structures in the universe to gravitational collapse of small perturbations in a quasi-homogeneous universe dominated by Cold Dark Matter (CDM). In this framework the collapse of structures

proceeds bottom-up on larger and larger scales, meaning that smaller structures, halos and galaxies ( $\lesssim 10^6 M_\odot$ ), appear first and are then incorporated into larger ones at later times (White & Rees (1978)). The first SMBHs should have formed within these proto-galaxies and then grown with them.

Among the theoretical scenarios, the most popular one associates the first supermassive black holes with the remnants of the first generation of stars, that formed out of zero metallicity gas (Madau & Rees (2001)). Indeed from simulations of the collapse of primordial molecular clouds (Bromm et al. (1999); Bromm et al. (2002); Abel et al. (2000); Yoshida et al. (2006); Gao et al. (2007)) it is expected that the first generation of stars contained many 'very massive stars' (VMSs) with  $M_\star > 100 M_\odot$  (Carr et al. (1984)). This is probably due to the slow subsonic contraction of the gas cloud, mostly composed of molecular hydrogen that is a much more inefficient coolant than the atomic line and dust cooling that takes over when heavy element are present. If these very massive stars manage to keep their masses until death, they will collapse after short life-time, of some Myrs. The final fate actually depends on the exact mass of the star. According to that different outcomes are possible:

- i) Low-metallicity stars with masses between  $\sim 25$  and  $140 M_\odot$  are predicted to form black holes directly. The mass of the remnant is nearly half of the stellar mass (Zhang et al. (2008)) and in this case it is probably too light to be dynamically stable within the center of its host, once stars populate the galaxy. It is more likely that the formed BH interacts with other stars and begins to wander within its host;
- ii) Between  $\approx 140$  and  $260 M_\odot$  it is believed to place the domain of pair instability supernovae. After helium burning, in the central region of stars temperature and density conditions allow the formation of abundant electron/positron pairs. Hence internal energy is converted into rest mass of the pairs without contributing much to the pressure (Barkat et al. (1967); Bond et al. (1984)). When such an instability occurs, the star enters in a rapid contraction regime until the oxygen and silicon burning is switched on and may reverse the collapse. These objects go finally to complete disruption due to nuclear-powered explosions. Stellar cores implode to a certain maximum temperature, burn fuel explosively and explode leaving no remnants (e.g. Fryer et al. (2001));
- iii) Stars with Main Sequence masses above  $260 M_\odot$  have still another faith. In these objects, the cores can become so hot that pair instability is reached before the explosive nuclear burning alters the collapse (Bond et al. (1984)). Hence instead of producing an explosion the mechanism accelerates the collapse, the nuclear energy released by pairs is not sufficient to reverse the implosion and the star becomes a black hole (e.g. Woosley & Weaver (1986)).

According to the scenarios just listed, if a VMS with a mass above  $260 M_\odot$  forms, it is highly probable that it will lead to the formation of a black hole with a final mass of the order of  $\sim 100 M_\odot$ . However it is still not clear whether many first stars were born with such high masses and actually some simulations have retrieved much lower initial estimates of stellar masses, up to few tens of solar mass (e.g. Hosokawa et al.

(2012)). If this is the case, then it is very hard that first stars have given birth to the first supermassive black holes.

Other possible paths for the formation of SMBHs with substantial initial masses, millions of  $M_{\odot}$ , involve dynamical instabilities pertaining both the gaseous and stellar components of proto-galaxies. In them, gas can cool and contracts until the equilibrium between gravitational and centrifugal forces is reached and this typically happens before densities required to the formation of the SMBH are achieved. However, gravitational instabilities may happen and transport mass at the expense of rotational support. At least a couple of situations may occur at this point. On the one side, if the galactic disk is globally unstable, a SMBH seed could form as a consequence of a very rapid accumulation of gas that produces a supermassive star with a mass of the order of  $\sim 10^6 M_{\odot}$  (e.g. [Begelman et al. \(2006\)](#); [Johnson et al. \(2012\)](#)). Such a gas accumulation needs to last less than  $\sim 2$  million years, more or less the nuclear time-scale, in order to avoid the star exploding as a supernova. Once the huge star has exhausted the hydrogen reservoir, its core starts to contract leading to the formation of a black hole of a few tens of  $M_{\odot}$  in the heart of the dying star. Gas continues to fall within it forming a system (a 'quasi-star') composed of a black hole that grows accreting the surrounding material until a maximum black hole accretion luminosity is reached, i.e. the one that equates the gravitational energy of the gas in-falling envelope. At that point the quasi-star dissolves leaving a black hole with a mass up to the 10 % of the mass of the quasi-star at the center of the galaxy. It is how a SMBH seed is formed and begin its life ([Begelman \(2010\)](#); [Ball et al. \(2011\)](#)). On the other hand, in galaxies just locally unstable ([Lodato & Natarajan \(2006\)](#)) SMBH seeds can form as a consequence of stellar dynamical instabilities, provided that gas is only mildly polluted by heavy elements ([Omukai et al. \(2008\)](#); [Devecchi & Volonteri \(2009\)](#)). Basically stars start to form in the central region creating a dense stellar cluster in which star-star collisions are common and can produce very massive stars of  $\sim 1000 M_{\odot}$  before the explosion of the first supernova. If heavy elements are still rare, up to about the second generation of stars, a very massive star is destined to collapse and form a black hole with a mass similar to the progenitor. This is not the case when heavy elements are more abundant because of the losing mass processes through strong winds occurring before the collapse into a stellar mass black hole. Hence this path of SMBH formation is available just in the early universe.

All of these possibilities, summarized in Figure 1.1 from the review of [Volonteri \(2010\)](#), are not mutually exclusive and actually observations that can probe possible scenarios are scarce. This is due to the fact that SMBHs in the early universe have relatively low masses and luminosities (from accretion mechanisms), with consequent limited capabilities of being detected. In this context much improvements would be achieved in the gravitational waves field, since these objects can be primary targets for instruments operating in frequencies of mHz. At subsequent epochs most of the information about the initial conditions is lost and that makes things even more complicated. Some clues about the mechanisms involved could be inferred from the lowest-mass SMBHs that are possibly nearer to be pristine objects because of the limited growth. Nevertheless, once a primordial black hole has formed, it then mainly grows its mass from in-falling gas from the surroundings. This process is accompanied to a release of a big amount of energy,

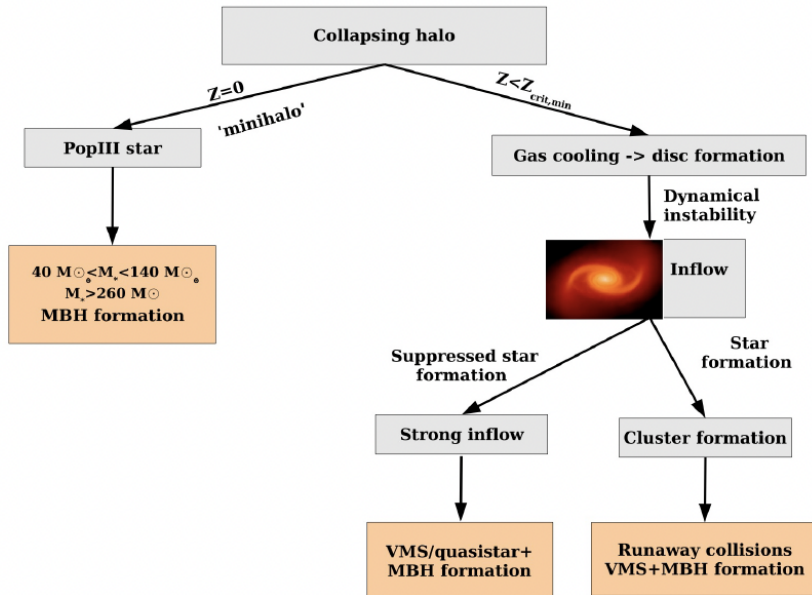


Figure 1.1: Scheme with possible supermassive BHs formation paths in high redshift galaxies.

in the form of radiation, that allows to identify supermassive black holes even at high redshift. This active phase, occasional and opposite to a dormant phase, is what defines the so-called Active Galactic Nuclei (AGN). In the next Section I am going to illustrate how this phenomenon is revealing important aspects about the evolution of supermassive black holes across cosmic time.

## 1.2 Evolution of SMBHs

Supermassive black holes are responsible for one of the most energetic phenomena in the universe, called Active Galactic Nuclei (AGNs). Many objects of this type can be observed and investigated in the distant universe. When matter falls onto a SMBH (accretion), it emits intense electromagnetic radiation, covering a wide range of wavelengths, as a consequence of the release of gravitational energy. The bolometric luminosity,  $L$ , is connected to the mass in-falling rate,  $\dot{M}$ , through the following equation:  $L = \epsilon \dot{M} c^2$ , where  $\epsilon$  is called the radiative efficiency, i.e. how much gravitational energy released is converted into radiation. Typically, for accretion processes characterized by optically thick disks (Shakura & Sunyaev (1973)), the radiative efficiency value considered is  $\epsilon \sim 0.1$ . AGN luminosities are huge and can reach up to  $10^{15} L_{\odot}$ , moreover they may produce powerful outflow in forms of jets and disk winds. Because of their strong radiation and kinetic power, active SMBHs assume a key role in the regulation of star formation in galaxies and are also able to affect their surroundings on galaxy clusters scale,  $\sim \text{Mpc}$  (e.g. Fabian (2012)).

As said, AGN represents the mechanism through which a SMBH acquires its mass. In particular the actual amount of gas that is used for this scope is given by:

$$\dot{M}_{\text{acc}} = \frac{1 - \epsilon}{\epsilon} \cdot \frac{L}{c^2}, \quad (1.1)$$

where  $L$ , a given bolometric luminosity, can be assigned to the mass of the growing black hole through the Eddington ratio,  $\lambda = L/L_{\text{Edd}}$ , with  $L_{\text{Edd}}$  expressing the Eddington luminosity at a certain  $M_{\text{BH}}$  (units of  $M_{\odot}$ ). More details will be given in Section 4.1. According to what just said, it is possible to have access to the growth history of a supermassive black hole through the study of the cosmological evolution of active galactic nuclei. The available information one reaches out of an AGN is its luminosity and, specifically, the main wave range of investigation is the X-ray regime. The SMBH and its accretion disk are believed to be surrounded by a wider structure, of  $\gtrsim 0.1$  pc, that consists of gas and dust and called 'torus'. This latter is usually assumed to have a donut-like shape and with clouds emitting broad emission lines (velocities of  $\gtrsim 1000$  kms $^{-1}$ ) inside its hole. This is the so-called broad line region (BLR) as opposite to the narrow line region (NLR), that is responsible of producing emission lines with velocity widths  $\lesssim 1000$  kms $^{-1}$  and located above and below the torus hole.

With reference to the unified scheme of AGNs by Antonucci (1993), what determines the observational characteristics of an AGN is the viewing angle with respect to the torus. In the first place it causes significant extinction of light, from optical to ultraviolet, that is emitted by the accretion disk and the broad line region. Also, it is responsible for the photoelectric absorption of the X-ray continuum. In fortunate cases, the line-of-sight toward the SMBH is unblocked by the torus. Thanks to this face-on view one can observe the broad line region and un-absorbed X-ray continuum. These are the 'type-I' or unobscured AGNs. On the other hand, when the torus completely block the light-of-sight, i.e. edge-on view, the broad lines can not be observed in the optical spectra and X-ray spectrum is almost entirely absorbed and becomes hard, meaning that the flux related to higher energies is more than what is received at lower energies (Awaki et al. (1991)). These objects are defined of 'type-II' or obscured AGNs. Naturally the latter are more difficult to detect, but may constitute a conspicuous part of the total population. For such reason, it is preferable to rely on surveys in 'hard' X-rays, e.g. above 2 keV, that provide the most efficient and complete way to treat AGNs. Rays of those energy have strong penetrating power against absorption. The other favorable aspect in the use of hard X-rays is the minor contamination from stars in the host galaxy with respect to other wavelengths. In this way it will be possible to reconstruct a clean AGN sample, even at low luminosities.

### 1.2.1 X-ray background

Almost isotropic X-ray radiation, observed from all directions of the sky, constitutes the so-called X-ray background (XRB). It was discovered through the famous experiment conducted by Giacconi et al. (1962) and, since then, much effort has been employed in trying to unveil the nature of this cosmic background. It is now established (Ueda (2015)) that, mainly, it is formed by the superposition of X-ray emission from the whole

AGN population in the universe. Hence understanding the origin of XRB is equivalent to revealing the cosmological evolution of AGNs. Actually to determine the redshift and type of the objects detected, multi-wavelength follow-up observations, in particular optical spectroscopic ones, are required. Then the most important quantity that allows to study the cosmological evolution of AGNs is the Luminosity Function (LF), i.e. the co-moving space number density as a function of bolometric luminosity and redshift. In order to build reliable statistics, it is of maximum importance to consider an unbiased AGN sample covering wide redshift and luminosity ranges through the combination of multiple surveys with different flux limits. The first time the hard X-ray luminosity function (XLF) of AGNs has been quantitatively determined is in the work of Ueda et al. (2003), in which authors compiled a sample made of 247 objects detected with *HEAO-1*, *ASCA* and *Chandra*. The luminosity function has been calculated in the 2-10 keV bands and in the luminosity range of  $10^{41.5} - 10^{46.5}$  erg s<sup>-1</sup> as a function of redshift up to  $z = 3$ , including both type-I and -II AGNs. The redshift completeness is very high of  $\sim 100\%$ , 97% and 93 % for the above-mentioned missions respectively. The final determination of the hard XLF,  $d\phi_X(L_X, z)/d\log_{10}L_X$  (Mpc<sup>-3</sup>dex<sup>-1</sup>), has been obtained through an analysis based on the maximum likelihood method fully corrected for observational biases. Figure 1.2 from Ueda et al. (2003) represents the resulting hard XLF of Compton-thin AGNs in five redshift ranges. With Compton-thin AGNs are intended those objects in which absorption is smaller than  $\log_{10}N_H = 24$ , that corresponds to an opacity for Compton scattering of  $\sim 1$ . The shapes of the luminosity functions are approximated as a double power-law function, with different slopes above and below a certain break luminosity. The evolution in shapes is rather complicated and, according to Ueda et al. (2003), a model that could describe the results is a luminosity-dependent density evolution (LDDE) model. Following this latter, the number density of AGNs rapidly increases with redshift, reaches a peak and then slowly declines towards higher redshift. An interesting finding is that the  $z$  at which the peak is reached increases with AGN luminosity, i.e. more luminous AGNs are more abundant than ones of lower luminosities at higher redshift. Such a behaviour is called 'cosmic downsizing' or 'anti-hierarchical evolution' of SMBHs. It implies the fact that more massive black holes formed at earlier epochs (see Section 6.3). A model of this kind was already introduced to reproduce data about XLF detected with *ROSAT* in the soft X-ray band (Miyaji et al. (2000)), even though in that case it has not been possible to detect the luminosity-dependence of the peak redshift. The discovery of the SMBH downsizing is something not really expected from a naively point of view, because it is apparently opposite to the prediction of the structure formation theory of the universe, based on cold dark matter models, before mentioned (bottom-up evolution). In scenarios of that type massive dark matter halos have formed more recently by merging from less massive ones. Some possible origins of the cosmic downsizing will be given in the following paragraphs. Many other works about X-ray surveys, followed by multi-wavelength identifications, have been conducted since that first work so to provide larger and larger samples of AGNs (Barger et al. (2005); Hasinger et al. (2005); Franca et al. (2005); Silverman et al. (2008); Ebrero et al. (2009); Yenko et al. (2009); Aird et al. (2010)). One of the largest is furnished by Ueda et al. (2014), that includes 4039 objects detected with *MAXI*, *ASCA*, *Chandra*, *XMM-Newton*, *Swift* and *ROSAT*. The

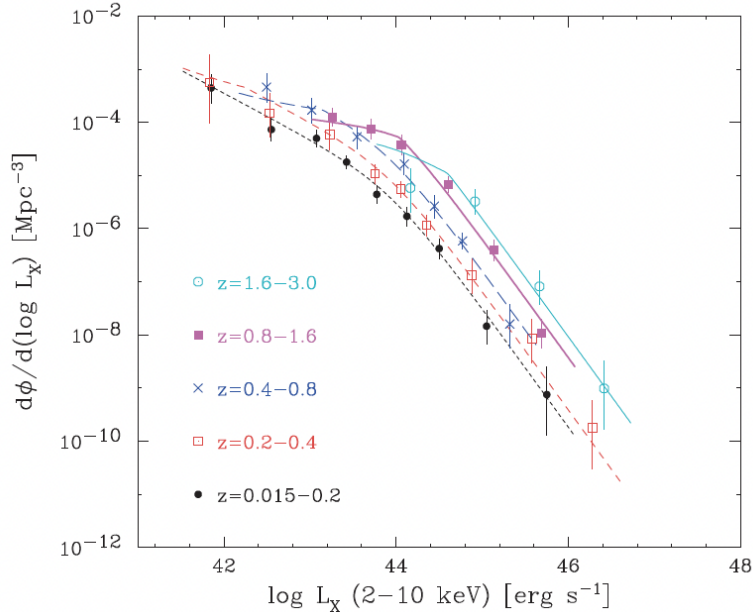


Figure 1.2: X-ray luminosity functions of Compton-thin AGNs at different redshift ranges:  $z = 0.015-0.2$  (short-dashed black),  $0.2-0.4$  (medium-dashed red),  $0.4-0.8$  (long-dashed blue),  $0.8-1.6$  (thick solid magenta) and  $1.6-3.0$  (thin solid cyan). The curves are obtained as best-fit LDDE models and data points have been assigned to their  $1\sigma$  statistical errors. Those are the results of the AGN sample analysis made in [Ueda et al. \(2003\)](#).

plot that illustrates all data luminosities as function of redshift can be visualized in [Figure 1.3](#). With more and more up-to-date luminosity functions it is then possible to better constrain the growing histories of supermassive black holes. The method to relate LF to the mass density of SMBHs, at each redshift, will be explained in the next Section.

### 1.2.2 Growth of SMBHs

As previously mentioned, the growth of a supermassive black hole is determined by mass accretion processes responsible for the high luminosity of AGNs. The link between the luminosity and the mass accretion rate of single SMBH is represented by the radiative efficiency,  $\epsilon$ . Once the AGN luminosity function is obtained as a function of redshift, this makes it possible to retrieve the global growth history of SMBHs. This argument was introduced by [Soltan \(1982\)](#), and states that the total mass density of SMBHs (including non active ones),  $\rho(z)$ , can be calculated by integrating the mass-accretion rate density,  $\dot{\rho}(z)$ , over cosmic time, i.e.:

$$\rho(z) = \int_z^\infty \dot{\rho}(z) dz \frac{dt}{dz}. \quad (1.2)$$

In turn the term  $\dot{\rho}(z)$  is related to the LF of AGNs in the following way:

$$\dot{\rho}(z) = \frac{1 - \bar{\epsilon}}{\bar{\epsilon}c^2} \int L \frac{d\phi_{\text{bol}}(L, z)}{d\log_{10}L} d\log_{10}L. \quad (1.3)$$

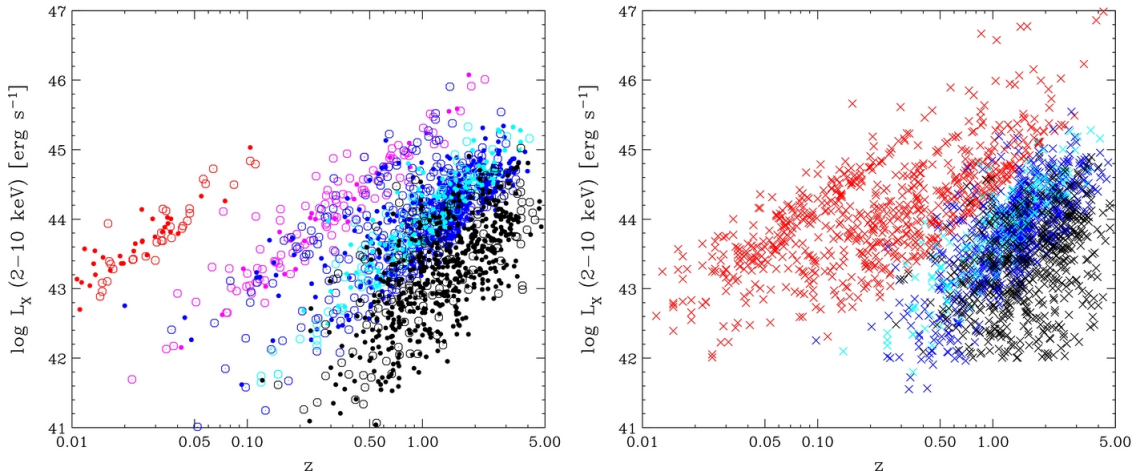


Figure 1.3: Redshift versus luminosity plot of the sample collected in Ueda et al. (2014). Left: sample detected in the hard ( $>2$  keV) band (red: *Swift* sample; magenta: *ASCA* sample; blue: *XMM-Newton* sample; black: *Chandra* sample). The open and filled circles represent X-ray unabsorbed AGNs (with  $\log_{10}N_{\text{H}} < 22$ ) and X-ray absorbed AGNs (with  $\log_{10}N_{\text{H}} \geq 22$ ), respectively. Right: redshift-luminosity plot of the sample detected in the soft (0.5–2 keV) band (red: *ROSAT* sample; blue: *XMM-Newton* sample; black: *Chandra* sample).

Here the luminosity considered,  $L$ , is a bolometric luminosity, i.e. integrated over all wavelengths, and  $\bar{\epsilon}$  is an averaged radiation efficiency assumed not to depend on  $z$  or  $L$  in the above Equation. This formula can be used to determine the value of mass density at  $z = 0$  and then compare the result to estimates of the same quantity but derived from independent methods, e.g. exploiting  $M_{\text{BH}}$  - galaxy properties relations (see Section 1.3). This would give constraints on  $\bar{\epsilon}$ , that characterizes the accretion modes of AGNs, e.g. standard disk (Shakura & Sunyaev (1973)) or radiatively inefficient accretion flows (Ichimaru (1977)).

The bolometric luminosity function of all AGNs, that should include both Compton-thin and Compton-thick ( $\log_{10}N_{\text{H}} > 24$ ) AGNs, can be derived from the XLF assuming luminosity dependent bolometric correction factors with their scatter, e.g. from Hopkins et al. (2007a). Adopting that types of corrections, it can be derived the trend of  $\rho(z)$  illustrated in Figure 1.4, from Ueda (2015). The curves have been obtained by assuming an average radiative efficiency of  $\bar{\epsilon} = 0.04$  and in luminosity ranges of  $\log_{10}L = 43-48$  (solid black) and  $\log_{10}L = 46-48$  (dashed red). As one expects from downsizing evolution, less luminous AGNs contribute more significantly to the global density at lower redshift. The value of  $\rho(z = 0)$  is not far from the observed local SMBH mass density,  $\rho_{\text{obs}} \approx 10^6 M_{\odot} \text{Mpc}^{-3}$  and calculated in Ueda et al. (2014) using the supermassive black hole - stellar bulge mass,  $M_{\text{BH}} - M_{\star, \text{bulge}}$ , scaling relation found in Kormendy & Ho (2013). Another application of this procedure can be the derivation of the mass function of SMBHs, including non active ones. Indeed, if mergers are neglected, the latter can be derived directly from the AGN luminosity function (Yu & Tremaine (2002); Marconi et al.

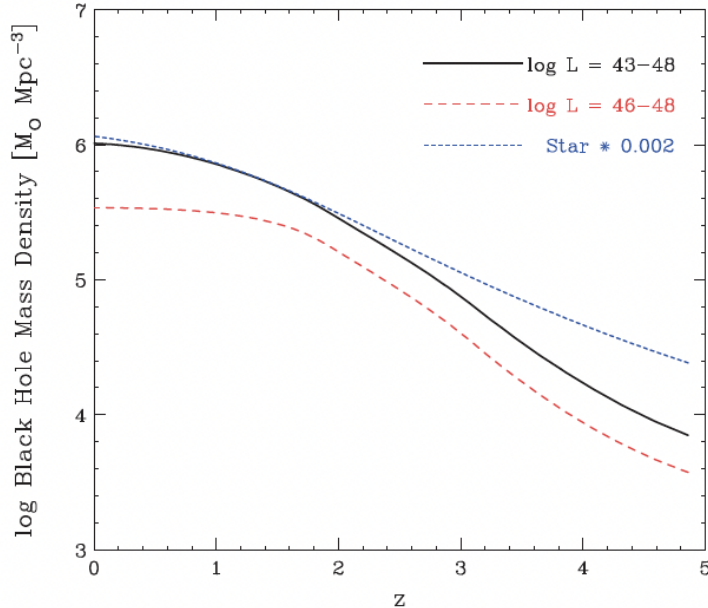


Figure 1.4: Evolution of SMBHs mass density derived by using Equation 1.2 with converted (bolometric corrections) X-ray LFs from Ueda et al. (2014) up to redshift  $z = 5$ . The assumed value of the average radiative efficiency is  $\bar{\epsilon} = 0.04$  and the related interval of luminosities are  $\log_{10}L = 43-48$  (solid black curve) and  $\log_{10}L = 46-48$  (dashed red line). Short-dashed blue curve represents the evolution of the co-moving stellar mass density (Madau & Dickinson (2014)) scaled by a factor of 0.002.

(2004); Shankar et al. (2004)). This implies the introduction of the Eddington ratio,  $\lambda$ , that is the bolometric luminosity divided by the Eddington luminosity, with the following expression:

$$L_{\text{Edd}} = \frac{4\pi GM_{\text{BH}}m_{\text{p}}c}{\sigma_{\text{T}}} = 1.25 \times 10^{38} \left( \frac{M_{\text{BH}}}{M_{\odot}} \right) \text{ erg} \cdot \text{s}^{-1} \quad (1.4)$$

with  $m_{\text{p}}$  the proton mass,  $\sigma_{\text{T}}$  the electron Thomson scattering cross-section and  $M_{\text{BH}}$  the mass of the central SMBH. The just explained scheme will be the one applied in Shankar et al. (2009) that leads to the retrieval of mean growing curves of supermassive black holes at different final masses (see Section 4.1 of Chapter 4) and that will be used as the model to be compared to the results of my work.

In Figure 1.4 it appears also the curve that delineates the growth history of galaxies (short-dashed blue one), obtained by the compilation of Madau & Rees (2001). The stellar mass density has been re-scaled by a factor of 0.002. The overall similarity between SMBHs and galaxies accretion supports a co-evolutionary scenario (already reported in Boyle & Terlevich (1998)) and further discussions will be given in the next Sections. Before going on, some hypothesis related to downsizing evolution of SMBHs are suggested in the following.

### 1.2.3 Downsizing evolution

Downsizing or anti-hierarchical evolution of SMBHs, found from AGN X-ray surveys, indicates that the actual more massive black holes formed earlier in cosmic time than less massive ones. Also star formation in galaxies has manifested a similar behaviour. This was firstly suggested by [Cowie et al. \(1996\)](#), and subsequent observations supported the results ([Kodama et al. \(2004\)](#); [Fontanot et al. \(2006\)](#)). If the co-evolution of SMBHs and galaxies goes at almost the same path, then it would mean that both downsizing of AGNs and star formation have the same origins.

This fact does not necessarily conflict with the well-accepted bottom-up structure formation models in cold dark matter dominated universe. Indeed it is not said that growing processes characteristic of SMBHs follow the assembly of dark matter halos. Actually, the observed decrease of the space density of luminous AGNs at  $z < 2$  ([Ueda et al. \(2014\)](#)) would lead to the conclusion that merging of massive dark matter halos does not imply rapid growth of SMBHs at low redshift. The main fact is that the accretion mechanism is governed by baryon specific physics rather than pure gravity governing the dynamics of dark matter halos. This particular phenomenon can be accessed through theoretical or semi-analytic models and cosmological hydrodynamic simulations (e.g. [Marulli et al. \(2008\)](#); [Fanidakis et al. \(2012\)](#); [Hirschmann et al. \(2012b\)](#); [Hirschmann et al. \(2014\)](#); [Enoki et al. \(2014\)](#)), but the actual origins have not yet been defined. A possible cause can be that the cooling of the gas that fuels the AGN is suppressed in very massive objects and at low  $z$  as a consequence of AGN feedback in 'radio mode' or 'kinetic mode' ([Fabian \(2012\)](#)). This, followed by a decrease of star formation due to lack of cold gas, can lead a quicker decrease of density of luminous AGNs ([Enoki et al. \(2014\)](#)).

Possible explanations could be linked to the difference in mechanisms of AGNs fueling. Two are at least proposed: major mergers on the one hand and processes such as disk instabilities and hot-halo accretion (e.g. [Marulli et al. \(2008\)](#); [Fanidakis et al. \(2012\)](#)) to the other. Such a picture goes in line with results on AGN morphologies, i.e. many of them are disk-dominated galaxies (e.g. [Kiuchi et al. \(2006\)](#); [Georgakakis et al. \(2009\)](#)). However, some of the models over-predict the space density of AGNs of low luminosities compared to observations at  $z > 1-2$  ([Miyaji et al. \(2015\)](#)). Actually some physical mechanisms may be still not clear and some observational biases can be on act.

Now that basic information on the histories of SMBHs has been acquired, in the following I will summarize other methodologies to investigate central massive black holes, i.e. how to infer their mass (locally) and which types of relations this seems to establish with the host galaxy properties.

## 1.3 SMBHs and host galaxies

In the previous Section I have discussed about possible studies that can be conducted in order to understand the formation and evolution of supermassive black holes. There could be many other ways available to explore these issues, in there I just limit the attention on one of the most common, that could give us general ideas on what happens for growing black holes and how to observe it. At this point the final result of all of the more or less defined processes is the presence of a supermassive black hole at the center of most of

galaxies. Once a SMBH has practically ended its growth it becomes no more visible, or at least in a direct way. Below I am going to give short list on the principal methods that allow to get mass measurements of supermassive black holes that are in their dormant or active phase.

### 1.3.1 Detection of SMBHs

Basically all massive black hole mass measurements rely on the gravitational effects it exerts in its surroundings. A SMBH at the center of a galaxy causes gas and stars to move on orbits that mainly follow the same Kepler's laws of planets around the central stars. If random motions are limited, then the mass that can be calculated within a certain radius  $r$  is given by:

$$M(r) = f \frac{V^2 r}{G}, \quad (1.5)$$

where  $V$  is the rotation velocity,  $G$  is the gravitational constant and  $f$  a factor that accounts for the geometry. If one measures the velocity as a function of distance from the center it is possible to calculate the mass of the SMBH, i.e. the larger is the mass, the faster would be the gas and stellar velocities. Many different techniques have been employed in order to measure, or at least estimate, the masses of SMBHs in nearby and also distant galaxies (when possible). Here below a probably not exhaustive list of them:

- Stellar dynamical measurements are typically conducted for quiescent SMBHs, so to avoid contamination from the light of active galactic nuclei. The case of the Milky Way is a special one because the proper motions of single stars in the proximity of the Galactic Center have been monitored for many years. Their orbits almost exactly trace the Keplerian potential generated by a dark object of a mass  $M_{\text{BH,MW}} \approx 4 \times 10^6 M_{\odot}$  (e.g. [Schodel et al. \(2003\)](#); [Ghez et al. \(2003\)](#)). For all other galaxies one should rely on integrated stellar dynamics, since single stars can not be resolved. In these situations the whole potential of the galaxy is modeled so to extract the signature of a central supermassive object from spectra of the central nucleus. A SMBH makes stars to move faster than they would in its absence. Since stars are actually affected only by gravitational forces, these methods are the most direct ones, even though may be subjected to systematic errors related to uncertainties in modeling the galaxy, e.g. anisotropy, stellar population mass-to-light ratios, triaxiality, inclusion of the dark matter halo and so on (see [Gebhardt et al. \(2011\)](#)). These could cause a factor of  $\sim 2$  of uncertainty in the mass measurements.
- Along with stellar dynamical techniques, there are gas dynamical measurements ([Barth et al. \(2001\)](#)) that, instead, are more suitable for low-luminous AGNs because they are made from the motion of ionized gas. Also for these techniques there could be many sources of uncertainty: the motion of gas is affected by pressure, including inflows and outflows, and the observed velocity can differ from the true nearly-circular velocity that probes just the SMBH gravitational potential.
- Another technique employs water masers that often form in the accretion disks of active galactic nuclei. Molecules that are on their higher energy state decay on the

lower state by emitting a photon corresponding to the energy of transition, typically at radio wavelengths. By taking measures of rotation of water masers, it is possible to achieve estimates of SMBH with good accuracy (Kuo et al. (2010)), since they consent to probe small scales (sub-light-year) that correspond to regions dominated by the black hole potential. This technique hence is by itself powerful and accurate but water masers are not easily detected.

- In active galactic nuclei that emits broad emission lines, originated in the vicinity of the black hole, it would be possible to estimate the mass from the average velocity of the gas and the radius of emitting region that probably is under the effect of the SMBH gravitational potential. To retrieve  $V(r)$  curves, a common technique is reverberation-mapping (Peterson (1993)), that uses the time delay in the response of spectral lines to the variation of the continuum. Since the speed of light is known, the size  $r$  of the emitting region can be estimated. Then the rotation speed  $V$  is evaluated from the width of emission lines, assuming the broadening is due to Doppler shift. Main uncertainties are related to whether inflows or outflows contaminate measurements and in the estimation of the geometrical factor  $f$ .
- In case of distant AGNs and quasars none of these techniques can be applied and one has to rely on secondary indicators. Most common techniques are based on an empirical relationship between the size of the broad-line region and the luminosity of the continuum in optical/UV. This scaling relation has been itself found through reverberation mapping and naturally uncertainties of the 'primary' method are summed to uncertainties of the secondary. Hence many errors can affect SMBH mass estimates for distant objects (Shen & Kelly (2012)).

Thanks to the methods just introduced it has been possible to get more and more estimates of supermassive black hole masses and start to see if some links exist between them and other galactic quantities. Indeed this is the case and the principal findings are summarized in the following.

### 1.3.2 Scaling relations: hints of co-evolution?

Many works have been trying to calibrate and unveil characteristics of scaling relations between supermassive black hole masses and host galaxy properties. First discovery of them has to be attributed to Dressler & Richstone (1988), that used stellar dynamical method to calculate the SMBH masses at the center of two neighboring galaxies: M31 and M32. They discussed of an upper-limit of  $\sim 10^9 M_{\odot}$  for SMBHs in galaxies with the largest spheroids, based on the ratio  $M_{\text{BH}}/M_{\star, \text{bulge}}$ , posing the idea of a relation between them. Later on Kormendy & Richstone (1995) found a linear distribution of  $M_{\text{BH}} - M_{\star, \text{bulge}}$  using only six galaxies. Much improvement in galaxy observations was achieved after the launch of the Hubble Space Telescope (HST) in 1990. In particular, thanks to HST data, Magorrian et al. (1998) proposed a log-linear relation to fit data relative to  $M_{\text{BH}}$  and  $M_{\text{bulge}}$ . With continuously increasing sample of objects, many other works have reported near-linear  $M_{\text{BH}} - M_{\star, \text{bulge}}$  (or using bulge luminosity  $L_{\text{bulge}}$ ) relation (e.g. Ho (1999); Haring & Rix (2004); Ferrarese & Ford (2005); Graham & Driver (2007); Gultekin

et al. (2009); Sani et al. (2011); Kormendy et al. (2011); Kormendy & Ho (2013)), even though in the last studies (Gultekin et al. (2009); Sani et al. (2011); Kormendy et al. (2011)) authors left out low-mass bulges and/or galaxies from their sample calling them ‘pseudo-bulges’.

In the meantime some works reported steeper  $M_{\text{BH}} - M_{\star, \text{bulge}}$  relations (e.g. Laor (1998); Wandel (1999); Salucci et al. (2000); Laor (2001)) because of the inclusion of smaller galaxies in the sample. Actually in Salucci et al. (2000), they hypothesized that LTGs (spirals) would follow a steeper  $M_{\text{BH}} - M_{\star, \text{bulge}}$  relation with respect to ellipticals. Graham (2012), with updating measures of BH masses and distances, observed a break in  $M_{\text{BH}} - L_{\text{bulge}}$  plot, i.e. different relations for Sérsic and core-Sérsic spheroids (Section 6.1.2). In particular it seems that (massive) core-Sérsic galaxies follow a near-linear relation, while Sérsic (most of which late-type galaxies) a super-quadratic (meaning a log-slope between 2 and 3) relation. Core-Sérsic galaxies are massive ones, that probably have undergone major dry (gas poor) mergers and, consequently, have a deficit of light in their spheroid cores. This can be explained by the fact that the massive BHs from the merging galaxies make stars depart from the center of the remnant galaxy (Begelman et al. (1980)). Galaxies with partially depleted cores were discovered by King & Minkowski (1966) and defined core-Sérsic galaxies described by a core-Sérsic function (Graham et al. (2003)). On the other hand, galaxies that grow over time through accretion or gas-rich mergers are likely to have Sérsic light profiles (Sérsic (1963)). Accepting the idea of co-evolution between the supermassive black hole and the hosting galactic bulge, a steeper  $M_{\text{BH}} - M_{\star, \text{bulge}}$  relation would imply the fact that the fractional growth of  $M_{\text{BH}}$  is greater than the fractional growth of the host  $M_{\star, \text{bulge}}$  in Sérsic galaxies, that have an evolution characterized by gas-abundant processes. On the other hand an almost linear  $M_{\text{BH}} - M_{\star, \text{bulge}}$  relation, that seems to pertain to core-Sérsic galaxies, may reflect their hierarchical growth through major dry mergers (Graham & Scott (2015)). A scenario of this type is in agreement with studies that have observed a parallelism between the AGN accretion rate with star formation rate (Diamond-Stanic & Rieke (2012); Seymour et al. (2012); LaMassa et al. (2013); Drouart et al. (2014)), as well as simulations (Fontanot et al. (2006); Hopkins & Quataert (2010); Dubois et al. (2012); Bonoli et al. (2013); Neistein & Netzer (2014)), and open new possibilities of investigation.

### Possible $M_{\text{BH}} - M_{\star}$ relation

By looking at all the above results, the existence of a strong relation between central black hole mass and its surrounding spheroid mass finds wide consensus among the scientific community. Another aspect concerns instead the possibility of scaling relations with global properties of the galaxy, i.e. the total galactic stellar mass,  $M_{\star}$ . In Läsker et al. (2014), authors used a sample made mostly of ETG galaxies and with some LTGs as well (total 35 objects) and inferred a relation between  $M_{\text{BH}}$  and the total galaxy luminosity equally strong as the one with the spheroid component. Moreover, the detection of many bulge-less galaxies with central black holes has accredited this hypothesis of a relation between  $M_{\text{BH}}$  and the total galaxy mass,  $M_{\star}$  (Reines et al. (2011); Secrest et al. (2012); Schramm et al. (2013); Simmons et al. (2013); Satyapal et al. (2014)). Actually it is still not clear whether a  $M_{\text{BH}} - M_{\star}$  relation exists for every type of galaxies, i.e. valid for both

ETGs and LTGs, or if there is a morphological dependence similar to  $M_{\text{BH}} - M_{\star, \text{bulge}}$  (see also [Savorgnan & Graham \(2016a\)](#)). What is true for sure is that if one could rely on a relation with the total mass of the galaxies, it would be much easier to evaluate supermassive black hole masses and even for distant unresolved galaxies.

### Black hole mass and stellar velocity dispersion

A self-gravitating system obeys to the virial theorem, according to which:  $M \propto rV_{\text{rms}}^2/G$ , essentially the Equation 1.5 seen before to determine the SMBH mass. The term  $V_{\text{rms}}^2$  for galaxies is the observed root-mean-square velocity, typically a combination of two velocity components: the stellar velocity dispersion,  $\sigma_{\star}$ , and the rotational velocity,  $V_{\text{rot}}$ . It is thus given by  $\sqrt{\sigma_{\star}^2 + V_{\text{rot}}^2/\sin(i)^2}$  ([Busarello et al. \(1992\)](#); [Ferrarese & Merritt \(2000\)](#)) with  $V_{\text{rot}}$  being the line-of-sight mean rotational velocity and  $i$  the inclination angle of the galaxy. The mass  $M$  in the Equation 1.5 is the mass enclosed in a radius  $r$  and  $G$  is the gravitational constant. In bulges of galaxies, usually the velocity is dominated by random motions, while in disks it is the rotational component the most important one. The virial theorem is a fundamental tool for many applications, and in here specifically it connects the velocity dispersion and the mass enclosed within a certain radius in galactic bulges. In combination with observed relations between black hole mass and host bulge stellar mass, Equation 1.5 constituted an incentive to question about an eventual  $M_{\text{BH}} - \sigma_{\star}$  relation. Indeed the very first discoveries have to be attributed to [Ferrarese & Merritt \(2000\)](#) and [Gebhardt et al. \(2000\)](#), that suggested this could be a fundamental relation between the central black hole and its host galaxy. The reason of such a supposition is because the correlation seemed to have minimal intrinsic scatter, consistent with zero. The problem was that the slopes reported in the two above-cited works were different, i.e. implying two different feedback mechanisms. According to [Ferrarese & Merritt \(2000\)](#),  $M_{\text{BH}} \propto \sigma_{\star}^{4.80 \pm 0.50}$ , supporting a energy-balancing feedback model ([Silk & Rees \(1998\)](#)); on the other hand in [Gebhardt et al. \(2000\)](#) the predicted relation was of the type  $M_{\text{BH}} \propto \sigma_{\star}^{3.75 \pm 0.30}$ , for which the feedback model of [Fabian \(1999\)](#) based on momentum conservation was more suitable. The discrepancy of the two was found ([Merritt & Ferrarese \(2001\)](#)) to be due to the different symmetrical and non-symmetrical regressions employed by the two studies respectively. This has pointed out the dependence of inferred scaling-relations on the regression procedure adopted.

Another important aspect to consider is the type of galaxies of which the sample is made. For example in [Graham & Scott \(2013\)](#) authors noted that there could be a substructure in the  $M_{\text{BH}} - \sigma_{\star}$  relation linked to the presence or not of the bar, e.g. barred galaxies followed a shallower slope scaling relation with respect to the non barred ones. In addition to that, in the work of [McConnell & Ma \(2013\)](#) they found that in the  $M_{\text{BH}} - \sigma_{\star}$  diagram, towards the high-mass end, some galaxies have offset  $M_{\text{BH}}$  (upturn) with respect to the best fit relation. These were presumably the massive core-Sérsic galaxies gone through multiple dry mergers. During a major merger indeed it is supposed that the mass growth of the galaxy and the black hole is not accompanied to a respective growth in the stellar velocity dispersion ([Burkert & Silk \(2001\)](#); [Ciotti & van Albada \(2001\)](#); [King \(2010\)](#); [Oser et al. \(2010\)](#); [King & Nealon \(2019\)](#)). Another problem has been more recently pointed out by [Shankar et al. \(2016\)](#), that have observed an offset in the  $M_{\star} - \sigma_{\star}$

diagram between the sample of ellipticals with dynamically measured black hole masses and a large sample of active galaxies from the Sloan Digital Sky Survey (SDSS), for which the sphere of influence is not resolved yet. Authors suggested that the black hole mass scaling relations inferred by using sample of objects with dynamical  $M_{\text{BH}}$  measurements are selection biased. This fact has not been addressed since then, and deeper analysis should be conducted to confirm the validity of the bias.

Despite all the issues connected to scaling relations, their study is by itself important to understand the relative growth of galaxy properties and black hole mass. It would give notable improvement in all those researches about black-hole and galaxy evolutionary interplay, e.g. the regulation of material (gas and dust) in the galaxy through AGN feedback, the relation between BH growth and star formation rate in the galaxy, where star formation is connected with the availability of gas and also about the galaxy morphology (e.g. [Marconi et al. \(2008\)](#); [Volonteri & Ciotti \(2013\)](#); [Heckman & Best \(2014\)](#); [Calvi et al. \(2018\)](#); [King \(2019\)](#)). In addition to that scaling relations allow to estimate BH masses in galaxies where the sphere of influence of the black hole is not resolvable due to technological limitations. They are also used to calibrate secondary BH mass measurements, e.g. constraining virial  $f$ -factors for reverberation mapping methods ([Bennert et al. \(2011\)](#); [Bentz & Katz \(2015\)](#); [Yu et al. \(2019\)](#)). SMBH - galaxy correlations, defined in the local universe at  $z \sim 0$ , can also work as a reference point for studies attempting to determine the evolution of these relations at high redshift (e.g. [Bennert et al. \(2011\)](#); [Sexton et al. \(2019\)](#)). Finally they are very useful to calculate the black hole mass function of the (local) universe (e.g. [Driver et al. \(2007\)](#)), to estimate supermassive black hole merger timescales ([Biava et al. \(2019\)](#)) and to constrain the SMBH merger rates (e.g. [Chen et al. \(2019\)](#)).

## 1.4 This thesis

The purpose of this thesis project is to connect the parts described so far, i.e. the formation and evolution of supermassive black holes and their relations with hosting galaxies, through the employment of a new Discrete statistical sEmi-empiriCal mODEL, DECODE. In brief such a model allows to generate mean mass assembly histories of galaxies within dark matter halos, and in particular the mean merger contribution to the growth of galaxies of given final masses. Through sets of re-parametrizations involving scaling relations it is possible to convert  $M_{\star} \rightarrow M_{\text{BH}}$  and obtain mean accretion paths for SMBHs assigned to each galaxy. At that point growing curves of supermassive black holes, appropriately subtracted by contribution of mergers, can be compared to models of SMBH accretion that are obtained from methodologies as described in Section 1.2.2, hence with the evaluation of AGN luminosity functions. Below I report the content summary of each Chapter.

- Chapter 2 describes all the details of DECODE implementation, its particularities and in which ways it can be defined a semi-empirical and statistical model.
- Chapter 3 presents first outcomes I derive from the running of the code. In particular I will explain what is expected from it and its dependence on the input

stellar mass function (SMF), that makes possible the passage from dark matter halo growth to the one of the stellar (galactic) component.

- Chapter 4 refers to the first and most direct application of DECODE outputs to the study of the SMBH growth: the employing of  $M_{\text{BH}} - M_{\star}$  scaling relation. By assuming particular shapes for it, I am going to show which one would be more suitable for the description of  $M_{\text{BH}}$  evolutionary tracks in comparison to the accretion model of reference throughout this work, the one described in [Shankar et al. \(2009\)](#).
- Chapter 5 is instead devoted to a second application of DECODE outputs that involves the probably most fundamental scaling relation,  $M_{\text{BH}} - \sigma$  relation. Velocity dispersions in this context can be only evaluated starting from  $M_{\star}$ , hence it is a less direct process with respect to the one of previous Chapter. Nevertheless it would be interesting to make comments about it so to have a more comprehensive view of the available roads opened by the model.
- Chapter 6 assembles the results obtained in precedent steps. In particular it summarizes the most interesting findings, the sources of uncertainties related to them, some alternative views to the ones adopted so far and the general idea behind the use of semi-empirical models of this type.
- Chapter 7 finally depicts some proposals for future applications. In order to improve evaluations made up in this project, two are the necessary fields of operation: increasing observations and looking at other models and simulations.

## Chapter 2

# Description of DECODE

The present Chapter is devoted to the presentation of DECODE, a new Discrete statistical sEmi-empiriCal mODEl designed by the research group of the University of Southampton (Fu et al. (in preparation), personal communication). The principal purpose of the model is to provide a flexible, fast and accurate tool to predict, in a full cosmological context, the average galaxy assembly and merger histories.

In what follows I will give a detailed description of how the code has been implemented, along with the consequent advantages and disadvantages related to it. Before addressing the characteristics and specifics of DECODE, I think it is important to familiarize with the concept of semi-empirical model (SEM).

### 2.1 Semi-empirical models

The study of the formation and evolution of galaxies in the universe is a field subjected to large debate, in particular about what concerns the relative roles of star formation and mergers in regulating their growth. In the last fifteen years, many works in literature have been conducted to this purpose, e.g. see Guo & White (2008); Oser et al. (2010); Cattaneo, A. et al. (2011); Lackner et al. (2012); Lee & Yi (2013); Pillepich et al. (2014); Rodriguez-Gomez et al. (2016); Qu et al. (2016); Clauwens et al. (2018); Pillepich et al. (2018b); Davison et al. (2020). The general idea is that galaxies are present at the center of Dark Matter (DM) halos and that they grow their mass either via mergers with other DM halos or through smooth mass accretion from their environments (Murali et al. (2002); Conselice & Arnold (2009); Genel et al. (2010) and L'Huillier, B. et al. (2012)). In order to have a clearer view of what is the process that dominates over cosmic epochs, it is first of all necessary to correctly predict the merger histories of the host DM halos in the context of a  $\Lambda$ CDM Universe; secondly it is important to well connect DM halos merger trees to galaxies and obtain their assembly histories.

Among the different techniques that have been proposed so far to get through this problem, we can cite hydrodynamic simulations (e.g. Vogelsberger et al. (2014); Schaye et al. (2014); Pillepich et al. (2018a)), and semi-analytic models, SAMs, (see Baugh (2006); Monaco et al. (2007); Hirschmann et al. (2012a); Shankar et al. (2012); Lacey et al. (2016a); Henriques et al. (2019); Jiang et al. (2021)). In both situations the

growth of galaxy follows from first principles that model the physical processes regulating baryon cooling, star formation and feedback mechanisms. The main problem related to such approaches is the fact that they are characterized by many input assumptions and related free parameters. Such large parametrization can induce strong degeneracies or divergences (e.g. [Lapi & Cavaliere \(2011\)](#); [González et al. \(2011\)](#)). Moreover there is still the issue connected to the relative roles of mergers and star formation in the accretion. It has been noted that quite different merger histories can lead to similar morphologies and kinematic properties in the remnant galaxies (e.g. [Bournaud, F. et al. \(2007\)](#)). Finally there is often the possibility that different hierarchical models return divergent balances between the quantity of stellar mass that is formed in-situ (star formation by cold gas) and the fraction of mass gained ex-situ, via mergers.

A way out in this context is represented by recently-developed semi-empirical models (SEMs) that avoid to evolve galaxies from first principles. Important steps in this direction have been performed in e.g. [Hopkins et al. \(2009a\)](#); [Cattaneo, A. et al. \(2011\)](#); [Zavala et al. \(2012\)](#); [Shankar et al. \(2014\)](#); [Moster et al. \(2018\)](#); [Grylls et al. \(2019\)](#). The approach adopted by SEMs is based on abundance matching techniques. They consist in the generation of a monotonic stellar mass - halo mass (SMHM) relation from the equivalence between the cumulative number densities of measured stellar mass functions (SMF) and DM halos mass functions (HMF) (e.g. [Kravtsov et al. \(2004\)](#); [Vale & Ostriker \(2004\)](#); [Shankar et al. \(2006\)](#); [Moster et al. \(2010\)](#); [Behroozi et al. \(2010\)](#)). Essentially galaxies are assigned to each halo at any epoch along dark matter merger trees via these relations, thus giving the possibility to track the full stellar mass evolution in, for example, the main progenitor branch of the merger tree. It has to be noted that, despite their flexibility, traditional semi-empirical models can suffer from volume limitation effects because of finite number of merger trees and/or dark matter halos. This becomes particularly relevant at high masses. In the context of the thesis project I will show how SMHM relation is computed and included in the model. I anticipate that the calculation follows from the formalism put forward in [Aversa et al. \(2015\)](#).

The predecessor of DECODE is the *STatistical sEmi-Empirical modeL*, STEEL, presented in [Grylls et al. \(2019\)](#) and [Grylls et al. \(2020\)](#). In this model the authors adopt the following method: they trace back in time the mean accretion histories of small bins in halo mass, weighted by the HMF; then, employing a mean SMHM relation, they can convert mean DM halo assembly histories into total mean galaxy accretion tracks and mean cumulative mass accretion by merging satellites. Star formation histories are then obtained subtracting the contribution of mergers to the total galaxy growth, and the results can be compared to independent observational data.

The method just outlined provides a powerful tool to investigate mean evolutionary trends, but it is significantly sensitive to the SMHM relation of input. Even small differences in the relation may bring to relevant discrepancies in the final evaluation of the galaxy merger rates. In this work I am going to analyse how a distinct choice of the SMHM relation impacts in the indirect derivation of growing curves of supermassive black halos hosted by galaxies.

## 2.2 DECODE implementation

As already mentioned, DECODE is a model that allows to investigate the evolution of galaxies within DM halos avoiding the adoption of a full SAM, hydrodynamic simulation or a complex cosmological SEM. It basically consists in the following few and simple steps:

- Generation of the central DM halo population;
- Generation of the DM subhalo population;
- Evolution of subhalos after infall;
- Generation of the galaxy population (baryonic component).

In fact, the last point can be directly achieved as an output of the program, or, as in the case of my thesis project, it can be considered independently and performed in a second moment. Hence, the main potentiality of DECODE resides in the creation of the mean merger histories of parent DM halos.

Figure 2.1, taken from Fu et al. (in preparation, p.c.), summarizes all the passages implemented in the code. Generally speaking, the program produces large catalogues of parent halos, starting from a HMF of input, and assigns to each of them a mean halo growth track based on N-body numerical simulations and analytic models. In this work the reference model for the global accretion of DM halos is the one described by [van den Bosch et al. \(2014\)](#). The population of subhalos linked to each halo is again created through sub-halo mass functions, SHMFs, that rely on accurate N-body simulations, as explained in [Jiang & van den Bosch \(2016\)](#).

The reason why DECODE can be described as discrete is related to the fact that it is built object-by-object, similarly to an N-body simulation, but, differently from the latter, it is almost entirely independent from volume and/or mass resolution limitations. Actually this should not be misinterpreted: DECODE does not produce single and specific evolutionary track for each object. The real information still consists in the *mean* halo/galaxy growth histories, as in STEEL ([Grylls et al. \(2019\)](#)) above-mentioned. The difference is that in the case of STEEL the model relies on continuous statistical weights, while in DECODE we have stochastic samples of halos that on average evolve in mass as predicted by STEEL.

Another aspect to be noted is the fact that, up to now, we never speak about the cosmological model to be used. Indeed the results are not strictly sensitive to the choice of the cosmological parameters because merger trees are built through the SHMF, that has been demonstrated not to differ much when studied in different simulations (e.g. [Jiang & van den Bosch \(2016\)](#); [Green et al. \(2021\)](#)). Nevertheless throughout this work I adopt the  $\Lambda$ CDM cosmological model with parameters from [Planck Collaboration et al. \(2020\)](#):  $(\Omega_m, \Omega_\Lambda, \Omega_b, h, n_S, \sigma_8) = (0.31, 0.69, 0.049, 0.68, 0.97, 0.81)$ .

In what follows I will describe in more details the features of each passage implemented in DECODE.

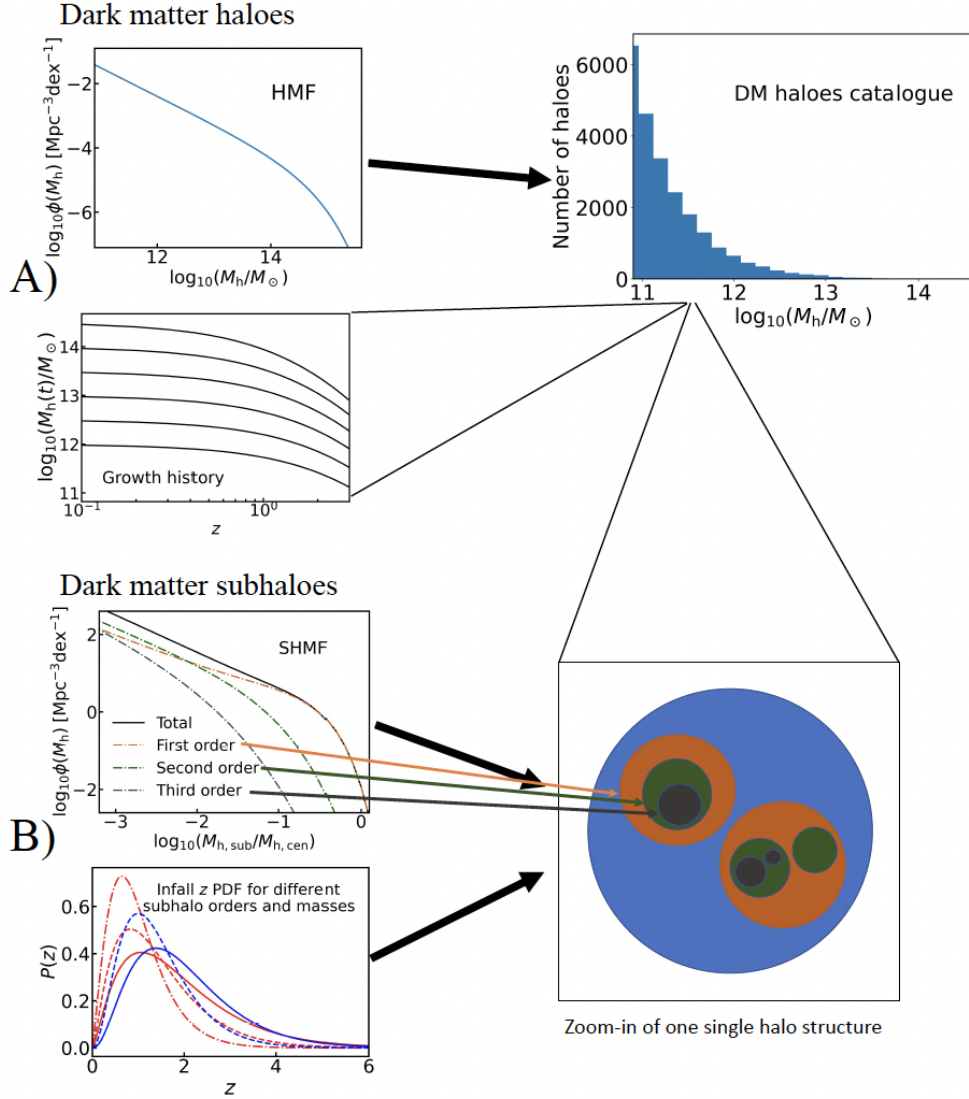


Figure 2.1: Schematic structure of DECODE for the part involving dark matter. Panel A shows the functions used to create the parent halos catalogue. The plot on the upper left corner displays the HMF from which the masses of dark matter haloes are generated. Below there are the curves of mean accretion history assigned to each halo through analytic fit. Panel B represents functions employed to create the population of sub-halos assigned to each halo. They are generated from the sub-halo mass functions, SHMFs, distinguished for orders of the sub-halos. I am going to focus on sub-halos just up to 1st order. As final step, redshift of infall is assigned through analytic fits that depend on the order and mass of the sub-halo (bottom right corner).

### 2.2.1 Catalogue of parent halos

Parent dark matter halos are extracted from an HMF given as input in the code. The choice for this work is the one that has been defined by [Tinker et al. \(2008\)](#). This density distribution function is valid just for central halos.

To extract halo masses the HMF is multiplied by a given input cosmological volume, arbitrarily chosen. A mass range is defined and some care should be put in this step to well calibrate the cosmological volume and the highest mass to be considered. Objects at the high mass end are more rare than the smaller ones and if not a sufficiently large volume is given, we end up with a very poor sample of high mass objects and need to run the program many times in order to have a good statistics.

Figure 2.2 presents an example of how to insert the parameters that are used for the creation of the parent sample. For this project, as I am going to specify in Chapter 3, the value of parameters chosen are: `cube_side` = 150, length of the side of the cubic cosmological volume in units of Mpc/h, and masses within `M0_host_min` = 11 and `M0_host_max` = 15 in units of  $\log_{10}(M/M_{\odot})$ . This method is extremely rapid and allows to create very large samples of objects at  $z = 0$ .

For what concerns the average mass accretion history, this is obtained for each central halo using the methodology described in [van den Bosch et al. \(2014\)](#). It has to be specified that DECODE does not give as direct output the total accretion tracks. These are included during the generation of the merger trees for each parent halo of a certain final mass in the way that will be clarified in the next Sections. The computation of the growth is, in fact, not performed for the single halo: the same mean history is assigned to all the DM halos falling within given mass bins of size  $\Delta\log_{10}M_{\text{bin}} = 0.5$  dex. For the purpose of the project presented here, having mean accretion curves is instead necessary. Hence the same function will be recalled again (see next Chapter) to reconstruct total mean accretion curves, this time for single values of halo final masses.

### 2.2.2 Population of subhalos

On average the number of subhalos of a given mass that fall onto the parent halo at a certain time is defined by a subhalo mass function (SHMF). In DECODE the adopted function is the time-independent one described in [Jiang & van den Bosch \(2014\)](#) and [Jiang & van den Bosch \(2016\)](#), that is computed by summing the contribution of distribution functions associated to subhalos of different orders. The order of a subhalo represents its hierarchical priority, meaning that first-order subhalos are the ones that directly fall onto the main branch, second-order subhalos are satellites of first-order ones at time of accretion onto the parent halo and so on. This can be visualized in Panel B of Figure 2.1, where the matryoshka-like scheme appears clear. In this project I will convert (sub)halo masses into stellar masses and then into central black hole masses. Subhalos of order higher than the first will be converted into a black hole of negligible mass when counted in the merging accretion process. Hence I consider only subhalos of first order.

In general the way to account for all subhalos that have ever fallen onto a parent halo is to use the cumulative total un-evolved SHMF. Then the SHMFs distinguished by order are considered (see again Panel B of Figure 2.1): for first-order subhalos the function

```

# -----
# ----> Mass functions:
# -----

# 1) Halo mass function.
#   Insert halo mass function model.
#   See https://bdiemer.bitbucket.io/colossus/lss_mass_function.html
#   for available models.
#   Default: tinker08
halo_mass_function = tinker08

# 2) Sub-halo mass function.
#   Currently developed only Jiang & vdB 2016, MNRAS 458, 2848–2869
#   This is assumed by default, no need to specify.

# -----
# ----> DM catalogue parameters:
# -----

# 1) Insert the length of the cube side.
#   Units of [Mpc/h]
cube_side = 150

# 2) Insert parameters for the redshift interval.
#   This is the range in which the infall redshifts will be generated,
#   subhalos which have in-falled before z_max will not be calculated.
#   z_bin indicates the resolution in redshift.
z_min = 0
z_max = 4
#z_bin = 0.1

# 3) Insert mass parameters for the host halos
#   M0_host_bin indicates the resolution in mass,
#   when drawing the halo mass function.
#   Units of [log10(M_sun)]
#   If you want outputs in [log10(M_sun/h)],
#   insert input parameters in those units.
M0_host_min = 11.
M0_host_max = 15.
M0_host_bin = 0.1

```

Figure 2.2: Example of input parameter file.

used can be found in [Jiang & van den Bosch \(2016\)](#), while for higher-orders subhalos the prescription is given by Equation (17) in [Jiang & van den Bosch \(2014\)](#). Each subhalo is at this point assigned with a probability of being of a certain order according to its mass. This probability is simply calculated from the ratio between first- or higher- order SHMF and the total SHMF computed in the chosen bin of (sub)halo mass.

### 2.2.3 Time of infall

The infall redshift,  $z_{\text{inf}}$ , is defined as the time at which a DM halo (subhalo) enters for the *first* time the virial radius of another halo. The procedure to determine this time is again built in a statistical way and it is distinguished for first-order subhalos and higher-order

ones. I have already specified the fact that I will focus just on subhalos of first-order, but for completeness I describe how the whole mechanism should work when considering also higher order subhalos.

- For **first-order subhalos**: the redshift probability distribution is directly calculated from the SHMF. A growing parent-halo, in a redshift interval of size  $dz$ , is subject to a change in mass of the order of  $dM_{h,par}(z)$ . Hence from  $M_{h,par}$  it gets a mass of  $M_{h,par} + dM_{h,par}$ , with a consequent slightly change in the SHMF associated to it. The probability density function (PDF) of infall redshifts related to a subhalo with a certain infall mass,  $M_{h,sub}$ , is then proportional to the derivative of the SHMF with respect to the redshift. This is represented by the following equation:

$$\text{PDF}(z_{\text{inf}}) \propto \frac{d}{dz} \phi(M_{h,sub}, M_{h,par}(z)). \quad (2.1)$$

In other words, since the un-evolved SHMF  $\phi(M_{h,sub})$  describes the total number and mass of the subhalos that have ever merged with the parent halo at any given epoch, the change of SHMF  $d\phi(M_{h,sub}, M_{h,par}(z))$  gives the number and mass of subhalos, with mass within  $M_{h,sub}$  and  $M_{h,sub} + dM_{h,sub}$ , that have merged with the parent halo in the redshift interval  $dz$ . Once normalized equation 2.1 provides the PDF for a subhalo of mass  $M_{h,sub}$  to be accreted at a redshift  $z$ , and the infall redshift for the subhalo is extracted from this distribution function. The SHMF only characterizes subhalos that merge with the parent-halo and this is the reason why such a method is only applicable to first-order subhalos.

- For **second-/third-order subhalos**: to assign infall redshift to second-order subhalos, the steps to follow are in a certain way analogous to the ones described in the previous point. First of all to each parent halo, named P0, it is assigned a full merger tree made by first-order subhalos, S1, with the specification of the infall time (Jiang & van den Bosch (2014); Jiang & van den Bosch (2016)). Then each S1 is assigned with its satellite accretion history using again a SHMF of first order. A satellite of a subhalo is a subhalo of second-order, S2, for P0. This loop can be repeated many times so to reach the order needed.

The whole process can be sped up after the first runs of the code. Indeed once the merger histories of all relevant subhalos S2 and S3 have been defined, it is possible to produce analytic fits out to the infall redshift distribution functions. The parametric form chosen for the PDF is given by:

$$P(z) = Az^\alpha \frac{1}{\delta e^{\beta z} - \gamma}, \quad (2.2)$$

with  $A$ ,  $\alpha$ ,  $\delta$ ,  $\beta$  and  $\gamma$  being dimensionless free fitting parameters, whose best values are not reported here because I am not going to use them. Anyway equation 2.2 is used to assign infall redshifts statistically to second- and third-order subhalos.

The technique just described has the big advantage of being fast and not affected by mass resolution limitations. On the other hand it does not generate specific accretion histories for single objects. What is actually obtained is a stochastic merger tree of subhalos for a

given average parent halo mass accretion track. This implies that to compute the 'right' merger histories, it is necessary to take the mean of many objects growing tracks that account for accretion through mergers.

### 2.2.4 Merging timescale

The merging timescale is the typical timescale that a subhalo needs in order to completely merge with its progenitor. For what concerns DM halos, this time is in good approximation expressed by the Equation (5) in [Boylan-Kolchin et al. \(2008\)](#), that is:

$$t_{\text{merg}} = t_{\text{dyn}} A \frac{(M_{\text{h,host}}/M_{\text{h,sub}})^b}{\ln(1 + M_{\text{h,host}}/M_{\text{h,sub}})} \exp \left[ c \frac{J}{J_c(E)} \right] \left[ \frac{r_c(E)}{R_{\text{vir}}} \right]^d. \quad (2.3)$$

In the above formula  $t_{\text{dyn}}$  is the halo dynamical timescale,  $J/J_c(E)$  is the orbital energy and  $A$ ,  $b$ ,  $c$  and  $d$  are free parameters. The parameters adopted in DECODE implementation are the ones found in [McCavana et al. \(2012\)](#). Last term of Equation 2.3 is the ratio between the average radius of the subhalo orbit,  $r_c$ , and the halo virial radius,  $R_{\text{vir}}$ , and it is computed assuming an orbital circularity,  $\xi$ . The latter is either assigned following [Khochfar & Burkert \(2006\)](#), i.e. extracted from a Gaussian distribution with a center value of  $\bar{\xi} = 0.5$  and a standard deviation of  $\sigma_\xi = 0.23$ , or it is assumed a constant value for it (see Section 3.1.1). Then the radii ratio is given by the formula reported below:

$$\frac{r_c}{R_{\text{vir}}} = \frac{\xi^{2.17}}{1 - \sqrt{1 - \xi^2}}. \quad (2.4)$$

All these expressions are approximation and in order to allow for some flexibility, the merging timescale is corrected through a fudge factor:  $t_{\text{merg}} \rightarrow f_{\text{dyn}} t_{\text{merg}}$ . It is found (Fu et al. (in preparation)) that the fudge factor is well represented by a linear relation that depends on the ratio  $q = (M_{\text{h,host}}/M_{\text{h,sub}})$ :

$$f_{\text{dyn}} = a \cdot q + b, \quad (2.5)$$

where best-fit values for the parameters  $(a, b)$  are  $(0.00035, 0.65)$ . In Figure 2.3, taken again from Fu et al. (in preparation), one can find the plot representing  $f_{\text{dyn}}$  factor as a function of  $M_{\text{h,sub}}/M_{\text{h,par}}$  on the top and the plot expressing equation 2.3, without the fudge factor correction (solid line from [McCavana et al. \(2012\)](#)) and with the correction (dash-dotted line), on the bottom.

At this point the last step is to assign merging timescales to all subhalos. They are initially computed for first-order subhalos through Equation 2.3 and considering the mass ratio  $M_{\text{P0}}/M_{\text{S1}}$ . Then taking into account the time of first accretion, we have at least three possibilities: 1) the first-order subhalo has survived today, and so its satellites; 2) the first-order subhalo has not survived and all its satellites are released to the parent halo; 3) the higher-order subhalos have been tidally disrupted before the first-order subhalo has merged (do not exist). The merging timescales are assigned to second-order subhalos using mass ratio  $M_{\text{S1}}/M_{\text{S2}}$ . For second-order subhalos released from first-order ones to the parent, a new  $t_{\text{merg}}$  is then calculated considering the ratio  $M_{\text{P0}}/M_{\text{S2}}$ .

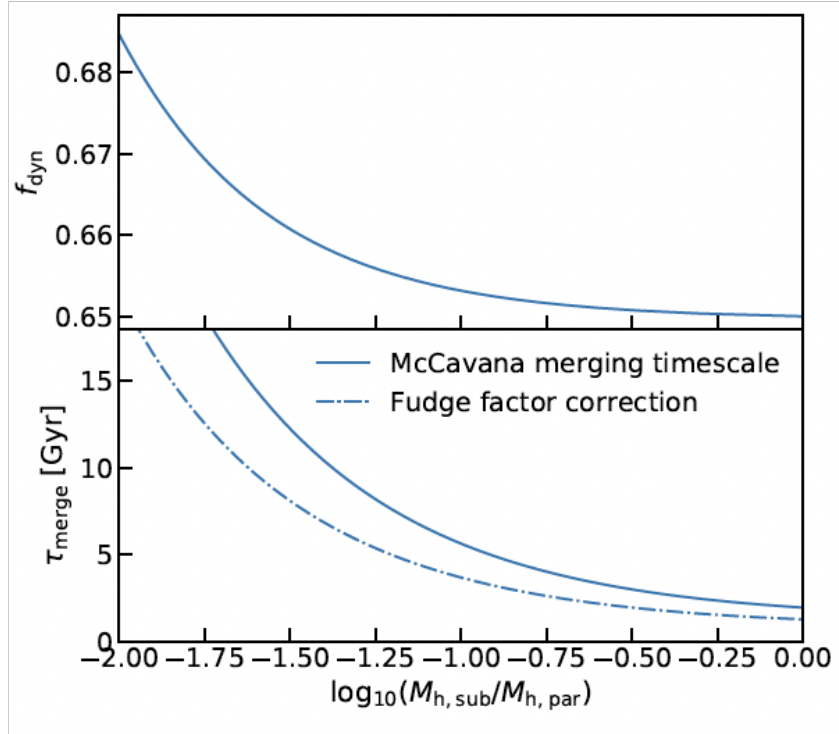


Figure 2.3: Merging timescale as a function of mass ratio (bottom plot)  $M_{h,\text{sub}}/M_{h,\text{par}}$ . Solid line is obtained using equation from [McCavana et al. \(2012\)](#), while dash-dotted line is the result of the fudge factor application (top plot).

Paragraphs [2.2.1](#), [2.2.2](#), [2.2.3](#) and [2.2.4](#) describe all the passages performed every time DECODE is run. Output data will be automatically stored into two ASCII files. One, named `output_parents.txt`, contains the information on the central halos. The other, named `output_mergers.txt`, contains the information on the mergers.

File `output_parents.txt` is organized as follows: it contains two columns reporting respectively the ID of the parent halo and its mass at  $z = 0$  in units of  $\log_{10}(M/M_{\odot})$ .

File `output_mergers.txt` is organized as follows:

- first column: ID of the corresponding parent halo;
- second column: ID identifying the  $(i - 1)$ -th order progenitor. It is -1 if the progenitor is the parent halo itself;
- third column: ID identifying the subhalo itself;
- fourth column: order of the subhalo;
- fifth column: subhalo mass in units of  $\log_{10}(M/M_{\odot})$ ;
- sixth column: redshift at first accretion ( $z_{\text{inf}}$ );

- seventh column: merging timescale in units of [Gyr].

As mentioned at the beginning of Section 2.2, for the moment I have left out the steps related to the halo-mass/stellar-mass conversion, since it is applied in a second moment and not made to be a direct output in my use of DECODE. The procedure implemented to address this point will be presented in the next Section.

## 2.3 Stellar Mass - Halo Mass (SMHM) relation

In Section 2.1 I have introduced the basic concept of the abundance matching technique when explaining the general characteristics of semi-empirical models. As said abundance matching is a standard way of deriving a monotonic relationship between galaxy and halo properties by connecting the corresponding number densities (e.g. [Vale & Ostriker \(2004\)](#); [Shankar et al. \(2006\)](#); [Moster et al. \(2010\)](#); [Moster et al. \(2013\)](#); [Behroozi et al. \(2013\)](#); [Behroozi & Silk \(2015\)](#)). It is possible to derive the relation  $M_\star(M_h, z)$ , with  $M_\star$  stellar mass and  $M_h$  halo mass, by solving the following equation (e.g. [White et al. \(2008\)](#); [Shankar et al. \(2010\)](#); [Aversa et al. \(2015\)](#)):

$$\int_{\log M_\star}^{+\infty} \phi(M'_\star, z) d\log M'_\star = \int_{-\infty}^{+\infty} \frac{1}{2} \operatorname{erfc} \left\{ \frac{\log M_h(M_\star) - \log M'_h}{\sqrt{2} \tilde{\sigma}_{\log M_\star}} \right\} \cdot \phi(M'_h, z) d\log M'_h, \quad (2.6)$$

which holds when a log-normal distribution of  $M_\star$  at fixed  $M_h$  with dispersion  $\sigma_{\log M_\star}$  is adopted. In the above formula I have defined  $\tilde{\sigma}_{\log M_\star} = \sigma_{\log M_\star} / \mu$  with  $\mu = d\log M_\star / d\log M_h$  the derivative of the SMHM relation. The only input parameter in equation 2.6 is this scatter. For what concerns the HMF, it should be a total one that considers both parent halos and subhalos; hence it is given by the sum  $\phi(M_{h,\text{tot}}) = \phi(M_{h,\text{par}}) + \phi(M_{h,\text{sub}})$ . The correction to the HMF (already specified as input in DECODE) follows an analytic formula presented in [Behroozi et al. \(2013\)](#), that accounts for the abundance of surviving satellite as a function of redshift. Essentially the HMF of input and the corrected one are similar, with the latter being just slight steeper at the low mass end as can be seen in Figure 2.4 (from [Fu et al. \(in preparation\)](#)). At this point the SMHM relation obtained from 2.6, at any redshift, is used to seed every parent halo and subhalo with galaxies. To be specified is the fact that subhalos are assumed to always maintain same mass after infall. Actually I will use a calculation of stellar mass from DM halo mass worked out with the mean SMHM relation, meaning the scatter term is not included. This is because DECODE, at this level of development, is mostly sensitive to mean galaxy and halo growth.

### 2.3.1 Stellar Mass Function

What I have just explained is a fast and flexible method that allows the computation of SMHM relation in a numerical way, without the need of applying a complex and pre-defined analytic fit. However, such SMHM relation is highly affected by the shape of

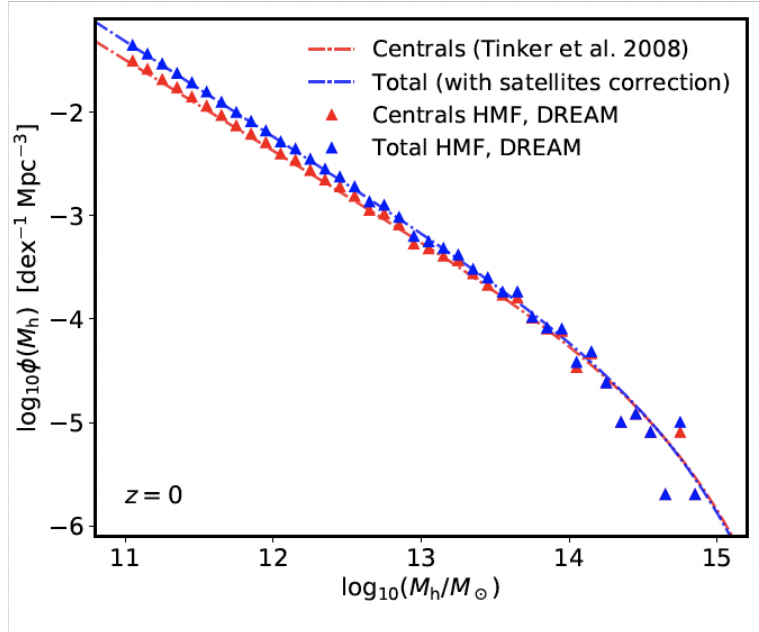


Figure 2.4: Halo mass function for parent DM halos by [Tinker et al. \(2008\)](#) (red dash-dotted line) and the HMF corrected for the abundance of satellites (blue dash-dotted line). Super-imposed there are triangles that represent mass functions calculated from DECODE.

the measured SMF,  $\phi(M_*, z)$ , which represents a major source of uncertainty. Indeed many works (e.g. [Bernardi et al. \(2013\)](#); [Bernardi et al. \(2016\)](#); [Bernardi et al. \(2017\)](#)) point out the fact that SMF is not easy to know with sufficient accuracy, even in the local universe, as it can depend for example on the light profile chosen to fit photometry. Other problems are related to the methodology used to measure stellar masses which can lead to different conclusions about the redshift evolution of SMF (e.g. [Shankar et al. \(2014\)](#) compared to [Bernardi et al. \(2017\)](#) and to [Davidzon et al. \(2017\)](#)).

Generally speaking, in the context of SEMs, what can be done is to evaluate to which extent the choice of the SMF, hence the resulting SMHM relation, impacts in results that are comparable with other observational data. In particular in this thesis project I am going to estimate which SMHM relation, assumed to convert halo mass into stellar mass, can best reproduce growing curves of supermassive black holes when compared to ones obtained through different methods (i.e. from continuity equations), see future Sections for details. Here I briefly report the features of the SMHM relations to be used: i) a first one is derived using SMFs of [Tomczak et al. \(2014\)](#); ii) a second SMHM relation is instead obtained from an empirical model set up in [Moster et al. \(2018\)](#).

## Tomczak SMF

In Tomczak et al. (2014), authors measure the galaxy SMF over a broad redshift range ( $0.2 < z < 3$ ) using observations from the FourStar Galaxy Evolution Survey (ZFOURGE). They build a large sample of galaxies complete to low stellar masses with accurate photometric redshifts. Actually their data allow to probe the SMF down to  $\approx 10^{9.5} M_{\odot}$  at  $z < 2.5$ .

Some studies (e.g. Baldry et al. (2008); Ilbert et al. (2013); Muzzin et al. (2013)) have noted that SMF at  $z \leq 1.5$  exhibits a steepening of faint-end slope at  $\sim \log_{10}(M_{\star}/M_{\odot}) \leq 10$  and so it is not well characterized by a single-Schechter function (Schechter (1976)). In Tinker et al. (2008) they fit both single- and double- Schechter functions to all SMFs and show that a low-mass upturn is present in the SMF up to at least  $z = 2$ . Also they find no evidence of evolution in the characteristic mass (turning point) of  $M_{\star} \approx 10^{10.65} M_{\odot}$  or in the slope at low masses which is  $\approx -1.5$ . Their stellar mass functions can be visualized in the Figure 2.5 (Figure (6) of their paper).

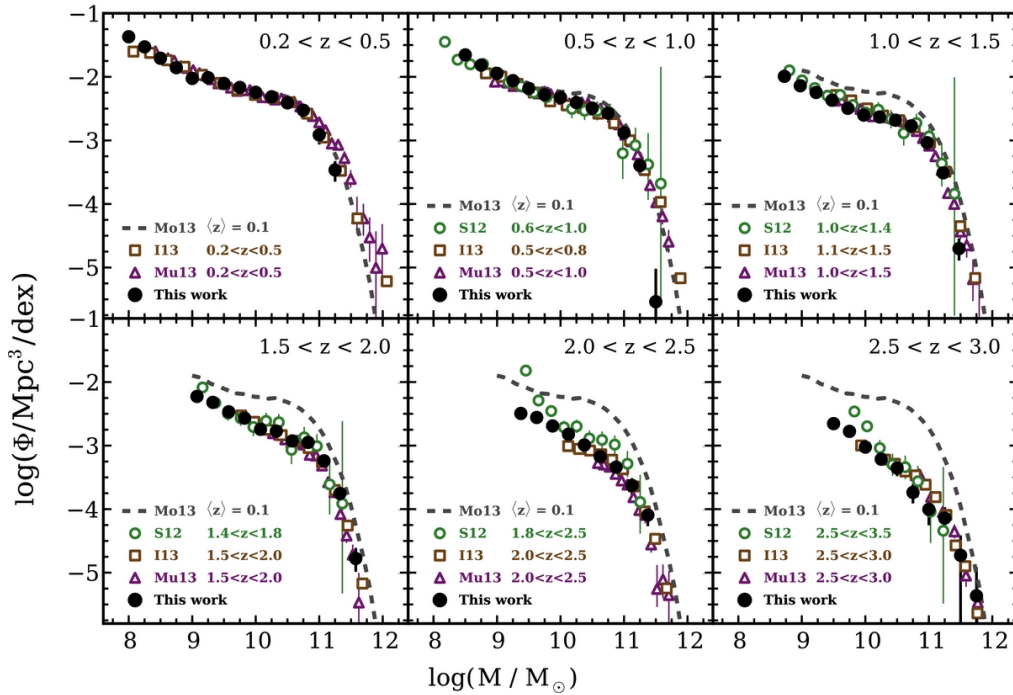


Figure 2.5: Stellar mass functions from Tomczak et al. (2014) for all galaxies between  $0.2 < z < 3$ . Their data are compared with results of other studies: Moustakas et al. (2013) (Mo12), Santini et al. (2012) (S12), Ilbert et al. (2013) (I13) and Muzzin et al. (2013) (Mu13).

### Moster model

[Moster et al. \(2018\)](#) provide a novel empirical galaxy formation model EMERGE, that reconstructs the evolution of galaxies in individual dark matter halos. The model is synthetically built in this way: halo merger trees are obtained from N-body cosmological simulations and for each of them it calculates the growth rate at every redshift; then the SFR of the galaxy is determined as the product of the halo growth rate (how much material is available) and the instantaneous baryon conversion efficiency,  $\epsilon(M_h, z)$ , (how efficiently the material can be converted into stars). Stellar mass of every galaxy is calculated by the integration of the star formation histories also taking into account mass loss from dying stars. Once the halo under consideration is captured by another one, becoming a subhalo, the seeded galaxy continues to form stars for a certain amount of time and then is rapidly quenched. The best model is finally constrained using several sets of observed data, including SMFs and sSFRs up to high redshift.

Once best-fitting values are found, from the instantaneous conversion efficiency it is possible to calculate the integrated baryon conversion efficiency  $\epsilon_{\text{int}}(M_h) = M_{\star}/M_b = M_{\star}/(f_b M_h)$ , or in other words the SMHM relation. In the previous expression  $M_b$  is the total baryonic mass in a halo and  $f_b$  is the universal baryon fraction. [Figure 2.6](#) shows the integrated conversion efficiency as a function of halo mass for each individual galaxy in the simulation box. It turns out that the low-mass slope is quite steep at low redshift and becomes shallower at high redshift. Instead high-mass slope is shallower and does not depend on redshift. Anyway [Moster et al. \(2018\)](#) find good agreement between these integrated conversion efficiencies and previous results for the SMHM relation from abundance matching methods.

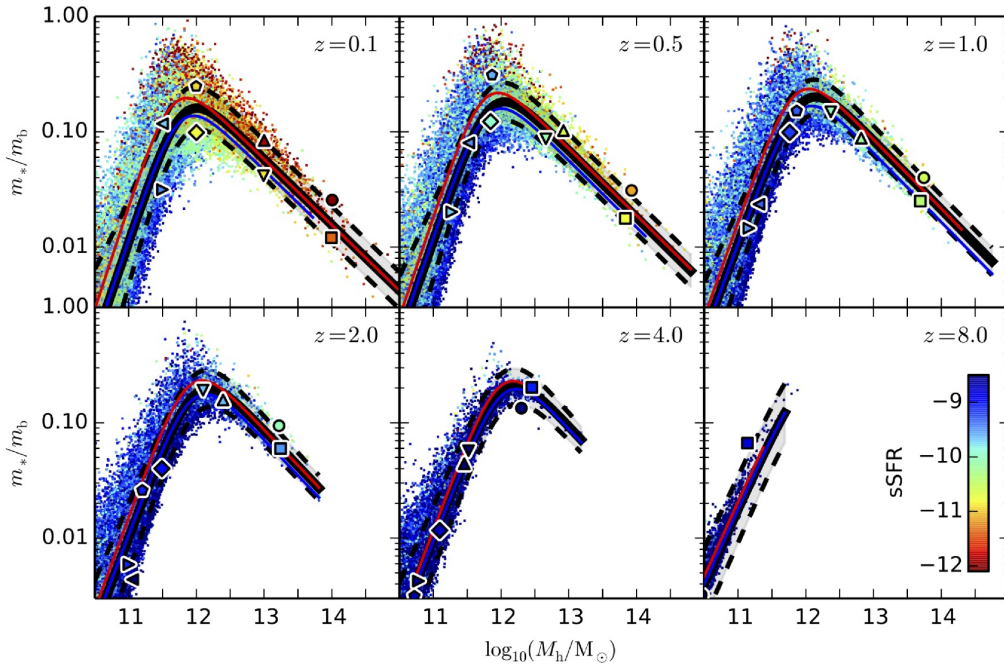


Figure 2.6: Integrated baryon conversion efficiency for central galaxies as function of halo mass at six redshift. Points are color-coded according to the sSFR ( $\text{yr}^{-1}$ ) of the galaxy. Solid black lines represent the median conversion efficiency at fixed halo mass and dashed black lines are  $1\sigma$  boundaries. The symbols are eight individual systems that have been selected at  $z = 0.1$ .

## Chapter 3

# Output of DECODE

In Chapter 2 I have introduced DECODE, in particular I focus on its implementation and main characteristics. At this point we dispose of a rapid and efficient tool that allows to probe, in a full cosmological context, galaxy assembly and merger histories for any given input stellar mass - halo mass (SMHM) relation. This model relies on minimal parametrization and its applications are numerous and approachable in an easy way.

The purpose of this project is to use the ability of DECODE to rapidly predict mean merger histories and to investigate the growth of supermassive black holes (SMBHs) believed to reside at the center of each galaxy. The mechanisms through which a BH acquires mass are basically two: accretion from infalling cold gas (see Section 1.2.2) and mass gain by BH-BH mergers. The relative roles of these two processes is still not well known, in particular how much is the contribution of mergers, if it has been always the same through cosmic time and for which systems (in terms of mass) it is more relevant. Trying to give answers to these questions is far from easy and the work conducted here is going just to give estimates in a wide more general and complex framework. Nevertheless some results obtained can be compared to other models (see Section 4.1 of Chapter 4) and observational data so that it is possible at least to get basic knowledge of what is happening in the growing path of a supermassive black hole.

I still miss the key ingredient that makes us able to relate the outputs of DECODE (mean halo/galaxy merger histories) to information on the accretion of black holes, specifically I am referring to models of gas accretion based on continuity equation (see Section 4.1). Such a bridge between them is represented by the scaling relations, a topic already discussed in Chapter 1.

Finally the outline of the project is schematize below:

- Reconstruct mean growing histories of DM halos from DECODE (Section 3.1);
- Convert halo masses in stellar masses of galaxies within them through SMHM relations (Section 3.2);
- Build SMBHs accretion curves through the following re-parameterization:  
 $M_h \rightarrow M_\star \rightarrow M_{BH}$ . The last conversion can be performed:
  - Directly through the employment of  $M_\star - M_{BH}$  scaling relations;

- With an additional step consisting in the computation of the stellar velocity dispersion,  $\sigma$  ( $\text{km s}^{-1}$ ), from the total galactic mass  $M_*$  and then the use of  $\sigma$  -  $M_{\text{BH}}$  scaling relations to obtain  $M_{\text{BH}}$ ;

(Following Chapters).

## 3.1 Dark-matter halos growth

This Section is dedicated to the analysis of DECODE output data and of the information one can get from them.

### 3.1.1 Input parameters

First of all, as mentioned in 2.2.1, it is necessary to set some input parameters in order to extract the sample of parent halos, to retrieve the sample of subhalos for each of them and to assign to these subhalos the respective redshift of infall,  $z_{\text{inf}}$ . The choices I made are reported below:

- `halo_mass_function = tinker08`  
It is the halo mass function used to generate the main progenitors and as already said is the one of [Tinker et al. \(2008\)](#);
- `cube_side = 150`  
It is the size of the simulated cosmological cube volume side in units of Mpc/h. This corresponds to a quite big cosmological volume and the exact total number of parent halos generated within it amounts to  $N_{\text{h,par}} = 166280$ . It allows to have a very high quantity of parent halos with low/intermediate masses and a more restricted but statistically good number of high-mass parent halos;
- `z_min = 0`  
`z_max = 4`  
`z_bin = 0.1`  
This set of parameters constraints the redshift interval within which the code will calculate the central halo accretion track and mergers. The parameters `z_bin` denotes the resolution for drawing the probability distribution of the redshift at first accretion. The maximum value of  $z$  has been set to  $z_{\text{max}} = 4$  in consideration of the redshift up to which stellar mass functions of use in this project are reconstructed (Subsection 2.3.1). Actually the one of [Tomczak et al. \(2014\)](#) has been obtained from observations at maximum redshift  $z_{\text{max}} \simeq 3$ , so my choice will imply an extrapolation of the SMHM relation at higher redshift, resulting in more approximated results;
- `MO_host_min = 11`  
`MO_host_max = 15`  
`MO_host_bin = 0.1`  
These are the parameters to set the mass interval, reported in units of  $\log_{10}(M/M_{\odot})$ ,

within which the code will generate the parent halos. The parameter `MO_host_bin` defines the resolution for drawing the halo mass function distribution. The extremes of the mass interval are decided so to produce, in a second moment, supermassive black holes with final masses between  $\sim 10^6 - 10^{10} M_{\odot}$ . Naturally these values and the exact halo mass that is converted into a SMBH of a certain final mass change depending on the scaling relation of use;

- `mass_definition = vir`  
It indicates the mass definition, which in this case is the virial mass. This is implemented via the Python `colossus` package;
- `use_mean_track = yes`  
This option states how to calculate the accretion track of the parent dark matter halos. The options allowed are 'yes' or 'no'. If 'yes' the code will assume a single mean track per halo mass bin, set to  $\log_{10}(M_{\text{bin}}/M_{\odot}) = 0.5$  dex. This is done according to the formalism of [van den Bosch et al. \(2014\)](#) as already mentioned. If 'no' then it will assign a single stochastic mass accretion assembly derived from the methodology of [Hearin et al. \(2021\)](#). In order to fulfill the purpose of this project the decision made is to use mean tracks, hence 'yes' option. I anticipate that a part of Chapter 7 will be devoted to a possible application of the second method, with a brief explanation of the code `diffmah` involved. It is built so to give the possibility of choosing which type of halo to generate, if of early or late type (distinction made clearer later on in that occasion);
- `M_sub_res = 1e-3`  
It gives the subhalos mass resolution. For a subhalo mass resolution set to  $f_{\text{res}}$ , the code will generate subhalos with masses higher than  $f_{\text{res}}M_{\text{h,par}}$ ;
- `max_order = 1`  
It specifies the maximum order of subhalos the program generates. As said several times in Chapter 2 I am going not to consider the contribution of subhalos of orders higher than one because black hole masses that will be derived from them have negligible contribution to the total mean merging mass;
- `use_merger_tree = no`  
This parameter gives the choice between a full merger tree and a statistical approach. Since the scope of using such a model is to keep a statistical-empirical approach, then the default option is set to 'no';
- `type_orbital_circularity = constant`  
`orbital_circularity = 0.5`  
`fudge = -1`  
This last set of parameters is needed to calculate the subhalos merging timescale as described in Subsection 2.2.4, using [McCavana et al. \(2012\)](#) fitting parameters. The first voice, `type_orbital_circularity`, specifies if one wants to extract the orbital circularity from a Gaussian distribution or let it to be a constant (0.5 in this case). As showed in Figure 2.3, a fudge factor correction is applied so to adapt

merging timescale to N-body simulations and semi-analytical works. If set `fudge` to a negative value the program apply the linear correction that depends on the progenitor/subhalo mass ratio, see Equation 2.4.

In fact such merging timescales are calculated for galaxy mergers, and in most of the work presented here they are not taken into account. The introduction of a  $t_{\text{merg}}$  is instead considered in a second moment to adjust results regarding high massive black holes. For such supermassive black holes, with final masses above  $10^9 M_{\odot}$ , merger contribution becomes very important at low redshift and that would create some problems if not limiting the amount of mergers in some way (see Section 6.2).

### 3.1.2 Running the code

Now that all the parameters have been defined it is possible to analyse what a run of DECODE produces. Figure 3.1 displays the distribution of parent halo log-masses generated, with a bin size of the order of  $\Delta \log_{10}(M_{\text{h,par}}/M_{\odot}) = 0.1$  dex. Superimposed there is the halo mass function of Tinker et al. (2008) (red dashed line) from which halos are extracted to build the catalogue. This is done to prove the correct behaviour of the program and to have an idea of the completeness of the sample so obtained. The mass function is indeed well represented by the parent halos available, with the only exception represented by the high mass end, where the sample is poor ( $N_{\text{h,par}} \approx 10 - 20$  objects). Masses that are actually considered when reconstructing SMBH histories are at most of the order of  $\sim 10^{14} M_{\odot}$  and up to there the number of halos created is enough to have good statistics.

For each halo in the local catalogue the model reconstruct the merger history (Sections 2.2.2 -2.2.4) but what is the real information of DECODE, as already mentioned during the description of the model, is the mean mass that is gained by mergers. I will define here the simple and general procedure to follow, applied to halos at this stage and repeated in an analogous way for black holes later on in the project. The main steps are:

- i) Select a bin of mass, e.g. halos between  $\log_{10}(M_{\text{h,par}}) = 12.5$  dex and  $\log_{10}(M_{\text{h,par}}) = 12.6$  dex;
- ii) Randomly extract 50/60 parent halos within that bin (such numbers of objects consist of good compromise between speed of calculation and right quantity to produce smooth mean merger curves);
- iii) For each of them compute the cumulative mass accretion through mergers. From now on and if not otherwise specified merger histories computed are the *maximal* ones. How?
- iv) Take all subhalos related to a main progenitor and the corresponding redshift at first accretion,  $z_{\text{inf}}$ ;
- v) Consider a redshift interval of interest, e.g.  $z = [0, 4]$  in step of  $dz = 0.1$ ;
- vi) For every  $z$ -step sum masses of all subhalos with  $z_{\text{inf}} \geq z$ ;

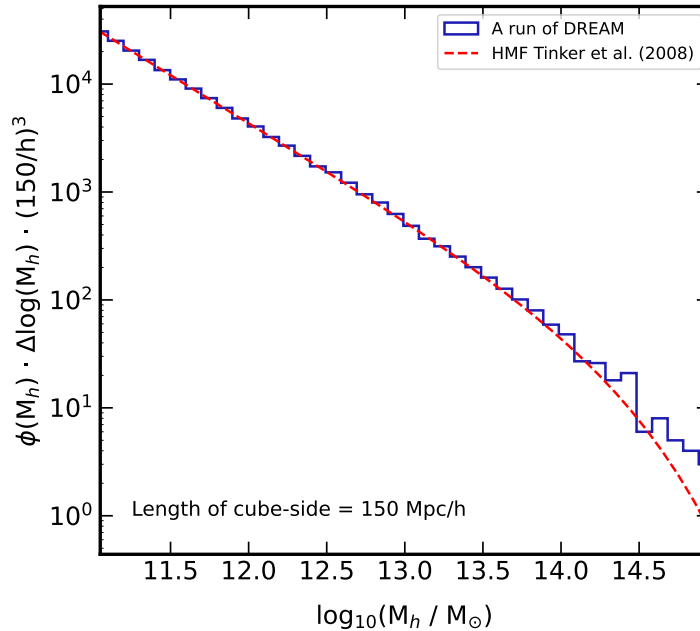


Figure 3.1: Hist plot representing the mass distribution of parent halos in the catalogue generated with input parameters in 3.1.1. Masses are in logarithmic units and binned in  $\Delta \log_{10}(M_{h,\text{par}}/M_{\odot}) = 0.1$  dex. Red dashed line is the analytic halo mass function of Tinker et al. (2008) used to extract the catalogue, multiplied by the size of the bin and the physical volume of the simulation =  $(150/h)^3$  Mpc<sup>3</sup>.

- vii) Once individual histories are obtained compute their mean,  $\langle M_{h,\text{merg}}(z) \rangle$ , and the error of the mean,  $\sigma_{\text{merg}}(z)$ .

To evaluate how much is the mass acquired through mergers compared to the total growth of a dark matter halo, I explicitly calculate these mean global accretion tracks following van den Bosch et al. (2014). For each bin of mass, the central value is chosen to be the final mass of the parent halo from which its past history is built. The function that works it out is already implemented in DECODE and it is sufficient to give as arguments the final mass and redshift interval,  $z$ -steps, selected. The curves so obtained can be visualized in Figure 3.2, where log-masses selected are within  $\log_{10}M_{h,\text{par}}(z=0) = 11.05$  dex and  $\log_{10}M_{h,\text{par}}(z=0) = 13.95$  dex. Finally all pieces of information achieved up to now are summarized in Figure 3.3. It includes the mean total accretion track of a dark matter halo with final mass  $\approx 10^{12.55} M_{\odot}$ , represented by the thick red curve, the cumulative merger histories of sixty halos selected in the mass bin bordered by  $\log_{10}(M_{h,\text{par}}) = 12.5$  dex and  $\log_{10}(M_{h,\text{par}}) = 12.6$  dex (gray thin lines), and the mean merger history obtained from them which is the thick blue curve. Errors are not visualized in order to keep clean the figure.

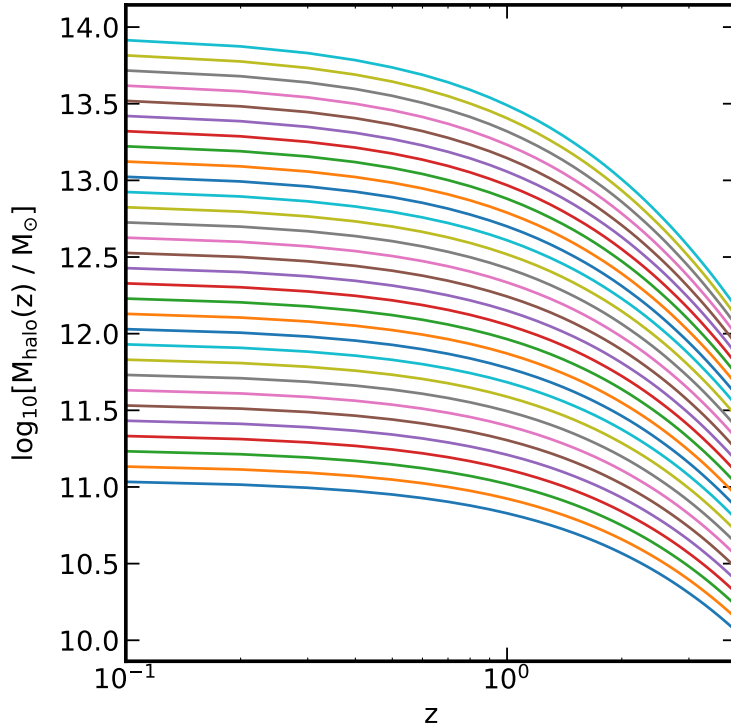


Figure 3.2: Total mean accretion histories of parent halos computed implementing the methodology in [van den Bosch et al. \(2014\)](#). The curves are reconstructed up to a  $z = 4$ , and for halos of final masses within the range  $[11.05, 13.95]$  in logarithmic units and with steps of  $\Delta \log_{10}(M_{h,\text{par}}/M_{\odot}) = 0.1$  dex.

### 3.2 From halo mass to stellar mass

The aim of this work is to reproduce curves similar to the one showed in [Figure 3.3](#) for black holes. This comes with the necessity to perform the intermediate and fundamental step consisting in the conversion of halo masses in masses of galaxies (stellar mass) growing within them. As explained in [Chapter 2](#), in particular in [Section 2.3](#), this passage is what makes DECODE truly a semi-empirical model. For what concerns which SMHM relation to use, the two possibilities introduced in [Section 2.3.1](#) are the ones I am going to apply. The choice made is in agreement with the work that presents DECODE as new model ([Fu et al. \(in preparation\)](#)). In there the authors analyzed different shapes of SMHM relation, evaluated starting from varying stellar mass functions or methods found in literature (e.g. [Baldry et al. \(2012\)](#); [Tomczak et al. \(2014\)](#); [Bernardi et al. \(2017\)](#); [Davidzon et al. \(2017\)](#); [Moster et al. \(2018\)](#); [Behroozi et al. \(2019\)](#); [Grylls et al. \(2020\)](#); [Leja et al. \(2020\)](#)), and compare results on galaxy formation and evolution (in particular merger rates, abundances of satellite galaxies, morphology of central galaxies and bulge-to-total ratios) with observational data and/or other cosmological simulations. They actually opt for a model made in this way:

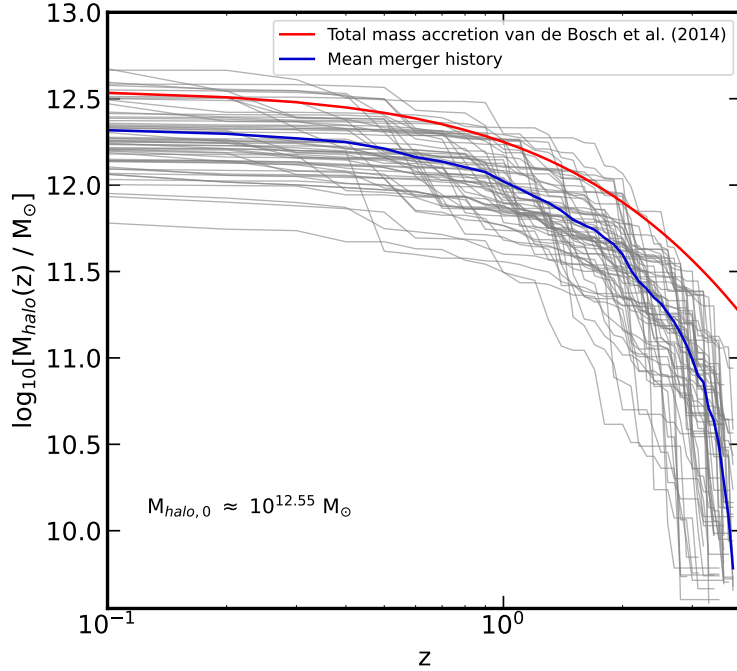


Figure 3.3: Total mean accretion track (red line) from [van den Bosch et al. \(2014\)](#); cumulative merger histories of sixty halos of final masses within  $\log_{10}M_{h,\text{par}} = 12.5 - 12.6$  dex (gray lines); mean merger history (blue line).

- SMF at  $z = 0$  adopted is the one from [Bernardi et al. \(2017\)](#), valid down to  $M_{\star} \sim 10^9 M_{\odot}$ ;
- At  $z > 0$  SMF is made to evolve consistently with the [Tomczak et al. \(2014\)](#) SMFs obtained between  $0 < z < 3$  (see Section 2.3.1);
- The correction made to the [Bernardi et al. \(2017\)](#) + [Baldry et al. \(2012\)](#) SMF at  $z = 0$  in order to apply [Tomczak et al. \(2014\)](#) evolution is given by:

$$\log_{10}\phi(M_{\star}(z)) \simeq (0.99 + 0.13z) \cdot \log_{10}\phi(M_{\star}(z = 0.1)). \quad (3.1)$$

Since SMF of this kind is close to SMFs obtained by the code EMERGE of [Moster et al. \(2018\)](#) at low redshift, it is interesting to observe how much results are effected by the choice of using one or another. In Figure 3.4 one can visualize the differences in SMFs with redshift evolution. The curves labelled as Model 2 are the SMFs( $z$ ) just described and considered as the reference model (RM) also in this project. They fit well data from [Tomczak et al. \(2014\)](#), as it is possible to note, with slightly deeper redshift evolution at low-mass end. As a general trend it appears that the SMFs modelled in [Moster et al. \(2018\)](#) have a milder  $z$  evolution at nearly all stellar log-masses than both [Tomczak et al. \(2014\)](#) data points and the reference model. About what concerns SMHM relations,

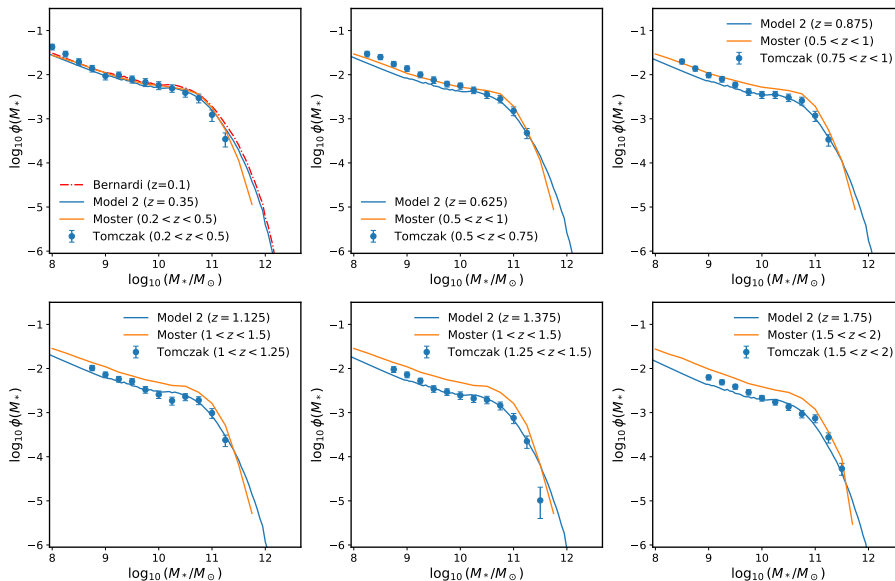


Figure 3.4: Comparison between SMFs by Tomczak et al. (2014) data (blue points), Moster et al. (2018) model (orange line) and Model of reference (blue line) in Fu et al. (in preparation) at six redshift intervals. Reference model well represents Tomczak et al. (2014) SMFs at any time steps, with small deviations at low stellar masses. Moster et al. (2018) modelled SMFs on the other hand differ to the ones of reference model and to Tomczak et al. (2014) data at higher  $z$ .

diversity among the realizations above-cited can be well visualized in Figure 3.5. The model of reference (RM), that is the one used in this work, is reproduced by the blue curve and the shaded region marks how the relation has changed through time up to a  $z = 4$ . Relation extrapolated from Moster et al. (2018) (Mo18), on the other hand, is defined by the red line, and again shaded region considers the evolution of the relation in  $z$ . At first glance it can be noticed the fact that, at least for DM halo masses  $\gtrsim 10^{11.8} M_{\odot}$ , in the case of the RM the relation is subjected to a broader change in time, while in Mo18 such a change is more limited. This is a consequence of what said above about the corresponding stellar mass functions. Another aspect to be pointed out is that in both cases one can perceive a variation in the slope of the relation; variation that is more accentuated in the case of the RM. This happens approximately at a characteristic mass of  $M_{\star} \sim 10^{10.1} - 10^{10.3} M_{\odot}$  and this will be reflected in the conversion of black hole masses. In that context interesting features will happen at an approximate characteristic mass of  $M_{\text{BH}} \sim 10^8 M_{\odot}$ . Real discordance between the two models characterizes the low-mass end. Actually at these mass ranges the RM has a lower and steeper trend (slope of the order of 2.3 - 2.4 with a normalization of  $\sim 7.3$  dex in  $\log_{10}(M_{\star}/M_{\odot})$ ) than Mo18 (slope of the order of  $\sim 1.55$  with a normalization of  $\sim 8.3 - 8.4$  dex in  $\log_{10}(M_{\star}/M_{\odot})$ ) at every epochs. It means that, at a fixed halo-mass, the RM produces a smaller stellar mass

and with a faster evolution (in the redshift range considered). This has non negligible consequences for what will be the behaviour of growing supermassive black halos. The situation is more comparable at the high mass end, at least at low redshift where curves (see Figure 3.5) can be approximated by a straight line of slope  $\sim 0.65$  and a normalization of  $\sim 9.5$  dex in log-stellar masses. It is important to underline the fact that all values reported in this last part are estimates, not fits of the curves; it is just to give orders of magnitude and errors are not considered. At higher redshift RM and Mo18 are again not in agreement at high mass end where the first becomes more and more steep backwards in time. This fact implies that accretion curves derived from RM are slightly less flat towards present times. Figure 3.6 helps to better understand and visualize how results

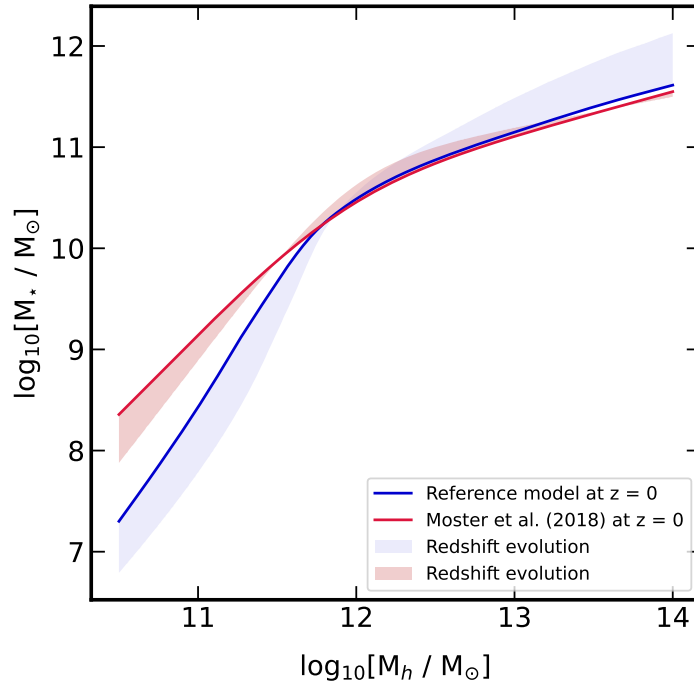


Figure 3.5: Stellar mass - halo mass relations derived from observational data combination of Baldry et al. (2012) + Bernardi et al. (2017) + Tomczak et al. (2014) (blue line and blue shaded area) and from Moster et al. (2018) empirical model (red line and red shaded area). Straight lines are referred to local ( $z = 0$ ) relations, while shaded areas consider redshift evolution up to  $z = 4$ . All masses are expressed in logarithmic units.

can differ case by case depending on which of the two relations is applied. Left panel is representative of the low-mass end situation since galaxies are seeded in a halo of final mass of the order of  $M_{h,fin} = 10^{12} M_{\odot}$ , hence at approximately the correspondence of the change in slopes of the SMHM relations. Right panel, instead, shows what happens if masses are converted starting from a dark matter halo with high final mass of  $M_{h,fin} =$

$10^{14} M_{\odot}$ . In this latter case the mass evolution of galaxies is almost all confined within the high-mass range, since masses at  $z \approx 4$  are of the order of  $M_{\star}(z = 4) \sim 10^{11} M_{\odot}$ . As

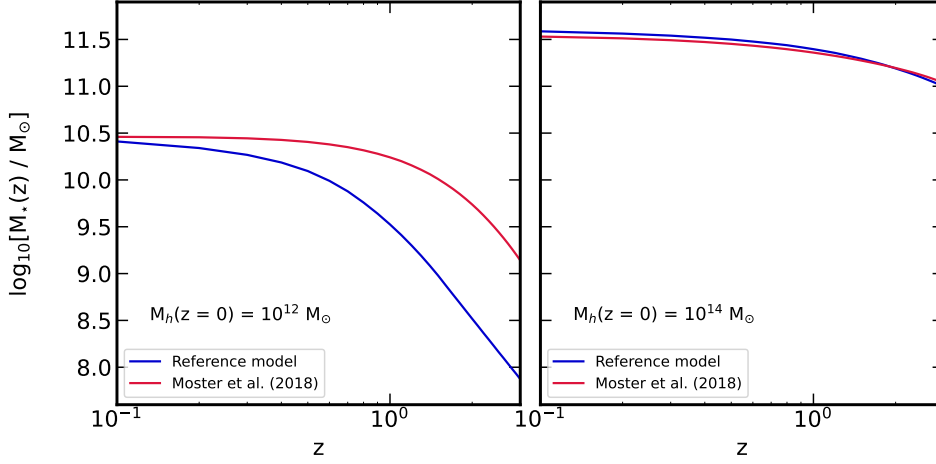


Figure 3.6: Galaxy evolution derived from the conversion of  $M_{\text{halo}}(z)$  (by van den Bosch et al. (2014)) at each redshift using either the RM and Mo18 relations. Left: curves are built starting from a DM halo with final mass of  $M_{\text{halo}}(0) = 10^{12} M_{\odot}$  (to investigate low-mass end of SMHM relations); Right: analogous but with the final mass of DM halo of  $M_{\text{halo}}(0) = 10^{14} M_{\odot}$  (to investigate high-mass end of SMHM relations). Blue lines are always related to the RM relation while blue curves to Mo18 relation.

expected much more profound deviations concern the low-mass end, where galaxy growth predicted by the RM is always 'behind' the one computed using Mo18. Similar trends are on the contrary found when accretion path regards especially high masses with only the exception that curves made from Mo18 flattens toward recent epochs as a consequence of very little evolution of the Moster et al. (2018) SMHM relation at high-mass end.

## Chapter 4

# Main: SMBH application I

This Chapter presents the main and truly original part of the thesis project and it is entirely devoted to the study of supermassive black holes accretion. The final purpose is twofold:

- 1) From one side it is to validate `DECODE` as an efficient, self-consistent and reliable model through the presentation of a new application of it;
- 2) From the other side it is to infer possible constraints on i) black hole mass - stellar mass relation, using an approach that allows to assign a temporal dimension to it; ii) black hole accretion curves, or in other words curves that describe the growth of a BH through infalling gas and strictly related to AGN light curves; iii) the black hole merger rates, more specifically the merger contribution to the evolution of a SMBH.

The interconnection between them is represented, as already stated, by scaling relations that have been known to subsist between SMBH mass and many properties of the hosting galaxies such as the luminosity ( $L_{\text{host}}$ ), stellar mass ( $M_{\star}$ ) and stellar velocity dispersion ( $\sigma_{\star}$ ). The tightness of these correlations may imply a connection between nuclear activity and galaxy formation and evolution (e.g. [Magorrian et al. \(1998\)](#); [Ferrarese & Merritt \(2000\)](#); [Gebhardt et al. \(2000\)](#); [Marconi & Hunt \(2003\)](#); [Haring & Rix \(2004\)](#); [Gultekin et al. \(2009\)](#); [Graham et al. \(2011\)](#); [Beifiori et al. \(2012\)](#)). Actually, the physical mechanism that is responsible for such tight relations is not yet well understood, mainly because of the huge diversity in scales under consideration: the dynamical sphere of the SMBHs ( $\sim \text{pc}$ ) and the dimensions of their hosts ( $\sim 10 \text{ kpc}$ ). A quite popular explanation invokes active galactic nucleus (AGN) feedback as the possible physical connection (see e.g. [Matteo et al. \(2008\)](#); [Hopkins et al. \(2008\)](#); [DeGraf et al. \(2015\)](#)). Other studies are based on the hypothesis that accretion of SMBHs and star formation in galaxies are fed by a common gas supply (e.g. [Cen \(2015\)](#); [Menci et al. \(2016\)](#)). Finally there are authors stating that there is no need of a physical coupling, since statistical convergence from galaxy assembly alone (i.e. mergers) may reproduced the observed correlations (e.g. [Hirschmann et al. \(2010\)](#); [Jahnke & Macciò \(2011\)](#)).

It is at this point evident why it becomes important to study these scaling relations as a function of redshift, determining how and when they emerge and evolve over cosmic

time (e.g. [Schramm & Silverman \(2013\)](#); [Sun et al. \(2015\)](#)). Addressing this task from an observational point of view is still not easy because of many problems that arise when taking measurements at high redshift, that especially are conducted on AGNs (far more luminous and with accessible measurements of SMBH masses). First of all one has to deal with the uncertainties in black hole mass estimates that rely on gas dynamics; secondly also measuring host galaxy properties can be challenging because of the overwhelming nuclear light; finally it has not to be underestimated the effect of the selection function when interpreting data (e.g. [Lauer et al. \(2007b\)](#); [Treu et al. \(2007\)](#)).

In this work the line of reasoning is the following:

- Observational data used to calibrate local scaling relations ( $z = 0$ ) are collected from different literature works;
- Due to the variations of technical methods implied, samples of objects selected and encountered problems in observational campaigns, these data do not represent a homogeneous group. The reason for accumulating some of them is to have a guide line in the choosing of shapes for scaling relations to adopt;
- Once a specific relation is arbitrarily set up, in a first moment it is assumed not to evolve with  $z$  and to be maintained up to epochs of  $z \approx 4$ . It is a strong assumption in consideration of what just written about difficulties in high redshift measurements.

In a second moment, there will be the possibility to allow for a mild  $z$  - evolution in the scaling relations of the form  $(1 + z)^\alpha$  (see Section 6.1.1).

- Finally the relation chosen is applied to results of growing galaxies (alias DM halo once given the SMHM relation) following analogous steps explained in Section 3.1.2;
- What is obtained, i.e. accretion curves of supermassive black holes, is then compared to gas-accretion curves derived by the employment of the continuity equation through the formalism and methods proposed in [Marconi et al. \(2004\)](#) and [Shankar et al. \(2009\)](#). Since those curves represent the ending and, in a certain sense, the starting point for the project developed here, the analysis made in the above-mentioned works is explained in more detail in Section 4.1;
- It is through this comparison, in particular with accretion curves found in [Shankar et al. \(2009\)](#), that some considerations can be made about the shapes of scaling relations.

Once having defined the evolutionary model of [Shankar et al. \(2009\)](#) (S09), I will analyse the way to build the results to compare, which scaling relations are chosen and why others are discarded. To be clear scaling relations that enter in this work are the  $M_{\text{BH}} - M_\star$  relation (this Chapter) and the  $M_{\text{BH}} - \sigma$  relation (Chapter 5).

## 4.1 SMBH evolutionary model

Since the discovery of quasars ([Schmidt \(1963\)](#)), it has been suggested that active galactic nuclei (AGN) are powered by mass accretion onto supermassive black holes (e.g.

Salpeter (1964); Lynden-Bell (1969); Rees (1984)), and the presence of remnant BHs in the spheroids of galaxies in the local universe (Richstone et al. (1998)) strongly supports the hypothesis. This scenario has consequently opened the road to the study of the correlated evolution of quasar and black hole populations. Again scaling relations discussed above play a key role in this framework because they make it possible to estimate the local mass function of black holes (Salucci et al. (1999); Yu & Tremaine (2002); Marconi et al. (2004); Shankar et al. (2004)). At this point the principal link is made between the integrated emissivity of the quasar population, the integrated mass density of remnant black holes, and the average radiative efficiency of black hole accretion (e.g. Soltan (1982), Fabian & Iwasawa (1999); Elvis et al. (2002)). Essentially given assumed values of the radiative efficiency and the Eddington ratio  $L/L_{\text{Edd}}$ , the observed luminosity function of quasars at different redshift can be connected to the mean growth rate of black holes of the corresponding mass. Once growth rates are obtained they can be integrated forward in time and track the evolution of the black hole mass function. I report below the formalism behind each passage and I am going to specify the assumptions made in Shankar et al. (2009) to reconstruct final BH accretion curves.

#### 4.1.1 AGN bolometric luminosity function

It is important to derive with accuracy the shape of the AGN luminosity function at single redshift step,  $\phi(L, z)$ , with  $L$  the bolometric luminosity. This is not immediate because usually observations are made at specific bands and then bolometric corrections are applied. It can be that these corrections are  $z$ -dependent or that they are in some measure related to the intrinsic luminosity of the object (e.g. Marconi et al. (2004); Richards et al. (2006); Hopkins et al. (2007a)). Another difficulty in the determination of a complete sample of AGN population is obscuration of the central engine made by dense gas and dust residing in a torus surrounding the growing BHs or in the interstellar medium of the host (e.g. Rigby et al. (2006)).

Shankar et al. (2009) base their calculations on the bolometric LF estimated in the work of Ueda et al. (2003) (see Chapter 1), where a vast sample of AGNs from *Chandra*, *ASCA*, *HEAO-1* surveys is considered along with absorption-corrected LF out to  $z \sim 3$ . The bolometric correction adopted is the one of Marconi et al. (2004) with the inclusion of a dispersion of 0.2 dex. The model of the AGN LF derived in Shankar et al. (2009) is shown in Figure 4.1 compared to a large collection of data from optical surveys (Pei (1995); Wisotzki (1999); Fan et al. (2001); Fan et al. (2004); Kennefick et al. (1995); Hunt et al. (2004); Wolf et al. (2003); Richards et al. (2005); Richards et al. (2006); Jiang et al. (2006); Cool et al. (2006); Bongiorno et al. (2007); Fontanot et al. (2007); Shankar & Mathur (2007)) and X-ray surveys (Barger et al. (2003); Ueda et al. (2003); Barger & Cowie (2005); Barger et al. (2005); Franca et al. (2005); Nandra et al. (2005); Silverman et al. (2008)) once converted into bolometric quantities and corrected for obscuration following Hopkins et al. (2007a).

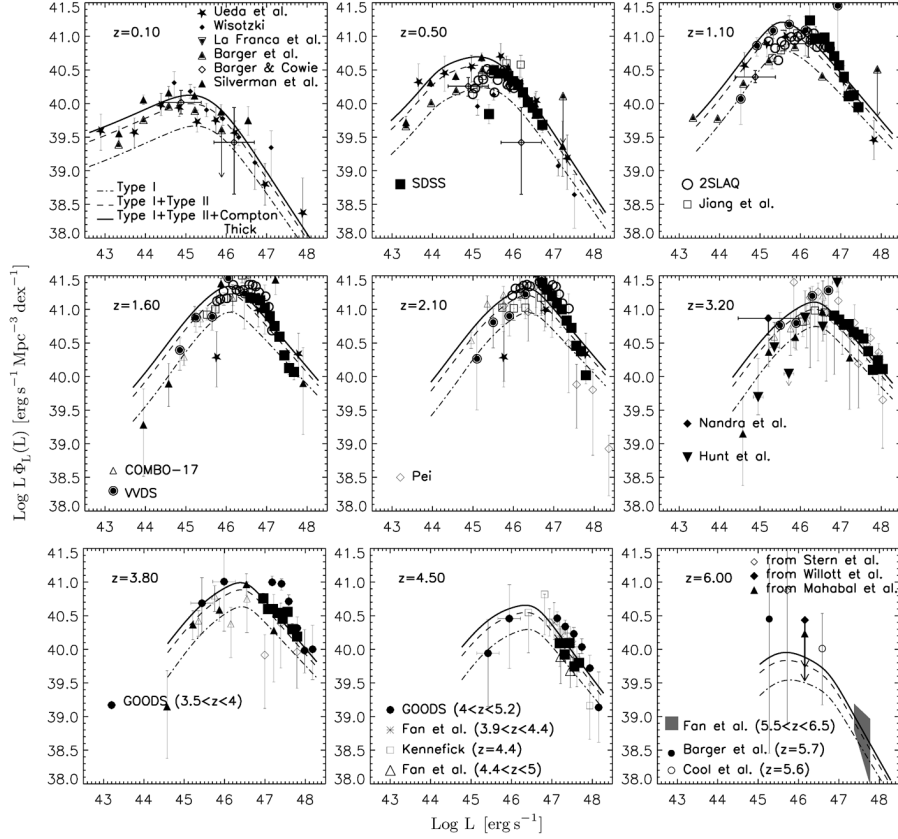


Figure 4.1: Bolometric AGN LF. Curves represent the model of Shankar et al. (2009), with solid line the total LF including very Compton-thick sources; short-dashed line includes sources with column densities up to  $\log N_{\text{H}}/\text{cm}^{-2} = 24$ ; dot-dashed line considers only sources with  $\log N_{\text{H}}/\text{cm}^{-2} \leq 22$ . Symbols are all data from optical and X-ray surveys reported in Section 4.1.1.

#### 4.1.2 Local black hole mass function

The principal observational constraint in models set up in Marconi et al. (2004) and Shankar et al. (2009) is represented by the local black hole mass function (BHMF). As I mentioned before, local  $\phi(M_{\text{BH}})$  can be determined through the use of scaling relations, especially between  $M_{\text{BH}}$  and stellar velocity dispersion,  $\sigma_*$  ( $\text{km s}^{-1}$ ), and  $M_{\text{BH}}$  - bulge luminosity,  $L_{\text{bulge}}$  ( $\text{erg s}^{-1}$ ), relations, applied to known galaxy luminosity and velocity dispersion functions (e.g. Nakamura et al. (2003); Sheth et al. (2003)). Figure 4.2 from Shankar et al. (2009) illustrates the local mass functions resulted from different relations between black hole mass and host galaxy properties. The solid line represents the result obtained using the  $M_{\text{BH}}$  -  $L_{\text{sph}}$  relation calibrated in McLure & Dunlop (2002), while solid squares the one found in Shankar et al. (2004). Other curves are evaluated with the application of  $M_{\text{BH}}$  -  $\sigma_*$  relation, for example the short-dashed line, gained from the relation of Tundo et al. (2007), the dot-dashed line from Marconi et al. (2004) and triple-dot dashed line from the one calibrated in Ferrarese & Ford (2005). The picture

also shows other estimates of the local BHMF, e.g. combining the galaxy baryonic mass function of [Bell et al. \(2003\)](#) with the relation between black hole mass and spheroid stellar mass of [Haring & Rix \(2004\)](#) (star symbols); and other two BHMFs, represented by the dotted curve and open circles, are the one derived in [Hopkins et al. \(2007b\)](#) and [Graham et al. \(2007\)](#) respectively. These two latter cases appear to be not consistent with other results. In [Shankar et al. \(2009\)](#) they adopt the gray band in Figure 4.2 as representative of the mean and the systematic uncertainties of estimates of the local mass function.

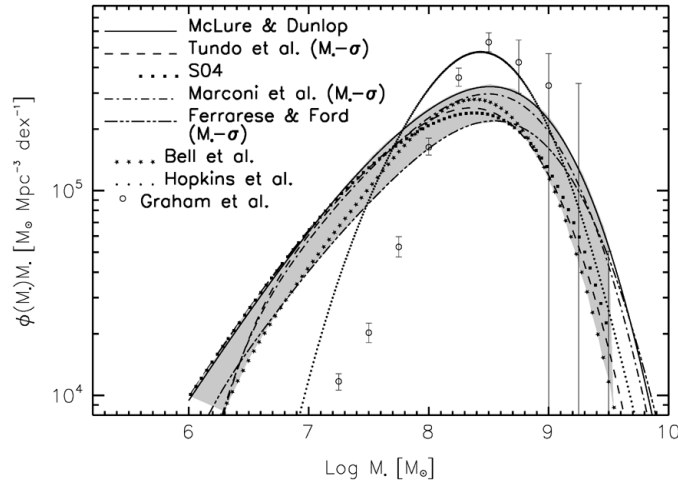


Figure 4.2: Local black hole mass function obtained from various calibrations of the  $M_{\text{BH}} - L_{\text{sph}}$ ,  $M_{\text{BH}} - \sigma_*$  or  $M_{\text{BH}} - M_*$  relations, assuming intrinsic scatter of 0.3 dex in all cases. Gray region is inclusive of all these estimates. Dotted curve is the local black hole mass function derived by [Hopkins et al. \(2007b\)](#) using the black hole fundamental plane and open circles represent the BHM-function from [Graham et al. \(2007\)](#) obtained using the relation between black hole mass and Sérsic index.

### 4.1.3 Evolved black hole mass function

The next step is to evaluate the evolution of the black hole mass function implied by the AGN bolometric functions described in 4.1.1. The formalism I will use is the one of [Shankar et al. \(2009\)](#). The expression  $\phi(X)$  will indicate mass and luminosity functions in logarithmic units, i.e.  $\phi(X) = n(X) \cdot X \cdot \ln(10)$ , where  $n(X)dX$  is the comoving space density of black holes in the mass or luminosity range  $X \rightarrow X + dX$  in  $\text{Mpc}^{-3}$ . The Eddington accretion rate is defined as:

$$\dot{M}_{\text{Edd}} \equiv \frac{L_{\text{Edd}}}{0.1c^2} \simeq 22 \left( \frac{M_{\text{BH}}}{10^9 M_{\odot}} \right) M_{\odot} \text{yr}^{-1} \quad (4.1)$$

with  $L_{\text{Edd}}$  the standard Eddington luminosity evaluated with Thomson scattering opacity and pure hydrogen composition at mass  $M_{\text{BH}}$ . The dimensionless accretion rate is given

by:

$$\dot{m} = \dot{M}_{\text{BH}}/\dot{M}_{\text{Edd}}. \quad (4.2)$$

The black hole growth rate is related to the large scale accretion rate by:

$\dot{M}_{\text{BH}} = (1 - \epsilon)\dot{M}_{\text{inflow}}$ , where  $L = \epsilon\dot{M}_{\text{inflow}}c^2$ , with  $\epsilon$  the radiative efficiency. It means a fraction  $\epsilon$  of in-falling mass is radiated away before entering the black hole. Defining  $f = \epsilon/(1 - \epsilon)$  and  $f_{0.1} = f/0.1$ , the relation connecting the bolometric AGN luminosity,  $L$ , and the mass of black hole,  $M_{\text{BH}}$ , growing at a dimensionless  $\dot{m}$  is written as:

$$L = \epsilon\dot{M}_{\text{inflow}}c^2 = 0.1f_{0.1}\dot{M}_{\text{BH}}c^2 = f_{0.1}\dot{m}lM_{\text{BH}}, \quad (4.3)$$

and  $l \equiv L_{\text{Edd}}/M_{\text{BH}} = 1.26 \times 10^{38} \text{ erg s}^{-1} M_{\odot}^{-1}$ . Since Eddington accretion  $\dot{M}_{\text{Edd}}$  is associated to a  $f = 0.1$ , then the Eddington luminosity is  $L_{\text{Edd}} = lM_{\text{BH}}$  and the link between the Eddington ratio  $\lambda = L/L_{\text{Edd}}$  and the accretion rate  $\dot{m}$  is given by:

$$\lambda \equiv \frac{L}{L_{\text{Edd}}} = \dot{m}f_{0.1}. \quad (4.4)$$

If a black hole grows at constant rate  $\dot{m}$ , then it evolves exponentially with a time-scale of  $t_{\text{grow}} = M_{\text{BH}}/\dot{M}_{\text{BH}} = t_s/\dot{m} = 4.5 \times 10^7 \text{ yr}$ , with  $t_s$  equal to the [Salpeter \(1964\)](#) timescale for  $f_{0.1} = 1$ .

The black hole mass function,  $n(M_{\text{BH}}, t)$ , evolves according to a continuity equation (see [Cavaliere et al. \(1971\)](#); [Small & Blandford \(1992\)](#))

$$\frac{\partial n}{\partial t}(M_{\text{BH}}, t) = -\frac{\partial(M_{\text{BH}}\langle\dot{m}\rangle n(M_{\text{BH}}, t))}{\partial M_{\text{BH}}t_s}, \quad (4.5)$$

with  $\langle\dot{m}\rangle$  is the dimensionless accretion rate average over the active and inactive population of black holes of mass  $M_{\text{BH}}$  at time  $t$ . Models proposed both in [Marconi et al. \(2004\)](#) and [Shankar et al. \(2009\)](#) assume constant accretion rates  $\dot{m} = \dot{m}_0$ , meaning that at any given time a black hole is either accreting at  $\dot{m}_0$  or not accreting. It is evident that adopting a single  $\dot{m}$  gives approximated results, especially for low-luminosity AGNs in the nearby universe with diverse values of Eddington ratios (e.g. [Heckman et al. \(2004\)](#); [Greene & Ho \(2006\)](#)). Nevertheless it constitutes a good starting point for the study of black hole growth. With a constant  $\dot{m}_0$ , the probability that a BH of mass  $M_{\text{BH}}$  is active or not, defined as the duty cycle  $P_0$ , is simply given by the ratio of luminosity and mass functions:

$$P_0(M_{\text{BH}}, z) = \frac{\phi(L, z) \left| \frac{d \log L}{d \log M_{\text{BH}}} \right|}{\phi(M_{\text{BH}}, z)} \leq 1. \quad (4.6)$$

As said before the mass  $M_{\text{BH}}$  and luminosity  $L$  conversion is:  $M_{\text{BH}} = L/(f_{0.1}\dot{m}_0l)$ . If also  $\epsilon$  is constant, then we have a relation of proportionality  $M_{\text{BH}} \propto L$ . The inequality in Equation 4.6 is necessary in order to have a physically consistent model.

## The algorithm

Here below I describe the method employed in [Shankar et al. \(2009\)](#) to retrieve BHMF evolution.

- A black hole mass function is assumed at initial redshift  $z_i$ :  $n(M_{\text{BH}}, z_i)$ ;
- Equation 4.5 is used to get characteristic curves  $M_{\text{BH}}(M_{\text{BH},i}, z)$ ;
- Logarithmic spaced values of  $M_{\text{BH},i}$  are defined and the integration forward in time is performed with a mid-point scheme from redshift step  $z_j$  to  $z_j - \Delta z$ :

$$M_{\text{BH},j+1} = M_{\text{BH},j} + \dot{m}_0 P_0(M_{\text{BH},j+1/2}, z_{j+1/2}) M_{\text{BH},j+1/2} \frac{dt}{dz t_s} \Delta z, \quad (4.7)$$

The values at mid-point  $j + 1/2$  are obtained by the extrapolation of the black hole mass at  $\Delta z/2$  using  $dM_{\text{BH}}/dt$  at the beginning of the step and the duty cycle  $P_0$  is computed with the mid-step mass function and the luminosity function evaluated at  $z_{j+1/2}$ ,

- The number of black holes is conserved, so  $n(M_{\text{BH}}, z) \Delta M_{\text{BH}} = n(M_{\text{BH},i}, z_i) \Delta M_{\text{BH},i}$ .

Basically all this procedure just depends on initial conditions, observed luminosity function and the values of  $\dot{m}_0$  and  $f_{0.1} = L/(M_{\text{BH}} \dot{m}_0)$  assumed.

Initial redshift considered is  $z_i = 6$ , and  $n(M_{\text{BH},i}, z_i)$  is evaluated from Equation 4.6 using the luminosity function at  $z = 6$  and an assumed  $P_0 = 0.5$ . A good overall agreement with the average estimate of the local black hole mass function is obtained setting the following parameters:

$$\dot{m}_0 = 0.60, \quad \epsilon = 0.065 \quad (f_{0.1} \sim 0.7). \quad (4.8)$$

Figure 4.3 shows the average accretion histories for black holes of different relic mass  $M_{\text{BH}}$  at  $z = 0$  as a function of redshift, obtained applying the reference model just described. It has to be pointed out that the derivation of tracks for lower BH final masses needs the extrapolation of luminosity functions at the very faint end using a power law fit, since no objects can be observed at such luminosities. Those are the accretion curves I am going to refer to when I will make the comparison between results of this work and the model for the growth of a supermassive black hole.

## 4.2 Building accretion curves: $M_{\text{BH}} - M_{\star}$ relation

In this Section I finally expose the method to reconstruct accretion curves illustrating the evolution in mass of supermassive black holes of different types, or in other words of different final masses. I recall that this is done starting from the assumption of a scaling relation that allows to relate, in an unambiguous way, the growing paths resulted from the analysis of DECODE output (see Figures 3.3 and 3.6) to tracks similar to what displayed in Figure 4.3.

In particular, since DECODE actually gives information just on the total mass a galaxy grows within a dark matter halo, the first immediate relation one should imply is the  $M_{\text{BH}} - M_{\star}$  relation, with  $M_{\star}$  the entire mass in stars of the hosting galaxy. In fact this is not the most intrinsically accurate relation, in the sense that observations have pointed out different behaviours depending on the galaxy morphology (see e.g. Davis et al. (2018)

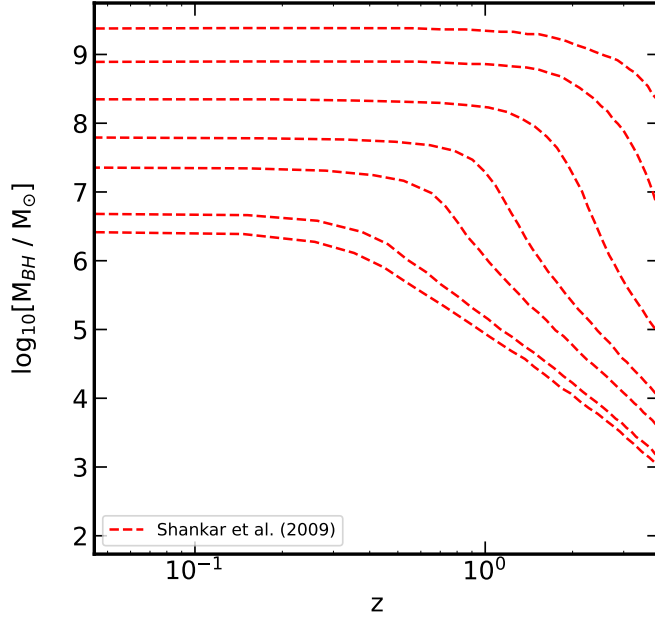


Figure 4.3: Log-mass growth along characteristic curves  $M_{\text{BH}}(M_{\text{BH},i}, z)$  derived in [Shankar et al. \(2009\)](#) through the procedure explained in Section 4.1. The highest redshift value is set to  $z = 4$  in the plot since it is the limiting  $z$  in my future calculation.

and [Sahu et al. \(2019a\)](#)) or on the fact the galaxy is active or not (e.g. [Reines & Volonteri \(2015\)](#)). In addition to that a relation of this type is more affected by selection bias (e.g. [Shankar et al. \(2016\)](#)), because of the prohibitive (in some cases) resolution needed to acquire a reliable black hole mass estimate from observations. Nevertheless many research groups have attempted to calibrate  $M_{\text{BH}} - M_{\star}$  relation, especially because it becomes very useful for observational campaigns at high redshift.

For the purposes of the project I choose not to rely on already calibrated relations and adjust parameters of them so to have good agreement with curves of Figure 4.3. Anyway I also collect sets of data from literature and test at least for coherency between observations and arbitrary chosen relations. An aspect it is important to underline concerns the normalization of these relations. In a certain sense it is less informative, in this context, than the slope because it is degenerate with the radiative efficiency of the curves of the reference model (S09). Since scaling relations are defined in log - log planes, a change in the normalization has the only effect of shifting curves upwards or downwards varying values of black hole masses of a fixed quantity at a given galactic mass. This is also true for variations in the choice of constant radiative efficiency,  $\epsilon$ , to create accretion curves. Indeed changing  $\epsilon$  makes curves in Figure 4.3 just to vertically translate in log-black hole mass.

I proceed presenting the collected data points and the scaling relations I am going to

apply.

### 4.2.1 Data sample and Chosen relations

Data are collected from the works of [Kormendy & Ho \(2013\)](#); [Reines & Volonteri \(2015\)](#); [Davis et al. \(2018\)](#); [Sahu et al. \(2019a\)](#). It does not constitute, and it is not intended to be, a complete selection of objects. Anyway it can be in some measure representative of differences connected to different classes of objects and hence of the difficulties found in having a  $M_{\text{BH}} - M_{\star}$  'all-inclusive'. Data are manifestly scattered (see [Figure 4.4](#)) with high variations in terms of supermassive black hole masses predicted at fixed galactic mass. To better clarify which types of objects I am referring to, a brief description of the data sets is reported below:

- In [Reines & Volonteri \(2015\)](#) authors investigate the relation between BH mass and their host galaxy total stellar mass using a sample made of 262 broad-line active galactic nuclei (AGNs) in the nearby universe ( $z < 0.055$ ). They also add 79 galaxies with dynamical measures of BH masses.

The sample of broad-line AGNs is built through the analysis of the Sloan Digital Sky Survey (SDSS) spectra of nearly 67,000 emission line galaxies in order to find objects with broad  $\text{H}\alpha$  emission, characteristic of dense gas orbiting a massive BH, and also with narrow emission-line ratios that indicate photo-ionization by an accreting massive black hole. The BH masses are estimated through virial techniques (e.g. [Greene & Ho \(2007a\)](#); [Vestergaard & Osmer \(2009\)](#); [Schulze & Wisotzki \(2010\)](#)), based on the assumption that the broad-line region (BLR) kinematics is almost only affected by the gravity of the BH, thus its mass is given by  $M_{\text{BH}} \propto r\Delta V^2/G$ . In particular [Reines & Volonteri \(2015\)](#) use the broad  $\text{H}\alpha$  line following approaches outlined in [Greene & Ho \(2005\)](#) and [Reines et al. \(2013\)](#). Total stellar masses,  $M_{\star}$  are instead obtained using mass-to-light ratios for  $i$ -band data ( $M/L_i$ ) as function of  $g - i$  color ([Zibetti et al. \(2009\)](#)). [Related data points in [Figure 4.4](#) are represented by sky-blue dots]

The authors collect additional objects to complete their work, including dwarf galaxies hosting broad-line AGNs (from [Reines et al. \(2013\)](#); [Baldassare et al. \(2015\)](#); [Thornton et al. \(2008\)](#)); reverberation-mapped AGNs, with BH masses evaluated through the time lag between the continuum flux and broad emission line variability, because it gives the light-travel time across BLR, hence the BLR radius (from the works of [Peterson et al. \(2004\)](#); [Bentz et al. \(2009\)](#); [Denney et al. \(2010\)](#); [Barth et al. \(2011\)](#)); finally galaxies with dynamically detected BHs, that rely on observations capable of spatially resolving the BH sphere of influence (inventory of BH masses from [Kormendy & Ho \(2013\)](#)); [Related data points in [Figure 4.4](#) are represented by orange dots]

- The sample from [Davis et al. \(2018\)](#) is made of 40 spiral galaxies with directly measured SMBH masses via proper motion, stellar dynamics, gaseous dynamics and/or astrophysical maser emission (see also the precedent paper of [Davis et al. \(2017\)](#)). For what concerns the galaxy stellar masses, imaging data are principally retrieved from the *Spitzer* Survey of Stellar Structure in Galaxies ([Sheth et al. \(2010\)](#)), with

central wavelength of  $3.6 \mu\text{m}$ , others from *Hubble Space Telescope* F814W and Two Micron All Sky Survey (2MASS) centered at  $2.2 \mu\text{m}$ . Then masses are calculated applying mass-to-light ratio following Meidt et al. (2014) and accounting for dust emission at  $3.6 \mu\text{m}$ .

The novelty in the work of Davis et al. (2018) is that it has the principal scope of studying late-type galaxies so to provide greater insight into the mutual growth of black holes and galaxies in a more gas-rich environment; [Related data points in Figure 4.4 are represented by green dots.]

- In Sahu et al. (2019a) authors report a data set consisting of 84 early-type galaxies (ETGs) with directly measured black hole masses, expanding the work done in Savorgnan & Graham (2016b). ETGs include elliptical galaxies (E), ellipticals with intermediate stellar disks (ES) and lenticulars (S0). BH masses are measured from direct methods, i.e. modeling of stellar and gas dynamics. Authors prefer to use masses calculated from stellar dynamics because stars are influenced only by gravitational forces, while gas dynamics is also subjected to non-gravitational forces (review of Ferrarese & Ford (2005)). For the galaxy images, the most part are *Spitzer Space Telescope (SST)*  $3.6 \mu\text{m}$  images taken with the Infra-Red Array Camera (IRAC). The remaining ones are Sloan Digital Sky Survey (SDSS) (York et al. (2000))  $r'$ -band images and Two Micron All Sky Survey (2MASS) (Jarrett et al. (2003))  $K_s$ -band images. Then masses are calculated again adopting mass-to-light ratio from Meidt et al. (2014) based on the Chabrier (2003) IMF. [Related data points in Figure 4.4 are represented by purple dots.]

This is the time to introduce scaling-relations I choose to convert  $M_\star$  into  $M_{\text{BH}}$ . I should stress again the fact that such relations do not fit the data collected above. The latter only serve as an indication and for this reason I do not even report errors assigned to them. The idea is indeed trying to find an optimal shape and parametrization of the scaling relations in use, so to produce the best possible concordance between growing curves that will be calculated and the ones predicted by the model of Shankar et al. (2009) (Figure 4.3). In this view, a fit of data would not be the best option because it does not let much space for variability. Actually what is needed is the possibility to test many guesses for parameters, even with small differences between each other, and then to decide what is the most suitable choice. In addition to that it is not said a fit would be really meaningful because, as explained before, the samples of data selected have been derived through different observational campaigns, hence employing different techniques right for the targets addressed to each time. They could be active or inactive galaxies, dwarf or giant ellipticals, ETGs or LTGs and so on. Indeed the data related to them have been treated time by time in a diverse way and even the fits that have been performed on them in the same works above cited are not compatible with each other.

In a first moment I have opted for a log-linear shape to assign to the relation that could be in some agreement with the previously cited works. The parametric form is defined by the following:

$$\log_{10}(M_{\text{BH}}/M_\odot) = \alpha \cdot \log_{10}(M_\star/10^{11}M_\odot) + \beta, \quad (4.9)$$

with  $\alpha$  that indicates the slope of the relation and  $\beta$  the intercept at a normalization of  $M_{\star} = 10^{11} M_{\odot}$ . The values I assigned by eye to  $\alpha$  and  $\beta$  are listed in Table 4.1 and represent an attempt to investigate if a general concordance is achieved between all what I have explained so far. In any literature work that tries to calibrate the  $M_{\text{BH}} -$

	$\alpha$	$\beta$ (dex)
1st	1.00	7.40
2nd	1.25	8.15
3rd	1.50	8.90

Table 4.1: Values chosen for parameters  $\alpha$  (slope) and  $\beta$  (intercept) to be inserted in Equation 4.9. They do not have errors with them because do not represent a fit of data.

$M_{\star}$  relation, when fitting their data authors consider a third parameter which accounts for the intrinsic scatter in the linear relation. Values for this range between  $\sim 0.20$  dex up to  $\sim 0.60$  dex for more scattered samples. Since it is difficult to introduce it when converted  $M_{\star}$  in  $M_{\text{BH}}$  at each redshift-step using one of the proposed relation, I will discuss a possible way to introduce some scatter later on. Figure 4.4 shows the arbitrary selected relations over-plotted to the scatter plot of data collected as explained above. As anticipated, it is evident the dispersion of observational points in the  $\log_{10}M_{\text{BH}} - \log_{10}M_{\star}$  plane. In particular it seems that the population of active galaxies (sky-blue points) stay systematically below data concerning quiescent objects. It is also notable the fact that late type galaxies (green points by Davis et al. (2018)) may be fitted by a steeper relation with respect to the one of early type galaxies (purple points from Sahu et al. (2019a)). Identifying possible reasons for such a behaviour goes beyond the scope of the present project, some suggestion will be given in future chapters.

#### 4.2.2 SMBH growing curves: first results

All steps traced up to now lead to the production of supermassive black holes growing histories. Once having selected a scaling relation, this is assumed to be valid up to redshift  $z = 4$  and the following chain of re-parametrizations is applied:  $M_{\text{halo}}(z) \rightarrow M_{\star}(z)$  (Section 3.2)  $\rightarrow M_{\text{BH}}(z)$ . If not otherwise specified the results presented are obtained using the stellar mass - halo mass (SMHM) relation defined as the reference model (RM) in Section 3.2. In order to construct accretion curves comparable to the ones in Figure 4.3 in a first approximation I use total mean accretion histories of parent halos that are derived through the application of van den Bosch et al. (2014) methodology as explained in Section 3.1.2 and showed in Figure 3.2.

Halo initial masses are made to vary from  $M_{\text{halo}}(0) = 10^{11.55} M_{\odot}$  to  $M_{\text{halo}}(0) = 10^{13.95} M_{\odot}$  and with logarithmic spaced values of step  $\Delta\log_{10}(M_{\text{halo}}/M_{\odot}) = 0.1$  dex. Once the halo masses are defined at each redshift step, they are converted into  $M_{\star}$  according to the given SMHM relation and finally into  $M_{\text{BH}}$  through Equation 4.9 and parameters in Table 4.1. The so-obtained black hole histories in mass do not yet distinguish between

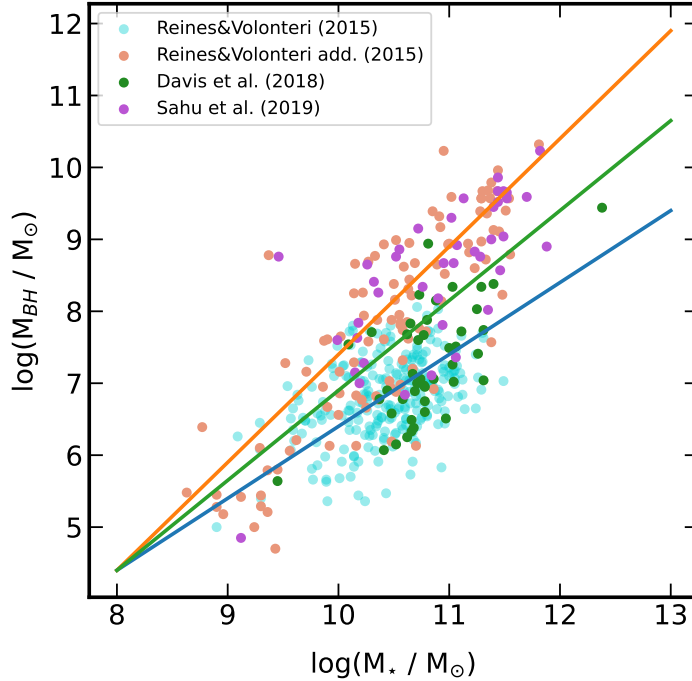


Figure 4.4: Different  $\log_{10}M_{\text{BH}} - \log_{10}M_{\star}$  relations arbitrarily defined. Blue line corresponds to 1st set of parameters ( $\alpha$ ,  $\beta$ ) reported in Table 4.1; Green line to the 2nd set (intermediate slope); Orange line is built using the 3rd set in Table 4.1. They are made to intercept each other in (8.00, 4.40) dex. Points indicate data collected from literature works of Reines & Volonteri (2015), Davis et al. (2018) and Sahu et al. (2019a) as described in Section 4.2.1.

merger contribution and gas accretion, they represent the total growth of a supermassive black hole with a given final mass. In fact, I will need to separate at a certain point the two contributions because red tracks in Figure 4.3, made following continuity equation models, assume that only gas accretion processes are in act. Figure 4.5 summarizes all what said and shows, from left to right, total black hole accretion histories respectively calculated with the first, the second and the third couple of parameters as presented in Table 4.1. Red curves in each panel are the ones by Shankar et al. (2009) and blue curves are those computed in this thesis. Immediate considerations can be made regarding the capability of the single relation to reproduce the model of reference (red curves).

- 1) On the left the assumed relation between  $M_{\text{BH}}$  and  $M_{\star}$  is a pure relation of proportionality, specifically  $M_{\text{BH}}/M_{\star} = \text{const}$ . This constant of proportionality evaluated from the parameters I have introduced is  $\approx 2.5 \times 10^{-4}$ . Actually it is not strictly significant in the sense that it is degenerate with the radiative efficiency  $\epsilon$  applied to get red curves and varying the constant has only the effect of rising up or down blue

curves. What is more important is the shape of the resulting tracks. In this case disagreement with curves of [Shankar et al. \(2009\)](#) can be highlighted in a twofold perspective: following curves from past to present epochs or the contrary. On one side it can be observed that the growing rate is not enough to match the accretion model; at low redshift, models of similar masses at  $z \approx 4$  to the ones predicted by [Shankar et al. \(2009\)](#) model, systematically stay below these latter. On the other side, if starting from similar masses at low  $z$ , blue curves systematically remain above curves of the reference model. In any case a relation of proportionality between  $M_{\text{BH}}$  and  $M_{\star}$  predicts black holes with a too low evolution, meaning that at each change in  $M_{\star}$  as function of  $z$  the change in  $M_{\text{BH}}$  should be more accentuated. This would imply a super-linear relation in terms of physical masses or a steeper linear relation in terms of log-masses;

- 2) The central panel of Figure 4.4 is representative of an intermediate situation between a linear  $M_{\text{BH}} - M_{\star}$  relation and a relatively high super-linear relation. Slope inserted in Equation 4.9 is  $\alpha = 1.25$ . In this second case the agreement is fairly good at smaller black hole final masses ( $z \sim 0$ ), up to approximately  $M_{\text{BH}}(0) \simeq 10^{7-7.5} M_{\odot}$ . From those values on the situation worsen, and again black hole differential growths appear to be much lower than what should be in comparison of the [Shankar et al. \(2009\)](#) model. One should search for a steeper log-linear relation, at least when considering conversion towards higher final black hole masses;
- 3) Last case, on the right, is related to a slope  $\alpha = 1.50$  which can be described as significantly steep. When compared to relations of lower slopes, relevant effects are observed at the two extremes of masses range. It means that, according to intercepts and normalization chosen, below  $M_{\star} \approx 10^8 M_{\odot}$  (see conjunction point of lines in Figure 4.4) predicted black hole masses start to be progressively much smaller than ones predicted by e.g. a relation of  $\alpha \sim 1$ ; on the opposite side instead the converted black hole masses begin to be much higher than the latter cases. This is reflected in the behaviour of blue curves in the respective panel of Figure 4.5, where resulted growing rates are slightly too high at smaller masses (maybe a less steep relation is needed there), while a not bad agreement is found at higher masses, probably because of a fortunate combination between black hole mass conversion and a slow evolution of the galaxy itself at that range of masses (see Figure 3.6).

To sum up, what emerges after this first tentative of reconstructing SMBH accretion curves is that a diverse behaviour is expected between black holes at low mass and high mass end. In my opinion, a consequence of such an observation, in terms of scaling relation, is the fact that it could be advisable also to take into consideration broken power law relations, i.e. a change of slope at a certain  $M_{\star}$  ( $M_{\text{BH}}$ ) characteristic.

### 4.2.3 Broken power law relation

The analysis made in the above Section has suggested that a broken-power law  $M_{\text{BH}} - M_{\star}$  relation would produce black hole accretion curves in better agreement with the model of growing proposed in [Shankar et al. \(2009\)](#). It is important to underline that in the present

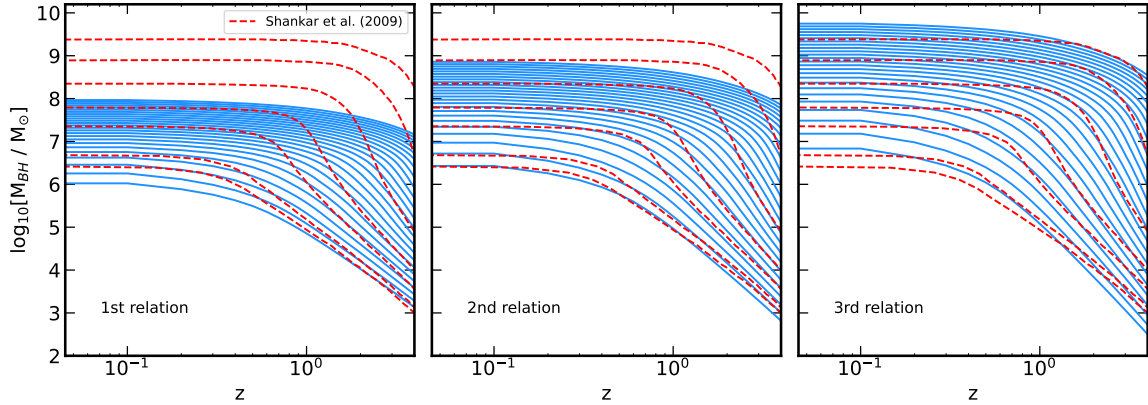


Figure 4.5: Supermassive black holes growing curves calculated following the procedure described in Section 4.2 are colored in blue, while the dashed-red curves are representative of the results obtained from the model of S09, outlined in Section 4.1. From left to right, the sets of lines (blue) are derived through the application of Equation 4.9 to global growths (gas accretion + mergers) of the stellar mass of hosting galaxies, and the parameters adopted can be found in the Table 4.1 respectively.

Section the solution I come up with is not necessary accompanied to physical explanation. It is just to show that the shapes of the growing tracks can reach an alignment to the ones of Figure 4.3, if one employs a certain type of scaling relation in this context.

The relation I am going to adopt has the following parametric form:

$$\log_{10}(M_{\text{BH}}/M_{\odot}) = \begin{cases} \alpha_1 \cdot \log_{10}(M_{\star}/10^{11}M_{\odot}) + \beta_1 & \text{if } M_{\star} < M_{\star,\text{ch}} \\ \alpha_2 \cdot \log_{10}(M_{\star}/10^{11}M_{\odot}) + \beta_2 & \text{if } M_{\star} \geq M_{\star,\text{ch}} \end{cases} \quad (4.10)$$

with  $M_{\star,\text{ch}}$  the characteristic stellar mass at which the change of slope (or of power-law) is applied. Values of  $\alpha_1$  and  $\beta_1$  selected are the same as the ones in the second line in Table 4.1:  $(\alpha_1, \beta_1) = (1.25, 8.15 \text{ dex})$ . This is because, as pointed out before, with these parameters the conversion  $M_{\star} \rightarrow M_{\text{BH}}$  predicts growing curves with shapes comparable to the ones of Shankar et al. (2009). For what concerns the characteristic mass, after some adjustments, the value I insert is  $M_{\star,\text{ch}} = 10^{9.8} M_{\odot}$ . Again this is only a consequence of my calculation and not intended to arrive to a physical hypothesis. Finally  $\alpha_2$  and  $\beta_2$  are chosen so to reproduce red curves of the model of reference and also to be in agreement with the findings of Sahu et al. (2019a) in their global fit of the entire sample of ET galaxies valid for  $M_{\text{BH}} \gtrsim 10^7 M_{\odot}$  (see Equation (11) of their paper). Given values are  $(\alpha_2, \beta_2) = (1.65, 8.63 \text{ dex})$  and the broken power law relation so built up is represented in Figure 4.6, analogous to Figure 4.4 with single-slope log-linear relations. Global accretion curves of supermassive black holes, obtained from initial halo masses between  $M_{\text{halo}} = 10^{11.55} - 10^{14.15} M_{\odot}$ , same SMHM relation (RM) as before and the broken-power low black hole - stellar mass relation, are showed in Figure 4.7a. I have increased a little bit the range of halo masses so to have clearer view of concordance.

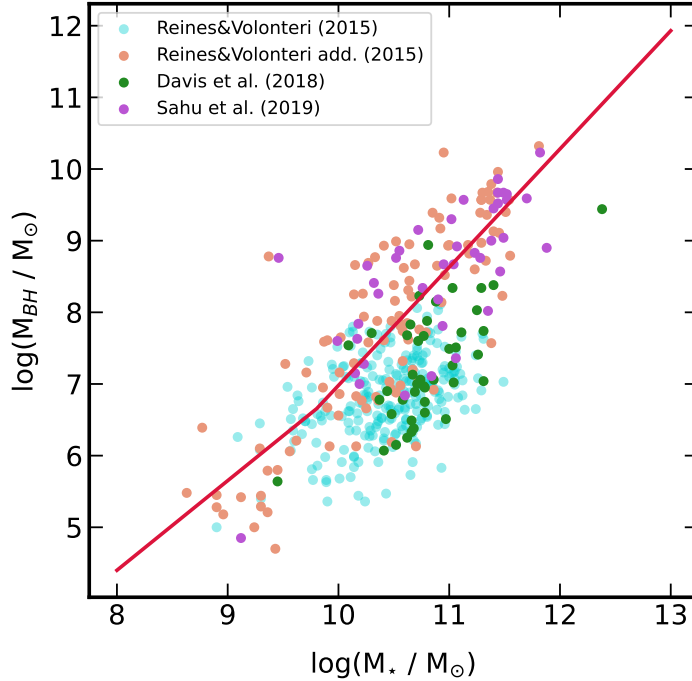


Figure 4.6: Broken power-law relation in  $\log_{10}(M_{\text{BH}}) - \log_{10}(M_{\star})$  plane (red curve). Data points are the same as described in Section 4.2.1, from Reines & Volonteri (2015), Davis et al. (2018) and Sahu et al. (2019a).

Indeed at smaller black hole final masses it seems that the adopted relation is effective in reproducing Shankar et al. (2009) red accretion curves. This is slightly less true at higher final masses, where resulted tracks appear to have exceeding growth rates with respect to what predicted by the RM. i) Surely this is in part due to the fact that the BHs growth taken in consideration so far is a global growth, hence I should subtract the contribution of mergers which can be conspicuous at low redshift for massive objects. ii) A secondary aspect may be responsible for such a behaviour, that is the role of the SMHM relation of use. In Figure 3.5 of Section 3.2, the RM SMHM relation is displayed along with the one obtained by the model of Moster et al. (2018) (Mo18). As anticipated in that occasion, the latter has similar trend in correspondence of high mass end as the one of the RM, but only at low redshift. When considering the evolution of such relations, instead, the one of RM has a manifestly wider scatter in this sense and that is reflected in the growing histories of stellar components. As one can perceive by looking at the right panel of Figure 3.6, growing curves of RM tend to stay above the ones of Mo18 that flatten at low redshift. In order to see the effects that a different choice of SMHM relation implies, I calculate total BH growing curves inserting Mo18 relation when converting from halo masses to stellar masses, instead of the RM one, and I decide to concentrate on the results

obtained at higher masses. In particular I start from final halo masses  $M_{\text{halo}} \gtrsim 10^{12.5} M_{\odot}$  so to have notable differences. Figure 4.7b visualizes curves obtained in the situation just depicted, and effectively a mild improvement is achieved in terms of growing rates of the curves compared to the model of reference. In particular the former follow better the flat (less and less accretion) trend of the latter ones. Anyway at this point a deeper

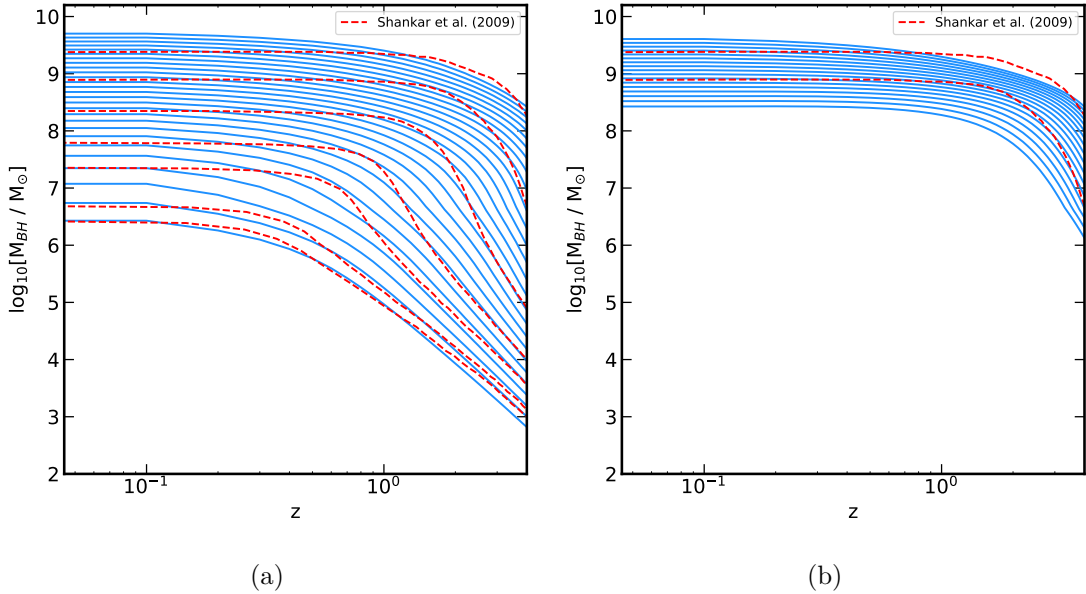


Figure 4.7: Panel (a) shows the global accretion curves (blue) of SMBHs that are evaluated using the broken power law relation of Equation 4.10 to convert  $M_{\star}(z)$  to  $M_{\text{BH}}(z)$ , and the stellar mass - halo mass relation of reference (RM, see Section 3.2) to convert  $M_{\text{halo}}(z)$  to  $M_{\star}(z)$ . Panel (b) is the same but the blue lines, this time, follows from a  $M_{\star}$  converted by the SMHM relation of Moster et al. (2018). Only growing paths of black holes with higher final masses are represented since at lower masses an agreement with red-dashed curves of S09 is not found, due to the shape of SMHM in that range.

analysis should be conducted in the evaluation of mergers contribution in the growing histories of supermassive black holes. In other words I investigate if DECODE information about mean merger accretion for each halo is compatible with the input scaling relation in terms of predicting the 'only' gas accretion curves of the reference model.

#### 4.2.4 Contribution of mergers

In this Section and for the rest of this Chapter, when making considerations about mean merger contribution what is intended is a *maximal* merger contribution. It means that I always make the assumption that for all subhalos that have ever fallen into the parent halo a BH-BH merger occurs. This is probably not the case, in the sense that the exact merger mechanism of two supermassive black holes is still not completely understood. However, as I am going to expose in a while, this maximal contribution approach has no

net impacts when applied at low mass regimes. On the other hand consequences become non negligible moving towards more and more massive objects, and that should imply further considerations and adjustments.

In the meantime the procedure followed in order to acquire mean merger histories is analogous to what I have presented in Section 3.1.2. I report below the main steps already discussed there and the additional ones that allow to retrieve something similar to Figure 3.3, but for supermassive black holes.

- i) Collect  $\sim 60$  parent halos among the `output_parents.txt` catalogue, derived by a run of DECODE, and within a single halo mass bin of size  $\Delta \log_{10}(M_{\text{halo}}/M_{\odot}) = 0.1$  dex. The chosen number is enough to have a good statistics;
- ii) For each of these parent halos retrieve all the in-falling subhalos related to them that can be found in the catalogue `output_mergers.txt`;
- iii) Convert each subhalo with mass  $M_{\text{subhalo}}$  in stellar mass,  $M_{\star}$ , through the SMHM relation of input (RM in our case), and then into black hole mass,  $M_{\text{BH}}$ , through the scaling relation defined (broken power law in Section 4.2.3);
- iv) For the time interval between  $z = 0 - 4$  divided in steps of  $dz = 0.1$ , calculate the merger cumulative accretion history of the single objects. This is done by summing at each redshift step,  $z$ , all the 'in-falling' black holes, meaning the ones associated to a  $z_{\text{inf}} \geq z$ ;
- v) Determine the mean of the  $\sim 60$  tracks so-obtained,  $\langle M_{\text{BH,merg}}(z) \rangle$  and the error of the mean  $\sigma_{\text{BH,merg}}(z)$ ;
- vi) Finally subtract the mean merger contribution to the average total growing curves, blue curves introduced in Section 4.2.3. The result of this operation is a set of mean tracks (of different final masses) that reproduce the gas accretion onto supermassive black holes and that can be coherently compared to the model set by Shankar et al. (2009).

Results related to two SMBHs with significant different masses are displayed in Figure 4.8. On the left it is shown the case of a typical black-hole of final mass  $\approx 10^7 M_{\odot}$  and on the right of a final mass slightly higher than  $10^8 M_{\odot}$ . In both of them the blue curve corresponds to the subtraction  $\langle M_{\text{BH,tot}} \rangle - \langle M_{\text{BH,merg}} \rangle$  with mean merger being traced by orange line. Light orange and light blue shaded areas account respectively for the  $1\sigma$  error of the mean merger history and for a scatter arbitrarily added to the accretion curve obtained from the subtraction. This latter is inserted firstly to have an idea of what would be the discrepancy between the model of reference and the results obtained, secondly because as mentioned in Section 4.2.1 an intrinsic scatter in  $M_{\text{BH}} - M_{\star}$  exists and it is not easy to compute. In this context, since there is not the possibility of evaluating a 'real' error, I assign a 'fake' scatter so to encompass the curves of the reference model within it. What can be noted is the fact that in the case of smaller supermassive black hole the concordance is better and the two curves (red and blue) are yet compatible if a scatter of  $\sim 0.25$  dex is included. On the other hand an higher value of  $\sim 0.35$  dex should be added

in the case of the black hole on the right of Figure 4.8 to have complete concordance. These values are just estimates of the order of magnitude of the discrepancies I obtain applying all the procedure described so far. Naturally this is only one example among

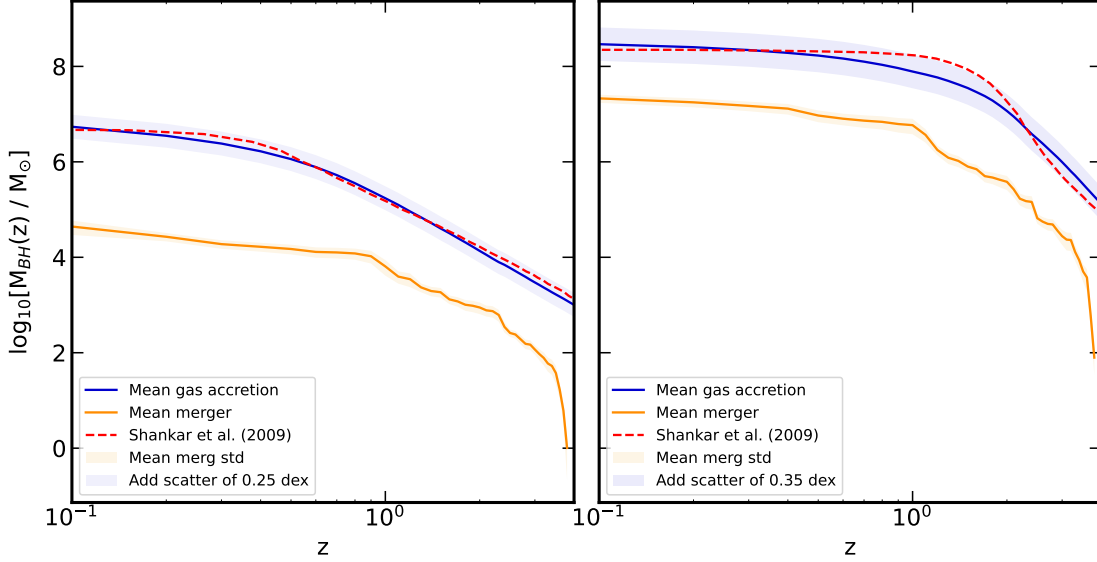


Figure 4.8: Left: blue curve traces the gas accretion history of a SMBH with a final mass of  $\approx 10^7 M_{\odot}$  as calculated from i) the application of the broken power law scaling relation (Equation 4.10) for the conversion  $M_{\star} - M_{\text{BH}}$  and ii) the subtraction of the mean contribution of mergers in that case, given by the orange curve (see Section 4.2.4 for the details of derivation). The orange shaded area considers the  $1\sigma$  error of the mean track, while blue shaded area represents an arbitrarily scatter (of  $\sim 0.25$  dex) added so to enclose the red-dashed curve, referred to the S09 model. Right: same as the panel on the left, but valid for a SMBH with a final mass of  $\gtrsim 10^8 M_{\odot}$ . In this second case the arbitrary chosen scatter is of  $\sim 0.35$  dex.

an infinite number of possibilities and the real result is not the exact parametrization of the scaling relation. What matters is to illustrate the potentiality of this application, that is indeed self-reliable and almost without the need of initial assumptions about the physical mechanisms involved. One could in a second moment adopt a more quantitative approach and make constraints about the evolution of a supermassive black hole.

At this level of analysis it is still possible to note some interesting characteristics of the curves derived. In the first place I repeat the fact that in order to obtain a general concordance with the lines of Shankar et al. (2009) one should introduce a variation in what is a perfect log-linear relation to be maintained in all past epochs. The solution for which I opted in this Chapter has been the introduction of a sort of *plateau* towards low mass end of the  $M_{\text{BH}} - M_{\star}$  scaling relation. In Chapter 6 I am going to mention another possible way out that consists in hypothesizing a redshift evolution of the relation in use,

with the effect of rising up values at low masses. Other possibilities are to consider non log-linear scaling relations, of second, third etc. order in the  $\log_{10}(M_{\star})$  variable. Actually the only method to get true indications would be the availability of data for low mass SMBHs (or galaxies) so to reduce the scatter, in particular in that region of the diagram (see again Figure 4.6).

Another piece of information regards the contribution of mergers, that will be discussed in more details in the future of this thesis. Focusing now on Figure 4.8, what can be pointed out is that the mass gained by mergers is, at least up to SMBH final masses of  $\sim 10^8 M_{\odot}$ , of second order with respect of the predicted contribution by gas accretion. In the case presented on the left panel actually the percentage of total merger contribution with respect to the global growth is negligible, of the order of 0.5 - 0.6 %; for a SMBH similar to the case found on the right panel the merger contribution is again of secondary importance even if ten times bigger than the former one: nearly 5 - 6 %. These percentages are actually quit surprising because, as said previously, what I am calculating is the *maximal* merger contribution. I am not going to expand about possible implications of such a finding. Another aspect that can be useful to introduce at this level is the fact that for higher and higher black hole masses (meaning higher starting halo masses) the merger contribution begins to be important, especially at low redshift. In that situation, it may also happen that the mass acquired through mergers is even larger than the total mass predicted and this produces something not physical and to be discarded. A suggestion to improve this will be given in Chapter 6, and will imply a delay time, actually the merging timescale,  $t_{\text{merg}}$ , explained in 2.2.4, in order to reduce the number of mergers that enter in the cumulative mean merger history.

Before going deeper in the analysis of all these issues, I would like to complete the discussion about scaling relations and their use in this project also showing how it can be feasible to obtain results through  $M_{\text{BH}} - \sigma$  relation. This is less obvious than before since no data about dynamics are given, the returns of DECODE are only in terms of total galactic masses. However, it would be a pity not to rely on  $M_{\text{BH}} - \sigma$  relation since it is thought to be the most fundamental one (e.g. Marsden et al. (2020)). I am going to devote next Chapter to the explanation of how the stellar velocity dispersion,  $\sigma_{\star}$ , can be inferred from global stellar mass,  $M_{\star}$ , and how, following the same passages, similar results are obtained. Strictly speaking not additional information is really added since the starting point is always the same, i.e.  $M_{\star}$ . Indeed the purpose is not to get to final solutions about scaling relations, but to make evident the fact that, with few and simple steps, the applications of DECODE are really manifold.



## Chapter 5

# Main: SMBH application II

The first observational works on the relation between central black hole mass,  $M_{\text{BH}}$ , and the stellar velocity dispersion,  $\sigma$ , of a galaxy (Ferrarese & Merritt (2000); Gebhardt et al. (2000)) revealed a relation with little or no intrinsic scatter, suggesting that this relation could be the most fundamental one. Since then, the  $M_{\text{BH}} - \sigma$  relation has been widely studied by the astronomical community since it is believed to be connected to the galaxy/halo gravitational potential well and hence to AGN feedback processes (see e.g. Granato et al. (2004)). The relation is typically written in the form:

$$\log_{10}(M_{\text{BH}}/M_{\odot}) = \alpha \cdot \log_{10}(\sigma/200\text{kms}^{-1}) + \beta. \quad (5.1)$$

The values for the slope and normalization in Equation 5.1 initially retrieved by Ferrarese & Merritt (2000) were  $\alpha = 4.80 \pm 0.54$  and  $\beta = 8.14 \pm 1.80$ . However other recent works have reported different values, e.g. Tundo et al. (2007) suggest values of  $\alpha = 3.83 \pm 0.21$  and  $\beta = 8.21 \pm 0.06$ . There is some debate in literature about the exact shape of the  $M_{\text{BH}} - \sigma$  relation and about its dependence on galactic properties, such as the morphological type, or even on the environment (see e.g. Wyithe (2006); Lauer et al. (2007a); Hu (2008)). There is a general consensus, instead, on the fact that  $M_{\text{BH}} - \sigma$  relation only weakly evolves with redshift (e.g. Gaskell (2009); Salviander & Shields (2013); Shen et al. (2015)). This has been also supported by other works that base their conclusions on direct observations of high redshift quasar samples (Woo et al. (2008)) or as seen in Shankar et al. (2009) from the comparison between the cumulative accretion from AGN with the local black hole mass density obtained through the employment of the  $M_{\text{BH}} - \sigma$  relation.

The questions to be addressed in this context are the following: i) how the velocity dispersion can be retrieved from the total stellar mass of galaxies? ii) Which type of  $M_{\text{BH}} - \sigma$  relation is better in describing SMBHs accretion curves when compared to the ones of Shankar et al. (2009)? iii) How much is the predicted contribution of mergers? iv) Is the whole process consistent in its results? I am going to answer to them in next Sections. Essentially, apart from a first part, the way of proceeding will be the same as what seen in Chapter 4.

## 5.1 Velocity dispersion from $M_\star$

The main equation of reference to relate the stellar velocity dispersion,  $\sigma_\star$ , to the total galactic mass,  $M_\star$  is the Equation (2) in [Bernardi et al. \(2018\)](#) reported below:

$$M_\star = k(n, R)R_e\sigma_R^2/G. \quad (5.2)$$

The above equation follows from the assumptions that the contribution of dark matter on the velocity dispersion  $\sigma_R$ , evaluated within the projected radius  $R$ , is negligible, that the galaxy is not rotating and has an isotropic velocity dispersion and that the total mass-to-light ratio is constant. In that case the Jeans' equation implies that the shape of the luminosity-weighted projected velocity dispersion profile is fully determined by the shape of the surface brightness profile ([Prugniel & Simien \(1997\)](#)). Therefore, the dynamical mass can be estimated by finding the mass-to-light ratio which correctly predicts the amplitude of  $\sigma_R$  on a scale; if all the assumptions before stated are accurate, then this same value will be returned whatever  $R$  one chooses to match.

The other terms in Equation 5.2 are the projected half-light radius  $R_e$ , i.e. the radius within which half of the galaxy's luminosity is contained, the universal gravitational constant  $G$  and the coefficient  $k(n, R)$  that is determined using the Prugniel–Simien methodology for each  $R$ , with  $n$  being the Sérsic index characterizing the surface-brightness profile. The  $k$  coefficient can be calculated for various ratios of  $R/R_e$  and I decide to use values related to  $R = R_e/8$  so  $R/R_e = 0.125$ . This is because the velocity dispersion within it,  $\sigma_{e/8}$ , should be in principle not much influenced by the presence of dark matter, hence being subjected only to the gravitational effect of the central supermassive black hole. In [Bernardi et al. \(2018\)](#) values of  $k$  are reported for different indexes  $n$  in the range  $[2, 10]$  and they can be found here in Table 5.1.

The terms  $R_e$  and  $n$  in Equation 5.2 are actually still missing because the only information we dispose of is the  $M_\star$ . Thus the former have to be related to the latter and this is done adopting both semi-analytic and observational prescriptions.

- The  $M_\star - R_e$  relation I am going to use is the redshift-dependent one found in [Marsden et al. \(2022\)](#), in turn derived following [Ricarte & Natarajan \(2018\)](#):

$$R_e(M_\star, z) = R_e(M_\star, 0)f(M_\star, z). \quad (5.3)$$

$R_e(M_\star, 0)$  represents the local relation between the effective radius and the stellar mass. The one I choose to adopt is obtained from the observational work of [Hyde & Bernardi \(2009\)](#). The parametric form used to fit data is given by:

$$\log_{10}R_e = p_0 + p_1\log_{10}(M_\star/M_\odot) + p_2[\log_{10}(M_\star/M_\odot)]^2, \quad (5.4)$$

with resulting best fit parameters  $p_0 = 7.55 \pm 0.44$ ,  $p_1 = -1.84 \pm 0.08$  and  $p_2 = 0.110 \pm 0.004$ .

The term  $f(M_\star, z)$  accounts for the redshift evolution of the relation and in [Marsden et al. \(2022\)](#) it is assumed the following expression for it:

$$f(M_\star, z) = (1 + z)^{-\gamma(M_\star)}, \quad (5.5)$$

---

n	R/R <sub>e</sub> = 0.125
2.00	7.20
2.50	6.46
3.00	5.76
3.50	5.15
4.00	4.62
4.50	4.17
5.00	3.79
5.50	3.46
6.00	3.17
6.50	2.92
7.00	2.70
7.50	2.50
8.00	2.32
8.50	2.16
9.00	2.01
9.50	1.88
10.00	1.75

---

Table 5.1: Dependence of coefficient  $k(n, R/R_e)$  in Equation 5.2.

and

$$\gamma(M_\star) = A \cdot \log_{10} M_\star [(B \cdot \log_{10} M_\star)^p + (C \cdot \log_{10} M_\star)^s]^{-1}, \quad (5.6)$$

with  $A = 3.05 \times 10^{-3}$ ,  $B = 9.67 \times 10^{-2}$ ,  $C = 0.204$ ,  $p = -39.0$  and  $s = -4.30$ ;

- For what concerns the  $M_\star$  -  $n$  relation the one I am going to use is evaluated by [Sahu et al. \(2020\)](#) for the spheroidal component of early type galaxies (ETGs) reported below:

$$\log_{10}(M_{\star, \text{bulge}}/M_\odot) = (3.27 \pm 0.25) \log_{10}(n_{\text{sph}}/3) + (10.50 \pm 0.06). \quad (5.7)$$

Actually this is valid just for spheroids but I decide to employ it in any case because it just enters in the calculation of the coefficient  $k(n, R)$  that is itself approximated.

At this point all ingredients entering in Equation 5.2 have been defined and it is possible to get values of  $\sigma_{e/8}$  at each wanted redshift. It is then straightforward to derive  $M_{\text{BH}}$  out of  $\sigma_e$  once a specific black hole mass - velocity dispersion relation has been identified. I am going to exactly apply the same steps as before: i) I collect an heterogeneous sample of local data concerning the  $M_{\text{BH}}$  -  $\sigma$  relation from different literature works; ii) try different values to assign to the parameters of the log-linear relation (i.e. Equation 5.1) and make considerations about the shapes of black hole accretion curves so determined, always in comparison of curves of the reference model; iii) evaluate the contribution of mergers in the growing process adopting the type of conversion (scaling relation) that better suits the curves of [Shankar et al. \(2009\)](#).

## 5.2 Data sample and Chosen relations

This Section is intended to present in some details the sets of data collected, with again the clarification that those data will not be used to perform a fit. I repeat the fact that it is just to have an indication of possible consistency between what will be my results and what one should expect from 'reality'. Since now, much effort has been made in trying to calibrate the  $M_{\text{BH}} - \sigma$  relation and choosing representative works is not an easy task. The ones I am going to describe are just a few, many others could have been considered.

- A first set of data is taken from [Xiao et al. \(2011\)](#), where the authors investigate the low mass end of the  $M_{\text{BH}} - \sigma_*$  relation. They present new measurements of stellar velocity dispersion for 76 Seyfert 1 galaxies selected from the sample of broad-line active galaxies with low-mass BHs in [Greene & Ho \(2007b\)](#) (BH masses estimated with single-epoch virial method). Observations are made with the use of the Keck Echellette Spectrograph and Imager (ESI) and the Magellan Echellette (MagE), and then results are combined with other ESI observations of similar objects so to have a final sample of 93 galaxies with BHs of masses below  $\sim 2 \times 10^6 M_{\odot}$ ; [Related data points in Figure 5.1 are represented by pink dots]
- Other data are retrieved from the work of [Kormendy & Ho \(2013\)](#) in which they review all the information available up to that time about the 87 supermassive black holes found at the center of galaxies.  $M_{\text{BH}}$  measurements are based on stellar dynamics, ionized gas dynamics, CO molecular gas disk dynamics, or maser disk dynamics. Host galaxies belong to different morphologies, some of them are ellipticals and others disk galaxies with classical or pseudo-bulges. For the stellar velocity dispersion,  $\sigma_e$ , they adopt the convention that  $\sigma_e^2$  is the intensity-weighted mean of  $V^2 + \sigma^2$  out of a fixed fraction of the effective radius  $R_e$ . In particular authors use  $R_e/2$  when  $\sigma_e$  is calculated from photometry and published kinematics. Otherwise  $\sigma_e$  is from the  $M_{\text{BH}}$  source paper from [Gultekin et al. \(2009\)](#). [Related data points in Figure 5.1 are represented by green dots]
- Next set of data collected comes from [Sahu et al. \(2019b\)](#). In this work the authors identify 145 galaxies, both early- and late-type (ETGs and LTGs), with directly measured SMBH masses obtained from stellar dynamics, gas dynamics, kinematics of megamasers, proper motion, or direct (recent) imaging techniques. Most part of data about ETGs galaxies are from [Savorgnan & Graham \(2016b\)](#) and [Sahu et al. \(2019a\)](#), the remaining from [Nowak et al. \(2007\)](#), [Gultekin et al. \(2014\)](#), [Huré et al. \(2011\)](#), [Nguyen et al. \(2018\)](#), [Thater et al. \(2019\)](#) and [Boizelle et al. \(2019\)](#). Data related to LTGs are mainly obtained from [Davis et al. \(2018\)](#) and [Davis et al. \(2019\)](#), the rest part comes from the works of [Combes et al. \(2019\)](#) and [Nguyen et al. \(2020\)](#). The velocity dispersion has been measured in many ways in literature, e.g. luminosity-weighted line-of-sight velocity dispersion within one effective radius,  $R_e$ ; luminosity weighted line-of-sight stellar rotation and velocity dispersion within one effective radius of either the spheroid or the whole galaxy; or velocity dispersions within an aperture of radius equal to one-eighth of  $R_{e,\text{sph}}$ ,  $\sigma_{e/8}$ . Due to the inconsistency in the use of aperture size and contamination linked to

disk rotation when considering large aperture, authors in [Sahu et al. \(2019b\)](#) decide to use the central velocity dispersion data taken from the HYPERLEDA database ([Paturel et al. \(2003\)](#)). Velocity dispersions found in there are homogenized for a uniform aperture of size of  $0.595 h^{-1}$  kpc; [Related data points in Figure 5.1 are represented by yellow dots]

- Other data included are from [de Nicola et al. \(2019\)](#) in which they use a sample of 83 BH masses collected from reliable spatially resolved estimates available from literature. Authors start with the big compilation of BH masses from [Saglia et al. \(2016\)](#), with some additional galaxies from [Kormendy & Ho \(2013\)](#), [van den Bosch \(2016\)](#) and from [Krajinović et al. \(2018\)](#). All BH masses are measured through stellar dynamics, gas dynamics or astrophysical masers, hence derived from spatially resolved kinematics. The authors then discard BHs with upper limits on their masses or estimates from reverberation mapping and virial methods, because these should be calibrated with  $M_{\text{BH}}$  - galaxy relations. Effective velocity dispersions are retrieved from the same sources as before ([Saglia et al. \(2016\)](#), [Kormendy & Ho \(2013\)](#) and [van den Bosch \(2016\)](#)); [Related data points in Figure 5.1 are represented by orange dots]
- The final set taken into consideration is collected from [Baldassare et al. \(2020\)](#). In this paper the authors obtain new stellar velocity dispersion measurements for eight active dwarf galaxies with  $M_{\star} < 3 \times 10^9 M_{\odot}$  and low mass black holes. These objects are drawn from the sample of [Reines et al. \(2013\)](#) dwarf galaxies with both broad and narrow optical emission line signatures of AGN activity. Measures for the velocity dispersion are taken again using the Keck Echellette Spectrograph and Imager (ESI) as in [Xiao et al. \(2011\)](#) and BH masses are obtained through virial methods. In addition to the eight galaxies, other systems are reported in the work so to investigate the low mass-end of  $M_{\text{BH}}$  -  $\sigma_{\star}$  relation. They are taken from [Filippenko & Sargent \(1989\)](#), [Barth et al. \(2004\)](#), [van den Bosch & Tim de Zeeuw \(2010\)](#), [Baldassare et al. \(2015\)](#), [Baldassare et al. \(2016\)](#), [Nguyen et al. \(2018\)](#) and [Nguyen et al. \(2019\)](#). [Related data points in Figure 5.1 are represented by blue dots]

Now that observational data have been collected, they can be represented as a scatter plot in the  $\log_{10}(M_{\text{BH}}) - \log_{10}(\sigma)$  plane so to observe what types of relation would possibly describe them. In a first moment a purely log-linear relation is considered, specifically the equation of reference is Equation 5.2. As done in the analogous Section 4.2.1 of Chapter 4, some values for the parameters  $\alpha$  and  $\beta$  are arbitrarily inserted in order to get basic understanding about the shapes of BH accretion curves derived from them, and to investigate if or not they tend to be in agreement with [Shankar et al. \(2009\)](#) model. It has to be said that many works in literature (including the above-mentioned ones) have found relations of type  $M_{\text{BH}} \propto \sigma^4$ , hence a reference value for the  $\alpha$  parameter I decide to adopt is right this one. Other two cases are then analyzed which are opposites, in a certain sense, to the former and all of them are listed in Table 5.2. Finally Figure 5.1 puts together all what explained so far: the sample of data selected is represented by colored dots, while straight lines are the scaling-relations related to parameters introduced. A

	$\alpha$	$\beta$ (dex)
1st	2.50	7.50
2nd	4.00	8.30
3rd	5.00	8.60

Table 5.2: Values chosen for parameters  $\alpha$  (slope) and  $\beta$  (intercept) to be inserted in Equation 5.2. They do not have errors with them because do not represent a fit of data.

thing that is interesting to note is the fact that, even though the observational data collected belong to variate samples and are obtained employing different methods, they are much less scattered than what seen in the complementary Figure 4.4. In the former plot data dispersion along the y-axis is at most of the order of 2 dex, while in the situation representing  $M_{\text{BH}} - M_{\star}$  it can reaches values above 3 dex.

For what regards the scaling relations, it is evident that the one assigned with the first couple of parameters in Table 5.2 (blue line in the Figure 5.1) is not compatible at all with the most of the considered mass ranges. This is in fact made on purpose so to investigate how the low mass end of the scaling relation, for which data are necessarily more sparse, tends to behave. The other two, instead, appear to be more reliable at intermediate and high masses, and less in line at low masses. Therefore it would be interesting to observe the black hole accretion curves resulting from them. Again at first approximation what is considered is the total accretion of a supermassive black hole, disregarding for the moment the role of mergers. This is to have a first feeling of which type of relation would be more suitable. Next Section is devolved to this purpose.

### 5.3 First results

In order to continue the parallelism of what done previously for the case of  $M_{\text{BH}} - M_{\star}$  relation, supermassive black hole growing curves are produced starting from the same initial halo masses, between  $M_{\text{halo}}(0) = 10^{11.55} M_{\odot}$  and  $M_{\text{halo}}(0) = 10^{13.95} M_{\odot}$ , making them evolve according to van den Bosch et al. (2014) and finally through the series of re-parametrization:  $M_{\text{halo}} - M_{\star}$  (RM) -  $\sigma - M_{\text{BH}}$  getting the accretion tracks to be compared to the ones of Figure 4.3. Applying scaling relations defined in the previous Section, what is obtained is depicted in Figure 5.2. At first glance, it can be pointed out that it is as if the resulting blue curves are shifted downwards with respect to the situation of Figure 4.5, in particular since I have made them start from same values of  $M_{\text{halo}}(M_{\star})$ . I have already discussed about degeneration between the normalization of scaling relations and the radiative efficiency used to calculate red dashed curves. Hence one could just change the  $\beta$  parameters, increase them by the same amount and re-align everything. However in doing so, log-linear curves in the  $\log_{10}(M_{\text{BH}}) - \log_{10}(\sigma)$  plane reach positions systematically above the data points and, even though such curves are not fit of them, that would be not desirable. A possible explanation is that I may have introduced a source of systematic in the passage from  $M_{\star}$  to  $\sigma$ . Indeed this is not absurd

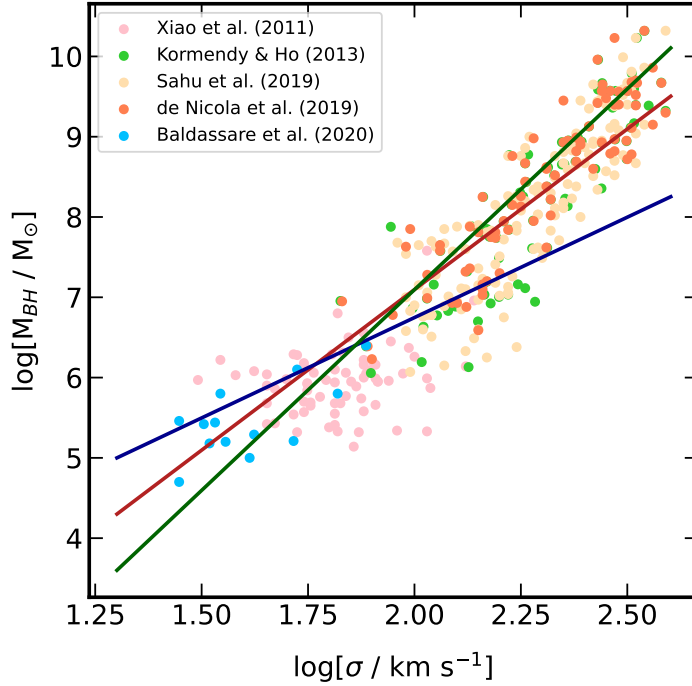


Figure 5.1: Different  $\log_{10}M_{\text{BH}} - \log_{10}\sigma$  relations arbitrarily defined. Blue line corresponds to 1st set of parameters ( $\alpha$ ,  $\beta$ ) reported in Table 5.2; Red line to the 2nd set (intermediate slope); Green line is built using the 3rd set in Table 5.2. They do not have a common interception since it would be more difficult than what done in the case of Figure 4.4 due to the less scatter in observations. Points indicate data collected from literature works of Xiao et al. (2011), Kormendy & Ho (2013) and Sahu et al. (2019b), de Nicola et al. (2019) and Baldassare et al. (2020) as described in Section 5.2.

since the relations considered are themselves models or calibrations out of observational data, hence in any case subjected to a part of uncertainty. Actually trying to define and adjust such errors is another matter and beyond the scope of the project. However if we trace back the steps made in Section 5.1 and consider that I am working with log relations, that I am starting from the same values of  $M_{\star}$  as in the previous Chapter, that variations in the  $k$  coefficient (see Equation 5.2) among the ones found in Bernardi et al. (2018) would be too mild to be responsible of the shift of curves in Figure 5.2, then the probably most influencing term is in the definition of the effective radius  $R_e$ . I find that if values assigned to it are reduced of almost a half, the parallelism with the situation in Chapter 4 is re-established without the need of shifting up all the normalizations in the  $M_{\text{BH}} - \sigma$  relations. In fact, it is not a negligible reduction the one applied to  $R_e$  and would imply a down-shift of nearly 0.3 dex in the  $\log_{10}(M_{\star}) - \log_{10}(R_e)$  relation. In any case I decide to opt for this type of adjustment so to maintain order and consistency

between all the passages I have performed so far, with some cautions including the fact i) that this could not be the best resolution, ii) that some other relations between  $M_\star - R_e$  could be investigated, iii) that it is not said the relations used are the optimal ones, iv) errors may have been made before in the part concerning  $M_{\text{BH}} - M_\star$  relation and v) that I am not taking into account what effect the variation of the radiative efficiency would produce in curves of [Shankar et al. \(2009\)](#). New results obtained with the reduced  $R_e$  are displayed in Figure 5.3. At this level some comments about the goodness of results are

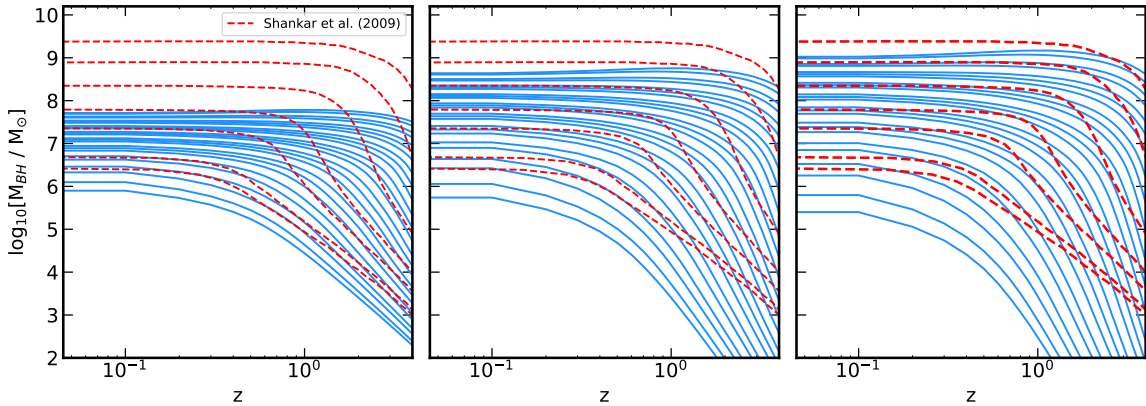


Figure 5.2: Supermassive black hole growing curves: blue ones represent total accretion (not subtracted by merger contribution) and red dashed ones are the tracks of [Shankar et al. \(2009\)](#). Redshift range is from  $z = 0$  and  $z = 4$ . In the left panel curves have been obtained employing the relation parametrized by the first couple of  $\alpha$  and  $\beta$  in Table 5.2, central panel is instead related to the second couple of parameters and on the right curves resulting from the third set are plotted. For all of the three situations the starting halo masses are the same.

needed, always in comparison to the reference curves of [Shankar et al. \(2009\)](#).

- 1) The first set of curves, found in the left panel of Figure 5.3, are referred to the parameters  $\alpha = 2.50$  and  $\beta = 7.50$ . I have already underlined that a relation of this kind is almost completely in disagreement with observational data. However, what can be evinced looking at the figure is the fact that at low masses the so-produced accretion tracks have growth rates of similar trend with respect to the ones of the reference model. Apparently this quite good behaviour is maintained up to nearly black hole masses of  $M_{\text{BH}} \sim 10^{6.5} M_\odot$ . Above these values of mass, the predicted growing rates appear to be too mild to correctly describe [Shankar et al. \(2009\)](#) curves, meaning a steeper log-linear relation is needed to make the former keep up with the latter;
- 2) The situation illustrated in the middle panel of Figure 5.3 is representative of results obtained applying a  $M_{\text{BH}} - \sigma$  relation of the type  $M_{\text{BH}} \propto \sigma^4$  that, as mentioned, is something expected from literature works. Indeed a fair agreement is not excluded

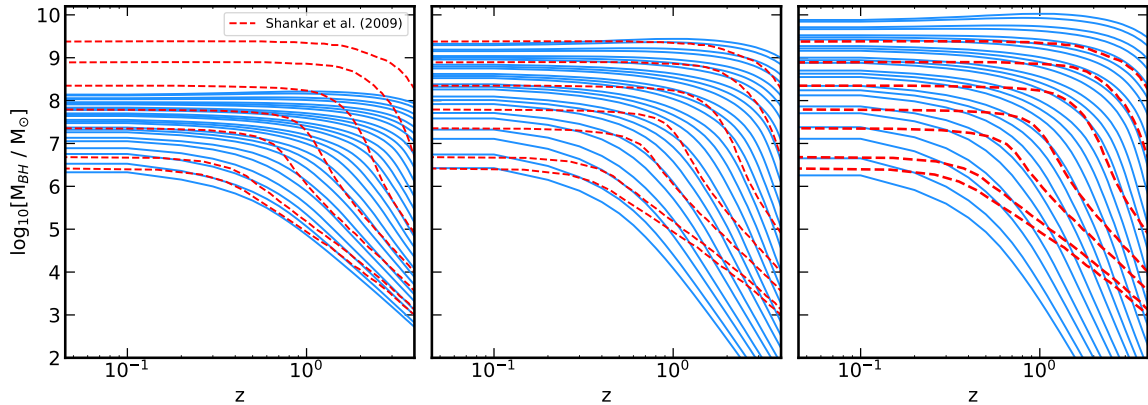


Figure 5.3: Same as Figure 5.2, but with curves obtained after the reduction of the  $R_e$  term evaluated from  $M_*$ .

at intermediate black hole masses, saying in between  $M_{\text{BH}} \sim 10^6$  and  $M_{\text{BH}} \sim 10^8 M_{\odot}$ , which is more or less the range where most part of observations is retrieved. At higher and higher masses, however, the rates of growth are again too slow in comparison the the ones related to the curves of [Shankar et al. \(2009\)](#) and another possible change of slope is advisable;

- 3) Final relation introduced is of the type  $M_{\text{BH}} \propto \sigma^5$ , which is not distant to some findings in literature (e.g. the slope in [Ferrarese & Merritt \(2000\)](#) of  $\alpha = 4.80 \pm 0.54$ ). In this case at low masses the curves produced have far too steep growing rates, and as it is notable also in Figure 5.1 values of BH masses predicted (green line) seem well below observational data in that range. For BH masses  $\gtrsim 10^7 - 10^{7.5} M_{\odot}$ , instead, we obtain fair good improvements in terms of comparison between blue curves growing rates and the ones of red curves.

As for the case of  $M_{\text{BH}} - M_*$  relation, a single slope log-linear scaling relation may not be the perfect choice when one uses it to reconstruct the mass growing history of supermassive black holes. In the next Section I am going to look for alternatives that would produce a general agreement, meaning at all mass steps considered. In particular two are the proposed relations: a broken power law type relation and a log-quadratic relation, or in other words a parable in the  $\log_{10}(M_{\text{BH}}) - \log_{10}(\sigma)$  plane.

## 5.4 Alternative relations

In consideration of the analysis made in the previous Section about results of Figure 5.3, if one wants to apply a single scaling relation to be valid at each redshift step between  $z \sim 0 - 4$  and for every SMBH of final mass in the range  $M_{\text{BH}} \sim 10^{6.5} - 10^{9.5} M_{\odot}$ , then a simple log-linear relation is not efficient in reproducing the results of the [Shankar et al.](#)

(2009) model. Hence I firstly decide to test if a broken power law type  $M_{\text{BH}} - \sigma$  relation would be more suitable for our purposes.

#### 5.4.1 Broken power law $M_{\text{BH}} - \sigma$ relation

The Equation to be parametrized in that case is of the form:

$$\log_{10}(M_{\text{BH}}/M_{\odot}) = \begin{cases} \alpha_1 \cdot \log_{10}(\sigma/200\text{kms}^{-1}) + \beta_1 & \text{if } \sigma < \sigma_{\text{ch}} \\ \alpha_2 \cdot \log_{10}(\sigma/200\text{kms}^{-1}) + \beta_2 & \text{if } \sigma \geq \sigma_{\text{ch}} \end{cases} \quad (5.8)$$

where  $\sigma_{\text{ch}}$  indicates the limiting value of velocity dispersion at which a change in the slope is expected. Naturally finding optimal parameters is not an easy task since the aim is to achieve a good, but qualitative, comparison with the curves of the reference model (still not considering mergers). Observing the trend of curves in Figure 5.3, the most intuitive options for  $\alpha_1$  and  $\beta_1$  parameters, at low mass ranges, correspond to the first couple in Table 5.2:  $(\alpha_1, \beta_1) = (2.50, 7.50 \text{ dex})$ . For the characteristic  $\sigma$  a tentative value could be  $\sigma_{\text{ch}} \approx 10^{1.9} \text{ km s}^{-1}$ , to which is assigned a  $M_{\text{BH}} \approx 10^{6.5} M_{\odot}$ . The other two parameters are defined after various attempts and the final values chosen are:  $(\alpha_2, \beta_2) = (4.80, 8.40 \text{ dex})$ . A slightly higher slope is necessary to rise values up of a 'correct' amount. The relation so built is represented in the left panel of Figure 5.4, again over-plotted to the same sample of data as before. The global accretion tracks that come out applying this type of scaling relation are illustrated in left panel of Figure 5.5. Generally speaking a similar trend is perceived, even if curves have growths not smooth in the region corresponding to change of slope because such a variation is quite brusque. In this view another option would be to consider a log-quadratic relation so to have gradual global variation of the slope. Actually there are some works, e.g. Gaskell (2009), that try to fit data with a relation quadratic in  $\log_{10}\sigma$ , hence that could not be so distant from 'reality'. In any case, mine is only a tentative to smooth the accretion tracks and at the same time maintaining a sort of consistency with observational data points.

#### 5.4.2 Log-quadratic $M_{\text{BH}} - \sigma$ relation

The equation that describes the conversion has the following parametric form:

$$\log_{10}(M_{\text{BH}}/M_{\odot}) = a \cdot [\log_{10}(\sigma/\text{kms}^{-1})]^2 + b \cdot \log_{10}(\sigma/\text{kms}^{-1}) + c, \quad (5.9)$$

with  $a$ ,  $b$  and  $c$  the parameters arbitrarily introduced. In choosing them I try to make the parable to be nearly tangent to the flatter part of the broken power law at low masses and to the steeper part at higher masses. In this way just mass values at intermediate steps would be subjected to a considerable change. The parameters I have adopted are given by:  $(a, b, c) = (1.10, -0.35, 3.45)$ . The relation in the  $\log_{10}(M_{\text{BH}}) - \log_{10}(\sigma)$  plane is displayed in the right panel of Figure 5.4. In this latter I have also reported again the log-linear relation pertaining to the second couple of  $\alpha$  and  $\beta$  in Table 5.2, in order to see that in the intermediate part of the range of masses considered the parable has a similar behaviour as such log-linear relation. The emerging series of accretion paths of supermassive black holes can be observed on the right panel of Figure 5.5.

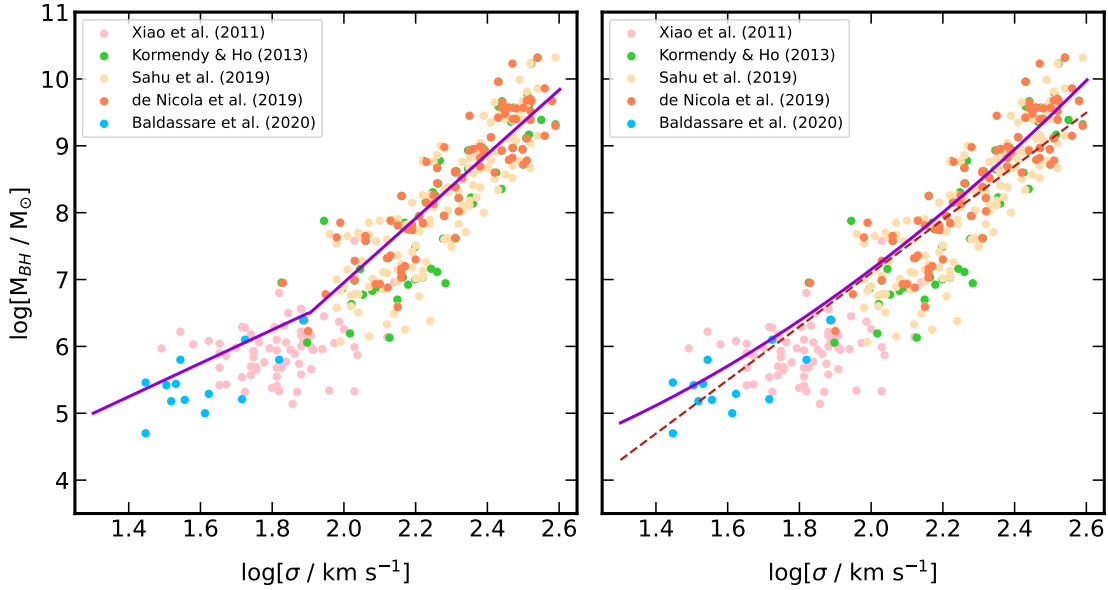


Figure 5.4: Alternative  $M_{\text{BH}} - \sigma$  scaling relations introduced in Section 5.4. Left: scatter plot of the data collected and presented in Section 5.2 with, superimposed, the broken power law relation represented by the solid violet line and defined by Equation 5.8. Right: the same as the situation in the left panel but with the violet line being the log-quadratic relation given by Equation 5.9. The dashed-red line is the log-linear  $M_{\text{BH}} - \sigma$  relation obtained by inserting in Equation 5.1 the second set of parameters in Table 4.1.

As expected the curves in this case evolve without sharp interruptions and have growing rates fairly in agreement with red dashed curves. The only unwanted issue that comes out in this occasion is at the very low mass end. Since the relation is a parabolic relation, at certain values of  $\log_{10}(\sigma)$  it enters its decreasing part and this leads to prediction of higher black hole masses at lower values of velocity dispersion. In Figure 5.5 this is perceived for the paths conducting to final BHs of small masses and at high redshift. The situation at a certain point can become not physical because, if the log-quadratic relation is kept always the same, then growing curves assume reverse trends. This would be actually a problem when it arrives the moment of evaluating the merger contribution. Indeed subhalos, then converted in stellar masses and then in velocity dispersions will be mainly confined to the very lower left angle of the  $\log_{10}(M_{\text{BH}}) - \log_{10}(\sigma)$  plane, towards the descending branch of the parable, resulting in an exceeding estimate of the cumulative merger contribution especially at high  $z$ . Hence either we adopt the broken power law relation to continue the calculation or approximate the parable to its tangent at a certain  $\sigma$  and keep it this way at smaller and smaller values. I decide for the latter alternative in order just to have smooth growing curves, with the awareness that it may not be adherent to a truly physical situation. Only data points down to that values of  $M_{\text{BH}}$  and  $\sigma$  could in the future reveal something about the shape of the scaling relation. To summarize,

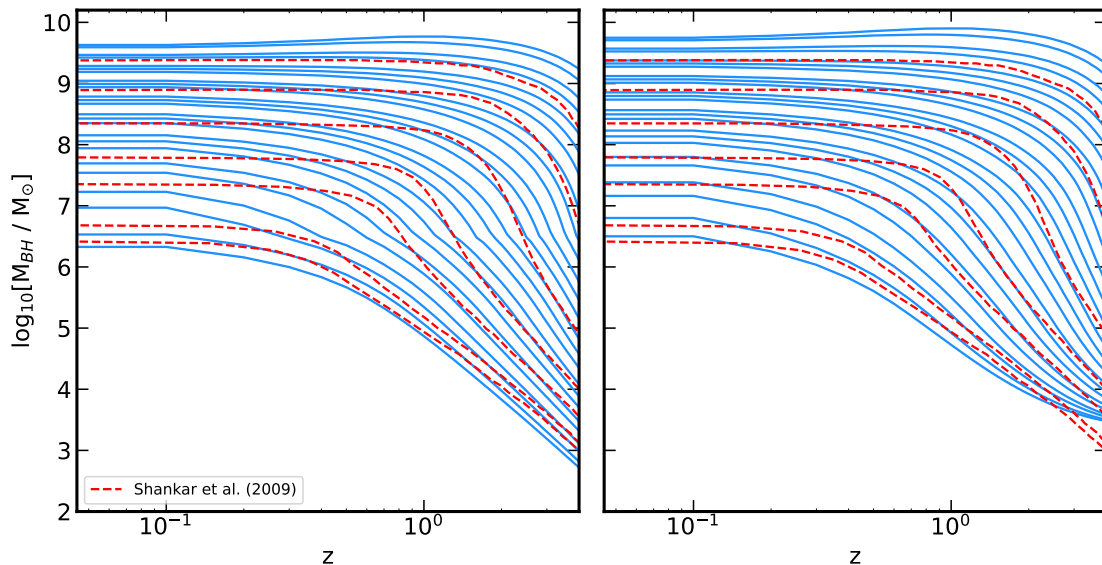


Figure 5.5: Blue curves are the global growing curves of supermassive black holes derived through the conversions  $\sigma \rightarrow M_{\text{BH}}$  defined in the parallel Figure 5.4. Left: mass histories obtained through the application of the broken power law scaling relation of Equation 5.8; Right: the same as the left panel but with blue curves derived from the employment of the log-quadratic  $M_{\text{BH}} - \sigma$  relation of Equation 5.9. As usual red-dashed lines are the ones of the S09 model, and with the function of term of comparison.

the conversion I am going to assume for further investigation about merger contribution is the following:

$$\log_{10}(M_{\text{BH}}/M_{\odot}) = \begin{cases} 2.20 \cdot \log_{10}(\sigma/200\text{kms}^{-1}) + 7.10 & \text{if } \sigma < 10^{1.25} \text{ km/s} \\ 1.10 \cdot [\log_{10}(\sigma/\text{kms}^{-1})]^2 & \\ -0.35 \cdot \log_{10}(\sigma/\text{kms}^{-1}) + 3.48 & \text{if } \sigma \geq 10^{1.25} \text{ km/s} \end{cases} \quad (5.10)$$

that finally produces the global accretion curves of Figure 5.6

This is the right moment to go deeper in the analysis and evaluate the role of mergers in the growing histories of SMBHs. Every passage is in analogy of what done in Chapter 4, with only the addition of the intermediate steps described in Section 5.1.

## 5.5 Contribution of mergers

In this Section I am going to retrieve the mean mass assembling histories of supermassive black holes that are evaluated from predicted BH-BH mergers. Again the contribution considered is the *maximal* one, that means black hole mergers are expected to occur whenever a subhalo enters the influence radius of the parent halo, i.e. we have a galaxy

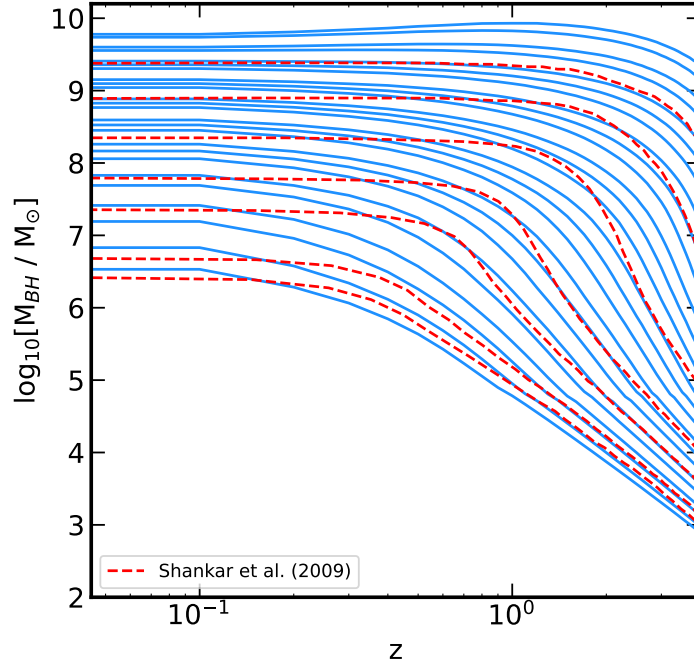


Figure 5.6: Total growths of supermassive black holes (blue lines) resulting from the employment of the relation described by Equation 5.10. Red dashed curves are always our reference term of comparison (by Shankar et al. (2009)).

merger. As anticipated this is quite improbable, since typically galactic mergers and the consequent merger of their hosted supermassive black holes require some time, called merging timescale. Also some mechanisms may prevent that the merger happens at all, but this is not to be discussed here. What is important is that in this framework the mean merger contribution subtracted from the global mean accretion is maximal and it is derived from the output of DECODE following exactly the passages enumerated in Section 4.2.4 with the additional conversions illustrated in this Chapter:  $M_{\star} \rightarrow \sigma$  and then  $\sigma \rightarrow M_{\text{BH}}$ . I would like to test for coherency between all the passages performed, hence I make an analogous plot as Figure 4.8 that shows the growing paths of supermassive black holes with final masses of different orders of magnitudes: one with a typical final mass of nearly  $M_{\text{BH}} \approx 10^7 M_{\odot}$  and another with final mass of the order of  $10^8 M_{\odot}$ . I also start from exactly the same values of  $M_{\text{halo}}$  at  $z = 0$ , so to build something comparable. What I get as output can be observed in Figure 5.7. In both panels the blue curves represent the mean subtracted growth, or in formula:  $\langle M_{\text{BH,tot}} \rangle - \langle M_{\text{BH,merg}} \rangle$ . They should trace the mean accretion of a typical supermassive black hole of that final mass due only to in-falling gas during phases of activity (AGN). Those are the histories to be compared to the model of Shankar et al. (2009) which, as already explained, is built

exactly considering AGN luminosity functions. The blue shaded areas around blue lines indicate a dex scatter arbitrarily added to get an estimate of the distance between the red-dashed curve and the blue one. On the left the scatter is of the order of  $\approx 0.25$ , while on the right panel the added scatter amounts to  $\approx 0.35$ . Such values have no real significance, but it is interesting to note that they are similar to the ones associated to intrinsic scatter in scaling relations from data points (see Section 5.2) that I do not take in consideration. Again the choice made to assign the scatter is in line of what done in Section 4.2.4. Another common feature as before is the need to adopt a scaling relation

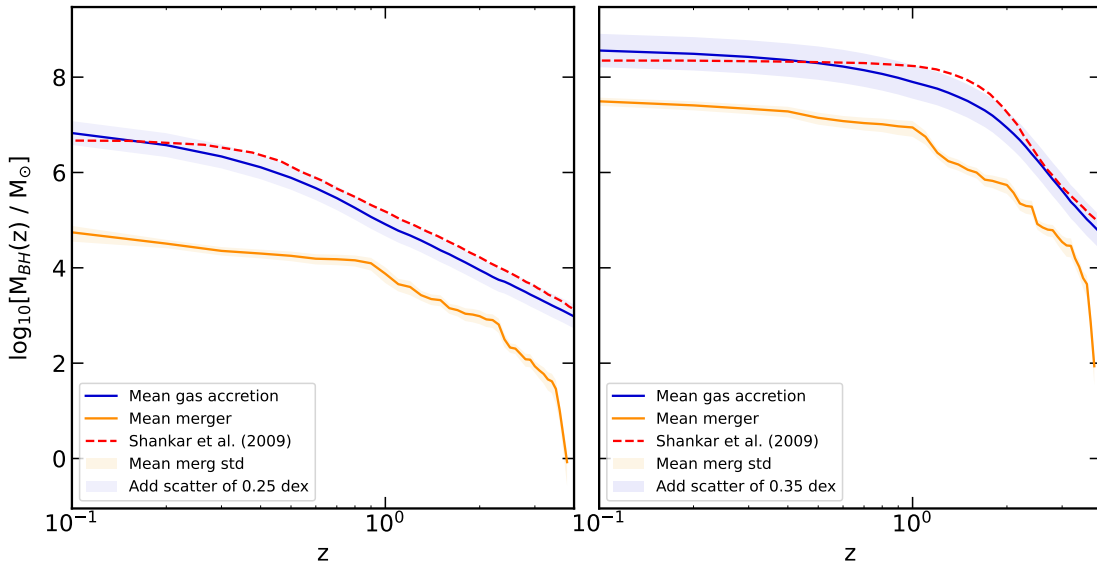


Figure 5.7: Left: blue curve traces the gas accretion history of a SMBH with a final mass of  $\approx 10^7 M_{\odot}$  as calculated from i) the application of the Equation 5.10 for the conversion  $\sigma - M_{\text{BH}}$  and ii) the subtraction of the mean contribution of mergers in that case, given by the orange curve (see Section 5.5 for the explanation of the derivation). The orange shaded area considers the  $1\sigma$  error of the mean track, while blue shaded area represents an arbitrarily scatter (of  $\sim 0.25$  dex) added so to enclose the red-dashed curve, referred to the S09 model. Right) Same as the panel on the left, but valid for a SMBH with a final mass of  $\gtrsim 10^8 M_{\odot}$ . In this second case the arbitrary chosen scatter is of  $\sim 0.35$  dex.

with a differential behaviour among the range of BH masses, in particular that flattens towards the low mass end and is steeper at higher orders. Actually the priority in this work has been given to the comparison with the model of Shankar et al. (2009) and not with observational data, that I repeat are local and rather dis-homogenized. Something that can be said is that if varied growing rates are expected at changing steps of BH mass, it is also as a consequence of the evolution of the host galaxy itself. Nevertheless what really matters is the possibility, with some adjustments, to investigate how all these considerations are related with each other through the use of the principal subject of this

project, the semi-empirical model DECODE.

I conclude this final Section by making a rapid comment about the role of mergers in the situations depicted in Figure 5.7, waiting for an expanded discussion about it in the next Chapter. Again the inferred maximum contribution of mergers is surprisingly low, even at relatively high black hole masses. Consistently with estimates found in Section 4.2.4, for a black hole of final mass around  $10^7 M_{\odot}$  this amounts to nearly 0.5 % of the mean global growth. It is ten times bigger for a final BH of mass  $\sim 10^8 M_{\odot}$ , about 6 %, but still much lower than what is considered the contribution of in-falling gas. The treatment of mergers at even higher black hole final masses need a deeper analysis for reasons already explained, i.e. the fact that at low redshift some undesired facts can happen that make the cumulative merger accretion exceed the global mean growth. Similar discussions can be done employing other scaling relations and/or different input SMHM relation, as mentioned in the previous Chapter. For this application I prefer not to investigate about the role of SMHM relation (e.g. [Moster et al. \(2018\)](#) model instead of our Reference-Model (RM)) because the galactic mass,  $M_{\star}$ , is subjected to repeated conversions and the exact propagation of all effects would be difficult to predict, hence to analyze.



# Chapter 6

## Results

The present Chapter aims at pointing out the principal results obtained from the whole procedure, especially for what regards the growing histories of supermassive black holes inferred through the methodology built so far. Two are the main branches along which the investigation has been oriented: understanding the role of scaling relations in the context of a semi-empirical model such as DECODE, and, on the other hand, using the information provided by the model itself, i.e. mean merger histories, so to refine and make constraints about these relations. Now that the general sense is given, I am going to describe the conclusions that I have come with when putting things together. In the first place some considerations are made about the type of scaling relation, either  $M_{\text{BH}} - M_{\star}$  or  $M_{\text{BH}} - \sigma$ , that is more convenient to employ in order to derive SMBH accretion curves in line with the ones that are calculated through the model of reference (Shankar et al. (2009)). In the second place I am going to define, in a more quantitative way, the amount of merger contribution to the global growth of a SMBH when a specific relation is used.

### 6.1 SMBH growth: scaling relations

The principal difficulty has been to find by hand parametrizations that could lead to concordance with the model of S09. Among the various attempts, some have been discarded because the resulting SMBH growing curves had a manifestly distant behaviour to S09. Constraints about scaling relations are acquired confronting the shapes of the black hole accretion tracks, meaning how much the  $M_{\text{BH}}$  predicted varies when changing  $M_{\star}$  ( $\sigma$ ) of small amounts. It means the derivative of scaling relations, or directly the slope if log-linear scaling relations are considered. This information has not to be confused with another that instead concerns the normalization, that is the scaling term between  $M_{\text{BH}}$  and  $M_{\star}$  ( $\sigma$ ). In the context of log-relations a scale becomes a constant and this means having the possibility of shifting upwards and downwards relations of an arbitrary amount with the only effect of moving the set of BH curves (e.g. Figure 4.5) up and down. Things are complicated by the fact that it is in principle not understandable from which halo masses (or stellar masses) to start to obtain the desired SMBH final masses. For example if one would like to achieve a SMBH with a certain final  $M_{\text{BH}}$  and adopts a

low normalization in terms of  $M_{\text{BH}}/M_{\star}$ , then it is necessary to invoke quite high values of  $M_{\star}$  to obtain the desired conversion. The behaviour of stellar mass growing curves is different according to the final value of  $M_{\star}$ , and a consequence of a bad calibration of the normalization is that one arrives at a mismatch between the shapes of SMBH growing curves evaluated from the conversion  $M_{\star} \rightarrow M_{\text{BH}}$  and the shapes of the model of reference (S09). Moreover the curves of the reference model itself are subjected to the possibility of being shifted if one changes the radiative efficiency to insert in the model and this implies a source of degeneration. The only way to come out of this issue is to have scaling relations correctly calibrated through observational data, that is not our case.

In choosing which parameters to insert in scaling relations, I have tried at least to maintain a sort of consistency with data points collected from various literature works, but without true adaptation to them. In the following Section I am going to summarize the types of scaling relations for which I have found good agreement with the reference model. Actually all what described so far did not take into consideration the possibility of evolving scaling relations. At the state of the art it is not well understood neither at what epochs in the past such relations have established neither if they have maintained the same form since then. Having a tool that consents to bring scaling relations in the past, linking them to other available information, could really represent a step forward in the study of co-evolution between supermassive black holes and their hosting galaxy properties.

### 6.1.1 Discussion: $M_{\text{BH}} - M_{\star}$ relation

All the literature works cited in Section 4.2.1 perform linear fits in the  $\log_{10}M_{\text{BH}} - \log_{10}M_{\star}$  plane and try to make constraints on the slope and normalization parameters. The results they obtain are not always in concordance between each other and seem to be slightly influenced by the galaxy properties, such as the morphological type (e.g. Sahu et al. (2019a), Sahu et al. (2019b)). Hence the perception is that a truly global relation, valid once and for all, struggles to exist. At the level of refinement of this project, I would like to find a general trend that could in some way be representative for each object type and for every mass step in the range considered. A deeper analysis could imply a separation of galaxies obtained from DECODE output catalogue into ellipticals and non-ellipticals by assuming some criteria based on the number of major mergers, e.g. that an elliptical galaxy is formed if a major merger has occurred in its past (Bournaud et al. (2007); Hopkins et al. (2009b); Hopkins et al. (2010); Shankar et al. (2013); Fontanot et al. (2015)). Another possibility may include the use of bulge-to-total ratios (B/T) as function of  $M_{\star}$  extrapolated e.g. from semi-analytical models (SAMs) that are usually implemented so to form stellar bulges through disc instabilities (e.g. Lacey et al. (2016b); Henriques et al. (2020); Oklopčić et al. (2017)). At that point the re-parametrization would be  $M_{\star, \text{tot}} \rightarrow M_{\star, \text{bulge}} \rightarrow M_{\text{BH}}$ , with the last step making use of another well known and discussed scaling relation that links the mass of the supermassive black hole and the mass of the galactic bulge. To this purpose I will mention in a while an interesting feature of  $M_{\text{BH}} - M_{\star, \text{bulge}}$  reported in Graham & Scott (2015) and suggesting something opposite to what retrieved in this project.

### Reference scaling relation

As extensively discussed in Section 4.2.3, a redshift-independent relation with manifest good agreement to the black hole accretion tracks calculated in Shankar et al. (2009) should have a change of steepness at a given mass range. Actually in order to reproduce the relatively slow growing rates towards low black hole masses, predicted in S09, such a change needs to be from a milder slope to a steeper relation. In other words the scaling relation employed to convert  $M_*$  to  $M_{\text{BH}}$  valid at each  $z$  presents a low mass plateau. The final form, reached after some adjustments as explained in Section 4.2.3, appears like:

$$\log_{10}(M_{\text{BH}}/M_{\odot}) = \begin{cases} 1.25 \cdot \log_{10}(M_*/10^{11}M_{\odot}) + 8.15 & \text{if } M_* < 10^{9.8} M_{\odot} \\ 1.65 \cdot \log_{10}(M_*/10^{11}M_{\odot}) + 8.63 & \text{if } M_* \geq 10^{9.8} M_{\odot} \end{cases} \quad (6.1)$$

that is Equation 4.10 with the parameters inserted made explicit. It is difficult to attribute to it a physical valence just looking at Figure 4.4. Data points are highly scattered and collected from samples of non homogeneous objects, and there is still the question of normalization which has been arbitrary inserted. Nevertheless this is what can be predicted with the available information: the observed data-sets, the growing curves of S09 and galaxy evolution obtained by the conversion of halo histories through the SMHM of the RM (see Section 2.3.1). About this latter, naturally things can be significantly different if one varies the SMHM of input. Again in Section 4.2.3 I have pointed out what happens to global growing BH curves if instead of RM stellar mass - halo mass, the one from Mo18 model is used (Moster et al. (2018)). In that occasion I have done the calculation just for high SMBH final masses because at low mass end no real concordance could be found due to the scarce evolution of SMHM relation in that part (see Figure 3.5). Hence I decide to continue the analysis just with the employment of the RM SMHM relation. A solution of the type 6.1 is thus in line with the findings of a model (Shankar et al. (2009)) that starts from different observables and reconstructs mean black hole gas-accretion tracks for given radiative efficiencies and Eddington ratios. A note of caution is at this point demanded. The results from the model itself may not be fully reliable, or at least less certain at higher redshift. This is because AGN luminosity functions are badly estimated at that  $z$  due to difficulties in observing faint distant objects. The curves in Figure 4.3 are based on an extrapolation of AGN LF at low black hole masses (i.e. low AGN luminosities) and that would potentially compromise the shape of curves at that epochs. Nevertheless I continue following that road and introduce an alternative to the broken power law relation which is to add a  $z$ -dependent term.

### Redshift evolution (?)

The time evolution of scaling relations is difficult to investigate in high redshift observations. As mentioned, studies are often based on broad-line AGN samples, with BH masses estimated through virial methods. The underlying assumption is that broad-line AGNs behave the same way as any other galaxy and follow the same scaling relations, which as seen in Reines & Volonteri (2015) may not be true. It has to be said that most observational studies have found mild or null evolution of scaling relations (e.g. Shields et al. (2003); Jahnke et al. (2009); Salviander & Shields (2013); Schramm & Silverman

(2013); Shen et al. (2015)). For instance Jahnke et al. (2009) find no  $z$  evolution of  $M_{\text{BH}} - M_{\star}$  relation when comparing objects at  $1 < z < 2$  with local  $M_{\text{BH}} - M_{\star, \text{bulge}}$  relations. Indeed the evolution of the scaling relation is often addressed by confronting the high-redshift  $M_{\text{BH}} - M_{\star}$  to the same relation scaled from the local bulge mass relation. The passage from  $M_{\text{BH}} - M_{\star}$  plane to the  $M_{\text{BH}} - M_{\star, \text{bulge}}$  one implies a redistribution of stellar mass from galactic disc to form a bulge and this can happen both because of mergers or through secular processes. The works above-cited indeed find that many galaxies at high  $z$  have a disc component. Hence the mild evolution coming out from observations would indicate that no addition of stellar mass is required to build the bulges, and the  $M_{\text{BH}} - M_{\star, \text{bulge}}$  relation, from high redshift galaxies. Also, the presence of discs at high  $z$  could imply the abundance of under-massive bulges with the consequence that time evolution of  $M_{\text{BH}} - M_{\star, \text{bulge}}$  relation may be stronger than the one with total  $M_{\star}$ . This suggests the idea that the assembly of BHs takes place before the assembly of their host galaxy bulges. More recently, Ding et al. (2020) used 32 X-ray selected broad-line AGNs at  $1.2 < z < 1.7$  and showed that the ratio  $M_{\text{BH}}/M_{\star}$  and  $M_{\text{BH}}/M_{\star, \text{bulge}}$  are larger than in the local Universe ( $\sim 0.43$  dex), that means such relations are slightly offset towards more massive BHs or lower stellar mass/bulge mass compared to the relation at  $z = 0$ . To sum up it can be said that there is no general consensus on the time evolution of the  $M_{\text{BH}} - M_{\star}$  mean relation and the only way to get to a clearer framework is to conduct more observations and analysis at high redshift. In any case, for the purposes of this project, it would be interesting to see which is the effect on the BH growing curves of increasing with  $z$  the normalization of the  $M_{\text{BH}} - M_{\star}$  relation. This is done by adding a term in the single-slope log linear relation:

$$\log_{10}(M_{\text{BH}}/M_{\odot}) = \alpha \cdot \log_{10}(M_{\star}/10^{11}M_{\odot}) + \beta + \gamma \cdot \log_{10}(1 + z), \quad (6.2)$$

where  $\gamma$  is a new parameter to be arbitrarily introduced. To maintain a continuity with what previously found I test the following solution: starting from the same slope  $\alpha$  and similar normalization  $\beta$  attributed to the high mass side of the broken power law in Equation 6.1, i.e.  $(\alpha, \beta) = (1.65, 8.70 \text{ dex})$ , I then assign a different  $\gamma$  value according to the final galactic mass. Specifically I have opted for a milder evolution in correspondence of SMBHs with final higher masses, whose shapes of accretion curves were already well described by a non-evolving scaling relation similar to the one now in consideration; towards smaller SMBH final masses instead I consider a more important evolution in normalization that has the same function as the introduction of a flatter non evolving scaling relations, i.e. the one of rising up the values of black hole masses converted from a fixed  $M_{\star}$ . This implies less deep growing rates ( $dM_{\text{BH}}/dz$ ) at the considered redshift ranges, but a speed up in terms of the whole accretion mechanism since the birth of the black hole. As boundary stellar mass I have considered  $M_{\star} \approx 10^{11} M_{\odot}$  since, by looking at Figure 3.5, it is where the evolution of SMHM is being already rising up. Hence above that  $M_{\star}$  I include a  $z$ -evolutionary term of the type  $M_{\text{BH}} \propto M_{\star} \cdot (1 + z)^{0.2}$ , i.e.  $\gamma = 0.2$ ; below that final  $M_{\star}$  I double the value of  $\gamma$  and adopt a relation  $M_{\text{BH}} \propto M_{\star} \cdot (1 + z)^{0.4}$ . The variation of the scaling relation between  $z = 0$  and  $z = 4$  can be visualized in Figure 6.1 represented by the colored shaded area. It characterizes the increase in normalization with growing  $z$ . In the Figure I also show as red dashed line the broken power law, our

reference  $M_{\text{BH}} - M_{\star}$  relation, in comparison. It can be said that the  $z$ -evolution assumed is actually very mild and it is well within the scatter in the  $\log_{10}M_{\text{BH}} - \log_{10}M_{\star}$  relation.

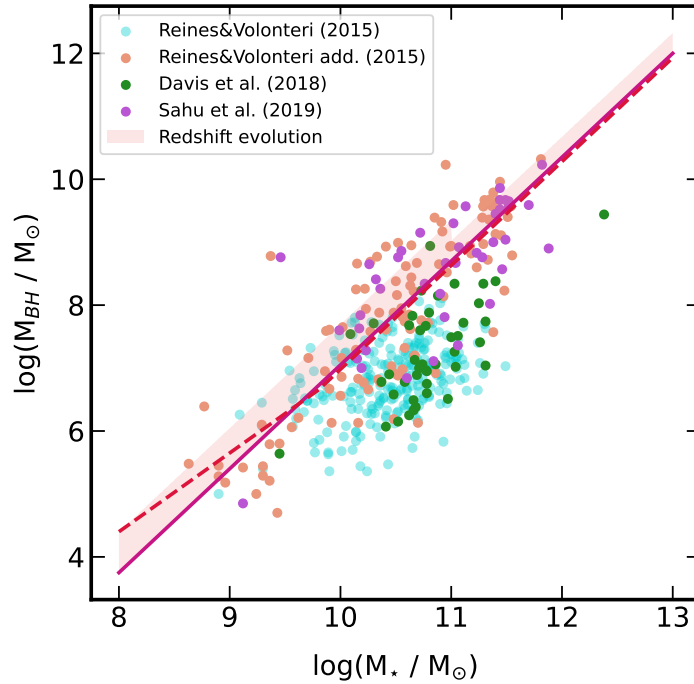


Figure 6.1:  $M_{\text{BH}} - M_{\star}$  scaling relations in the log - log plane. Violet straight line is the chosen log-linear relation at  $z = 0$  with slope and normalization given by  $\alpha = 1.65$  and  $\beta = 8.70$  dex respectively. To that a differential redshift evolution is applied and represented as the pink shaded area. Last value of  $z$  taken is 4. Broken power law of reference is also displayed as red dashed line. This is applied without an evolution in  $z$ .

The tracks of BH global growing that emerge from an evolving scaling relation are illustrated in Figure 6.2. Different colors indicate the lines that have been obtained with different redshift evolution treatments. Towards lower masses, at high  $z$ , the curves still have the tendency to fall down slightly faster than the prediction of S09, but the overall trend is reproduced. Naturally one should subtract the contribution of mergers also in this case and this is done respecting the usual method adopted during the whole project. The results presented in Figure 6.3 are again for typical supermassive black holes of final masses of  $M_{\text{BH}} \approx 10^7 M_{\odot}$  and  $M_{\text{BH}} \approx 10^8 M_{\odot}$ . The orange lines that reconstruct the cumulative merger growths appear more discontinuous and with less smooth trends because the scaling relation in use is continuously changing its normalization with redshift. With a choice of this type I obtain global merger contributions of  $\sim 0.3\%$  in the case of the smaller black hole and of  $\sim 5-6\%$  for the more massive one. Discrepancies with

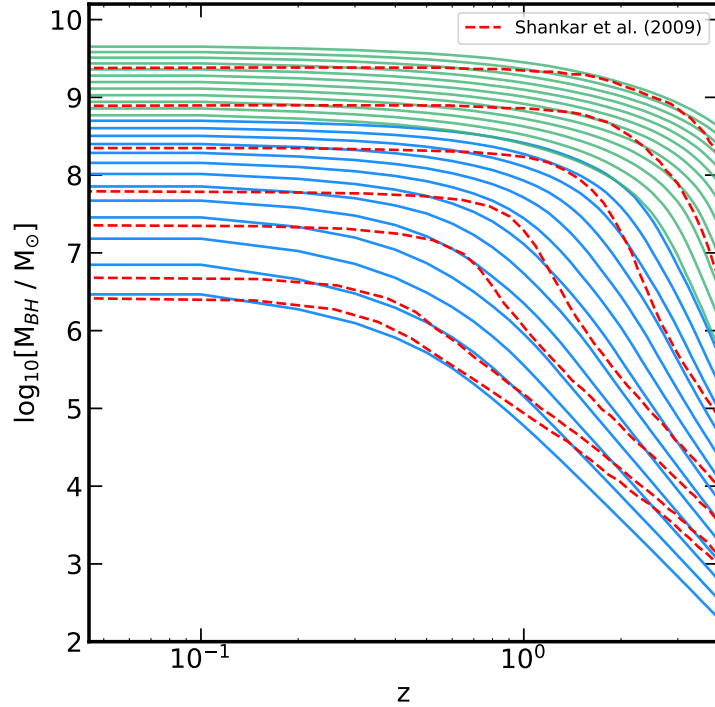


Figure 6.2: Global (gas + mergers) growing of SMBH of different final masses obtained through the conversion of  $M_*$  with the  $z$ -evolving log-linear relation. Blue and green curves start from the same relation defined at  $z = 0$ , then depending on the  $M_*(z = 0)$  they are assigned with a stronger ( $\gamma = 0.4$ ) redshift evolution (blue curves) or milder ( $\gamma = 0.2$ ) redshift evolution (green curves).

the reference model of S09 are of the order of 0.50 dex towards low mass end and always of the order of  $\sim 0.3$  dex at higher masses. This is not bad in consideration to the fact that I have treated the question of redshift evolution in a quite rough way, and probably a further investigation, e.g. adopting different scaling relations or forms of  $z$ -evolution, is necessary. Anyway this is to show another possible approach to the study of SMBH scaling relations in the context of semi-empirical models. Now that I have introduced in the discussion the chance of redshift evolving scaling relations and mentioned about the  $M_{\text{BH}} - M_{*,\text{bulge}}$  relation, I would like to briefly look at an interesting aspect about the latter. In [Graham & Scott \(2015\)](#), authors suggest that the relation between black hole and bulge mass becomes steeper, quadratic like, at roughly  $M_{*,\text{bulge}} \lesssim (0.3 - 1) \times 10^{11} M_{\odot}$ . Since this is nearly an opposite behaviour of what corresponds to our reference  $M_{\text{BH}} - M_*$  relation it would be nice to make a sort of parallelism between them, by applying same procedures. This is done in the following Section.

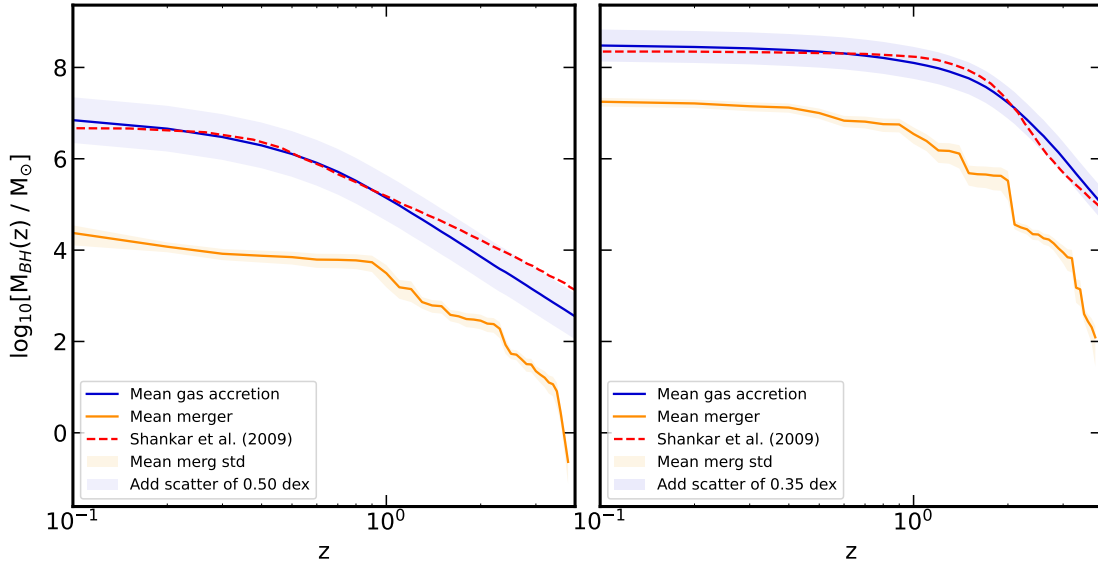


Figure 6.3: Mean supermassive black hole accretion tracks subtracted for the merger contribution. Left: history of a SMBH with final mass of the order of  $M_{\text{BH}} \approx 10^7 M_{\odot}$ ; Right: analogous but valid for a SMBH with final mass of the order of  $M_{\text{BH}} \approx 10^8 M_{\odot}$ . Blue curves in both panels indicate the retrieved mean accretion due to gas (global - mergers) with an additional scatter represented by blue shaded areas. Orange lines are the mean merger contributions,  $\langle M_{\text{BH,merg}} \rangle$ , extrapolated from DECODE through all the conversion steps that include a  $z$  evolving  $M_{\text{BH}} - M_{\star}$  scaling relation, with dashed regions around them the error of the mean. Red dashed curves are from the model of S09.

### 6.1.2 $M_{\text{BH}} - M_{\star,\text{bulge}}$ Scaling relation

In this Section I am going briefly through some aspects of the relation between the black hole mass and the stellar mass of the spheroidal component of a galaxy, i.e.  $M_{\text{BH}} - M_{\star,\text{bulge}}$ . Having an idea of how such a relation can be defined and change through cosmic time is important because it gives insights into the evolutionary scenario which is jointly related to the central supermassive black hole and the central region of a galaxy. In [Graham & Scott \(2015\)](#), authors make considerations about  $M_{\text{BH}} - M_{\star,\text{bulge}}$  relation that can have consequences for what just said about growing histories. They start by noting that a near-linear scaling relation between  $M_{\text{BH}}$  and host spheroid stellar mass,  $M_{\star,\text{bulge}}$ , is not perfectly efficient in describing the black hole - spheroid interconnection (see also [Graham \(2012\)](#)), and that for the description of Sérsic spheroids a non-linear relation would be more suitable. To clarify, Sérsic spheroids are elliptical galaxies and bulges of disk galaxies that do not have partially depleted cores, that instead happens for the so called core-Sérsic galaxies (e.g. [Graham & Driver \(2005\)](#); [Graham et al. \(2003\)](#)). Objects of the first type have typically B-band absolute magnitudes of  $M_{\text{B}} \gtrsim -20.5$

$\pm 1$  mag and Sérsic indices  $n \lesssim 3 - 4$ . Actually [Graham \(2012\)](#) has pointed out that the relationship between  $M_{\text{BH}}$  and  $M_{\star, \text{bulge}}$  pertained to that galaxies should be better described by a near-quadratic relation as subsequently confirmed in [Graham & Scott \(2013\)](#) and [Scott et al. \(2013\)](#). In these works it has been observed that only at high masses  $M_{\text{BH}} \gtrsim 10^8 M_{\odot}$  a near-linear  $M_{\text{BH}} - M_{\star, \text{bulge}}$  is evident. Due to the scatter in the  $M_{\text{BH}} - M_{\star, \text{bulge}}$  diagram and the location of bright Sérsic galaxies at the high-mass end of the near-quadratic relation, surveys that have not probed enough the region below  $M_{\text{BH}} \approx 10^7 M_{\odot}$  can already miss the bend in the scaling relation (e.g. [van den Bosch et al. \(2012\)](#); [McConnell & Ma \(2013\)](#); [Feng et al. \(2014\)](#)).

These scaling relations as said are important for several reasons. Given the broken, or rather bent,  $M_{\text{BH}} - M_{\star, \text{bulge}}$  relation, it implies that within Sérsic galaxies, the supermassive black holes grow more rapidly than the stellar spheroid ([Graham \(2012\)](#)). That is, there is no conjunct and lockstep growth of black holes and bulges in these galaxies since the  $M_{\text{BH}}/M_{\star, \text{bulge}}$  ratio is not a constant value. An additional, connected, interesting aspect regards feedback from supermassive black holes (e.g. [Page et al. \(2012\)](#); [Wurster & Thacker \(2013\)](#); [Fanidakis et al. \(2013\)](#)) that is believed to regulate star formation in the spheroid and provide potential solution to the overabundance of massive galaxies predicted by dark matter only simulations. This process has been also invoked to produce the turnoff in the galaxy luminosity function at high luminosities (e.g. [Benson et al. \(2003\)](#); [Bower et al. \(2006\)](#); [Croton et al. \(2006\)](#)). The  $M_{\text{BH}} - M_{\star, \text{bulge}}$  relation then tends to flatten and to settle into a relation with a slope close to unity for the brighter core-Sérsic galaxies ([Graham \(2012\)](#)). The presence of partially depleted cores in these bigger spheroids is thought to indicate that they and their black hole have formed through simple, additive, dry major merger events that led to the establishment of the near-linear  $M_{\text{BH}} - M_{\star, \text{bulge}}$  relation. The process of 'kinetic' or 'radio mode' AGN feedback may therefore subsequently maintain such a relation.

Now that a general framework is given, I report what are the findings of [Graham & Scott \(2015\)](#), who investigate AGNs with low mass black holes using data from many authors so to avoid possible biases. I do not describe here how BHs and relative spheroid masses have been calculated, what matters for our purposes is to understand location of these data (nearby objects) in the  $\log_{10}M_{\text{BH}} - \log_{10}M_{\star}$  plane. This is showed in [Figure 6.4](#), where data points collected are represented by colored dots, the broken power law relation related to  $M_{\text{BH}} - M_{\star, \text{bulge}}$  corresponds to the blue line and the red dashed line is our reference  $M_{\text{BH}} - M_{\star}$  relation. Even though these last two do not constitute the same type of relation they have been put together in the plot because the ranges of spheroidal masses considered are overlapping. Actually massive elliptical galaxies are totally described by bright core-Sérsic spheroids, hence towards high mass end we should have  $M_{\star} \approx M_{\star, \text{bulge}}$ . The blue line equation is given by:

$$\log_{10}(M_{\text{BH}}/M_{\odot}) = \begin{cases} 2.20 \cdot \log_{10}(M_{\star, \text{bulge}}/10^{11}M_{\odot}) + 9.35 & \text{if } M_{\star, \text{bulge}} < 10^{10.5} M_{\odot} \\ 1.10 \cdot \log_{10}(M_{\star, \text{bulge}}/10^{11}M_{\odot}) + 9.00 & \text{if } M_{\star, \text{bulge}} \geq 10^{10.5} M_{\odot} \end{cases} \quad (6.3)$$

whit slopes and intercepts inserted so to respect the mean values reported in [Graham & Scott \(2015\)](#). Once the scaling relation is defined it would be interesting to include it in the process of deriving growing curves of SMBH as done so far. However it is

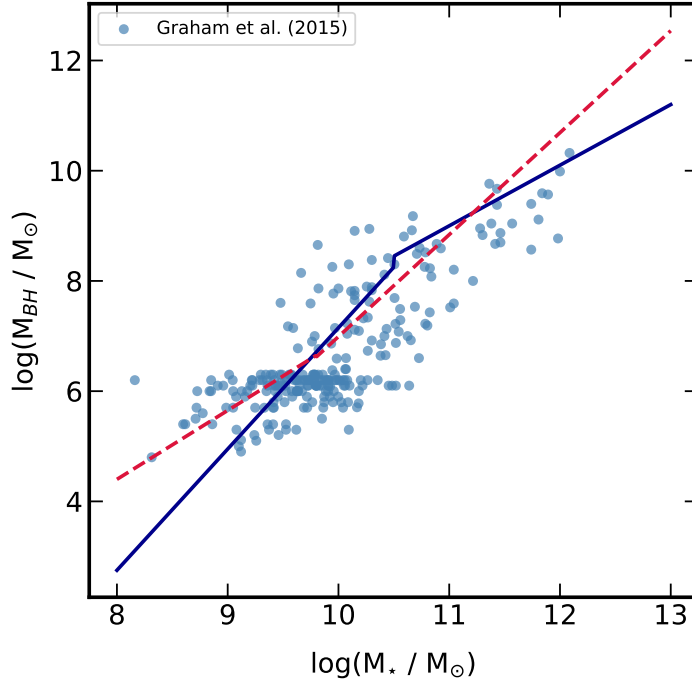


Figure 6.4: Scatter plot of the data sample extracted from [Graham & Scott \(2015\)](#) and representative of the  $M_{\text{BH}} - M_{*,\text{bulge}}$  scaling relation. The solid blue line corresponds to the broken power law defined in Equation 6.3, with slopes and normalizations similar to the ones found in [Graham & Scott \(2015\)](#), but adjusted in order to reproduce growing black hole curves slightly more in agreement with [Shankar et al. \(2009\)](#) model (see Figure 6.6 later on). This refers again to the scaling relation between the black hole mass and the stellar mass of the spheroidal component of the hosting galaxies. The dashed-red line is the  $M_{\text{BH}} - M_*$  relation of reference, described by Equation 6.1 and valid for the total stellar mass of the galaxy. It is inserted so to have an idea of the different behaviours.

not advisable to use  $M_{\text{BH}} - M_{*,\text{bulge}}$  relation, instead of the one with the total mass, in a straightforward way because the information at our disposition only concerns the growing history of the whole galaxy which is not the same as the one of bulges. An appropriate treatment would require to separately derive, at different galaxy mass steps, the evolution of the bulge component and then use it for the conversion to black hole masses. This is far from trivial and implies the assumption of a bulge formation process, which can only be addressed through analytical models to be implemented in hydrodynamic simulations. Therefore, considering all of this in full details is something well beyond the scope of our project, which has the prerogative of being simple and not relying on pre-assumed models. In any case something can be inferred by looking at Figure 6.5 from [Fu et al.](#) (in preparation). Thick blue curves represent mean growth of galaxies with different final

masses, extrapolated by the mean total accretion of DECODE halos (van den Bosch et al. (2014)) converted through the RM SMHM relation. The formation and evolution of the bulge are then calculated by the implementation of simple models, e.g. by assuming that once a major merger occurs,  $M_{*,1}/M_{*,2} > 0.25$ , the descendent galaxy is strictly elliptical with bulge-to-total ratio  $B/T = 1$ . For a complete descriptions of the models adopted I leave to the lecture of Fu et al. (in preparation). In all panels of the Figure 6.5 the curves of bulge accretion are colored in orange, while green lines are accounting for the disks. It can be noted that, for low massive galaxies, the growth of the bulge follows nearly the same rate as the growth of galaxies, naturally scaled for an almost fixed fraction. For higher stellar masses, e.g. above  $M_*(z=0) \sim 10^{10.5} M_\odot$ , the bulge has a rapid growth until it becomes the dominant component of the galaxy (massive elliptical galaxy) for the most part of their accretions. Because of such diversity in the evolution of the bulge

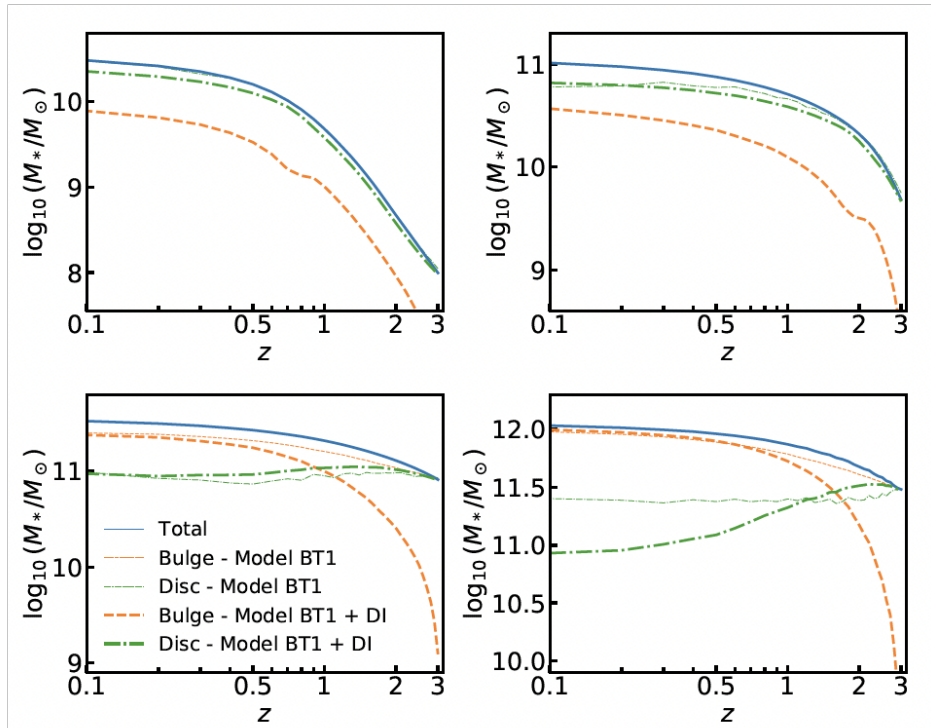


Figure 6.5: Figure taken from Fu et al. (in preparation) showing the mean evolution of the galactic components, e.g. the bulge (orange curves) and disk (green curves), as evaluated from a procedure explained in the paper above-mentioned. Basically the total galaxy growth (solid blue lines) is the same as the one considered in this work and the bulge and disk evolution are extrapolated adopting some recipes based on the occurrence or not of major mergers in the mean merger histories of the considered galaxies with different final masses.

component in galaxies, it is not easy to retrieve general solutions regarding the growth of SMBHs starting from  $M_{\text{BH}} - M_{\star, \text{bulge}}$  relations. In order to keep things on a simple ground the method I adopt is the following:

- i) I calculate the galaxy growing histories in the same way as always done, using the RM SMHM relation;
- ii) For galaxies with  $M_{\star}(z = 0) \lesssim 10^{10.7} M_{\odot}$ , I re-scale the total stellar mass at each redshift for the same quantity of  $\sim 1/4$  to get an estimate of the  $M_{\star, \text{bulge}}$ . I convert these bulge masses to black hole masses adopting the scaling relation defined by Equation 6.3. Without any kind of evolution that would produce black hole growing curves with far too steep descending towards high redshift. Indeed, I am not considering the  $M_{\text{BH}} - M_{\star}$  relation that refers to the total galactic mass; the bulge and the supermassive black holes are expected to have connected growth but not at the same path. According to the study of [Ding et al. \(2020\)](#) I apply a redshift evolution of the kind  $\propto (1 + z)^{1.7}$  which is substantial but consistent with data found at  $1 < z < 2$  (see their Figure 13);
- iii) For galaxies with  $M_{\star}(z = 0) \gtrsim 10^{10.9} M_{\odot}$  the situation is slightly more complicated because bulges have an almost exponential growth till they reach the entire galaxy mass. In this case I do not scale the mass of the galaxies and maintain it at each redshift step. I subsequently apply the same  $M_{\text{BH}} - M_{\star, \text{bulge}}$  relation of Equation 6.3 but this time with much milder redshift evolution, of the type  $\propto (1 + z)^{0.2}$  to compensate the fact that  $M_{\star} > M_{\star, \text{bulge}}$  at high  $z$  (see Figure 6.5). At that masses, at a certain point, I have the brusque change of the slope of the scaling relation.

This is a very simplistic way to treat a complex issue and all values of parameters used are not to be considered 'real' in a physical term. The intent is to have a qualitative understanding of the processes that regulate the growth of a supermassive black hole and how they could be investigate in a context like this. The plot I obtain following the procedure just described is given in Figure 6.6. Naturally the agreement with the curves of S09 can not be perfect because of the very approximated process employed. Nevertheless it is neither extremely bad and at least it gives the possibility to make some considerations. About the Sérsic and core-Sérsic separation, [Graham & Scott \(2013\)](#) identify two regimes of black-hole growth: gas-dominated processes occurring in Sérsic galaxies and gas-poor (dry) major merging forming the core-Sérsic galaxy sequence. In this scenario, it seems that the low mass spheroids grow their black holes rapidly, relative to the spheroids, through the accretion of gas and stellar material. Moreover the growth of the black hole and the spheroid is in a certain measure linked because they both rely on the same reservoir of cold gas in the galaxy. This could explain the establishment of the quadratic or super-quadratic scaling relation  $M_{\text{BH}} - M_{\star, \text{bulge}}$ . Such a mechanism continues until a critical point is reached, that is when the mass of the spheroid rises up approximately the value of  $M_{\star, \text{bulge}} \sim 10^{10.5} M_{\odot}$ . At this stage radio-mode feedback from the black hole may become important. This means that large part of the energy of an active galactic nucleus is released in a kinetic form via radio-emitting jets, which are able to expel the majority of the galaxy's cold gas supply and prevent this from cooling

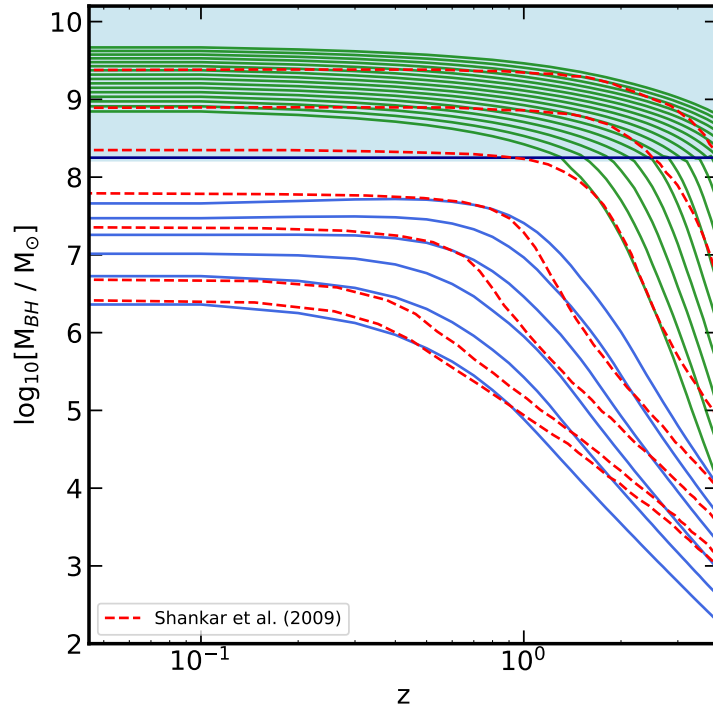


Figure 6.6: Supermassive growing curves calculated following the procedure outlined in Section 6.1.2. In particular the blue curves (point ii) of the list present in the same Section) are those that, according to the separation made in [Graham & Scott \(2015\)](#), would trace the global accretion of black holes within the so called Sérsic galaxies; while the green ones (point iii) of the list) are related to the core-Sérsic galaxies. The solid blue line in correspondence of  $M_{\text{BH}} \approx 1.8 \times 10^8 M_{\odot}$  gives the turning point of the broken power law type relation adopted (Equation 6.3). The blue shaded region should indicate the SMBH growing phases dominated by merger processes.

again. Actually this feedback is not thought to be the responsible for the un-setting of the scaling relation between  $M_{\text{BH}}$  and the host spheroid. With little reservoir to accrete from, the supermassive black hole now grows predominantly through dry merging with other massive black holes, leading to the core-Sérsic relation with linear growth of the black hole and the host spheroid. Indeed, the growing curves in Figure 6.6 seem to concord with such an explanation. The ones colored in blue are referred to hosts with smaller final masses (ii) and behaves like Sérsic galaxies in a certain sense. These objects have very low probability of having had a major merger in their past, hence their growth is almost totally due to gas accretion processes. This fact would be clarified in the following Sections when the percentage of merger contribution will be given at each step of mass. For now this just comes out from the behaviour of curves (blue), which are entirely confined within that range of mass populated by Sérsic galaxies according to [Graham & Scott \(2015\)](#). The turning point is indicated in the Figure 6.6 as a thick and horizontal

dark-blue line, at  $M_{\text{BH}} \approx 1.8 \times 10^8 M_{\odot}$ , and the shaded region indicates the subsequent change of slope in the  $M_{\text{BH}} - M_{\star, \text{bulge}}$  relation, speaking in strictly terms, and a possible change in the growing mechanism as hypothesized in [Graham & Scott \(2015\)](#). Green curves are those obtained applying the passages of point (iii) in the previous list. Indeed it is plausible that in that context, at a certain point, the total growth is regulated by mergers because of higher discrepancies between green curves and the ones of S09. That is again addressed in next Sections. Anyway, I am still in the field of speculation and, since the steps made to calculate that curves are subjected to high amount of uncertainty, they should be considered with caution.

What has been depicted so far is or would be another useful application of the very flexible procedure adopted in this work. It allows to investigate about scenarios that lead to the formation and evolution of supermassive black holes. Before finally passing to the part concerning the role of mergers, I conclude the series of scaling relations by briefly discuss the results found in Chapter 5 about the  $M_{\text{BH}} - \sigma$  relation.

### 6.1.3 Discussion: $M_{\text{BH}} - \sigma_{\star}$ relation

The  $M_{\text{BH}} - \sigma_{\star}$  scaling relation is possibly the one most studied and discussed since it is believed the most fundamental of all black hole - host galaxy scaling relations ([Marsden et al. \(2020\)](#)), and Chapter 5 is entirely devoted to it. In here I just briefly summarize the main results.

The  $M_{\text{BH}} - \sigma$  relation is thought to arise as a consequence of AGN feedback mechanisms (review of [King & Pounds \(2015\)](#)), specifically the black hole in these models is expected to grow until it reaches a critical point (as mentioned in the previous Section) at which it is massive enough to drive energetic/high-momentum large scale winds that can potentially remove residual gas and inhibiting further star formation and black hole growth. The limiting mass reached by the black hole, which is dependent on the potential well of the host, would provide an explanation for the existence of the  $M_{\text{BH}} - \sigma_{\star}$  relation. Indeed by looking at data points collected in Figure 5.1, it can be observed that such a scaling relation has a tight and rather well established behaviour at higher masses, while towards low mass end the situation is less clear and subjected to higher scatter. This should be investigated a little more, but in the meantime, for our purposes, I would like to introduce a scaling relation that can be suitable in the providing of black hole accretion curves. This is done after having calculated the velocity dispersion  $\sigma$  ( $\text{kms}^{-1}$ ) from the stellar mass of the galaxy, following the steps highlighted in Section 5.1. Such a calculation implies as 'input' other scaling relations, i.e. the  $M_{\star} - R_e$  and  $M_{\star} - n$ , with  $R_e$  and  $n$  being the effective radius (alias half light radius) and the Sérsic index respectively. This does not come without problems because the just mentioned relations are subjected to errors themselves. However since all quantities at the end enter in logarithmic units, each systematic is transformed into a constant value that can be adjusted almost freely as needed because of the degeneration to which normalization is subjected (see Section 5.3). After that it has been possible to calculate the  $M_{\text{BH}}(z)$  histories starting from velocity dispersions and by the use of an arbitrarily decided scaling relation. First choices have been naturally oriented to log-linear type scaling relations because of all the literature works. However a solution like that, in parallel to what noted also in the case of  $M_{\text{BH}} -$

$M_*$  relation, seems not efficient in reproducing black hole growing curves compatible with the model of S09. Hence I turn the attention towards other types of relation, that would include changes of slope (thus of growing rates when converted). A broken-power law relation proved to be not bad, but the apparently much diverse slopes considered make the curves to have non smooth trends. Hence I decide to use a log-quadratic relation that is turned in a log-linear one at low masses to avoid taking values in correspondence of the descending branch of the parable. The relation of reference in this occasion is finally given by Equation 5.10. The resulting mean global growing paths of supermassive black holes are showed in Figure 5.6 and the accretion curves subtracted by the mean merger contribution (for SMBHs of  $\approx 10^7$  and  $10^8 M_\odot$  final masses) are displayed in Figure 5.7. For this type of application I do not further consider the role of a redshift dependent term since something related to the evolution is already inserted during the derivation of  $\sigma_*$  from  $M_*$ , when calibrating the relation  $M_* - R_e$  (see Equations 5.3, 5.5, 5.6). Indeed, due to this, the resulting growing curves are already 'enhanced' at higher redshift and leads also to slightly decreasing behaviours towards higher masses (where  $M_*(z)$  are characterized by very slow evolution).

Now that all aspects about scaling relations have been analysed is the time to discuss about how much is the contribution of mergers derived from the combination of DECODE and such relations. In particular the main goal is to understand: i) what is the amount of mass acquired *at most* by a supermassive black hole from mergers; ii) how much this depends on the scaling relation employed; iii) what happens at high masses (not yet investigated in previous treatment) and what if a merging timescale is introduced to limit the global contribution of mergers at that range. All of these issues will be explained in the next Section.

## 6.2 Mergers

Despite the fact that I have always led the calculation of merger contribution as a final passage in the procedure outlined, it is the essential information retrieved from the model. Actually, as explained in Chapter 2, what confers to DECODE the characteristic of being statistical is the treatment of mergers themselves. Merger trees are derived from probability distribution functions and not through hydrodynamic simulations that imply the movement of dark matter particles according to some physical mechanisms of input. The main advantages of this are the extreme rapidity and the almost limitless resolution achievable by the model in the determination of number of mergers. To the other side, results obtained by the application of this approach are inevitably intended to trace *mean* behaviours rather than specific and detailed growing histories. Indeed any time I am going to speak about merger contribution, what I am supposing is the average cumulative accretion that a supermassive black hole of a certain final mass has gained from mergers. The way to build it is explained throughout the previous Chapters and it is not repeated here. The aspect that is instead important to underline at this point is how well the contribution of mergers can be predicted by the employment of scaling relations. In other words I would like to investigate the interplay between the adoption of a specific scaling-relation and the amount of merging mass inferred through it. At the

end, this could help to better define the suitability of a choice with respect to another one.

### 6.2.1 Global merger contribution: percentages

It has been repeated many times the fact that, up to now, the contribution of merger considered in the whole project is a maximal one. Therefore each sub-halo that have ever entered the sphere of influence of another halo (at the in-falling redshift  $z_{\text{inf}}$ ) is taken into account in the calculation. The real situation is naturally different and, at least for what concerns galaxy mergers, this imply some time from the moment called  $z_{\text{inf}}$  to the one of complete merger, as mentioned in Section 2.2.4. Nevertheless the approximation adopted here may still represent a good one, especially in the case of low mass objects in which the impact of mergers is very limited. To have an idea: for a galaxy with a final mass of the order of  $M_{\star} \approx 10^{10.8} M_{\odot}$ , the probability that a major merger ( $M_{\star,1}/M_{\star,2} \gtrsim 0.25$ ) has occurred in its past is of about 10 %. This value rises up to  $\sim 70$  % for galaxies with final masses of the order of  $M_{\star} \approx 10^{11.5} M_{\odot}$ . Hence, in these latter cases, it is plausible that adopting maximal merger histories is no more a comfortable solution.

For what concerns black holes, things are not so different because, in the first place, their masses are converted starting from stellar ones through our agreed scaling relations. The way they are involved in this scenario, and how different it becomes if one relation is selected instead of another, can be evaluated taking the final ( $z = 0$ ) mass ratio  $\langle M_{\text{BH,merg}} \rangle / \langle M_{\text{BH,tot}} \rangle$  for each choice of scaling relation and mass step. In practice I have obtained mean cumulative merger accretions for all mass steps related to the sets of global black hole growing curves (e.g. Figure 4.5) and compared their final values to what is the prediction of the total final mass of a supermassive black hole. The percentage contribution of mergers as a function of  $\log_{10} M_{\text{BH}}(z = 0)$  can be visualized in the Figure 6.7. Points labelled with 'log-linear1', 'log-linear2' and 'log-linear3' are referred to log-linear  $M_{\text{BH}} - M_{\star}$  relations parameterized by values of slope ( $\alpha$ ) and normalization ( $\beta$ ) found in Table 4.1. Red squares represent instead results coming out from the use of the reference  $M_{\text{BH}} - M_{\star}$  broken power law type relation, described by Equation 6.1. Finally orange points are the ones retrieved through the modified log-quadratic  $M_{\text{BH}} - \sigma$  relation (see Equation 5.10). Gray horizontal dashed lines sign the moments at which the contribution of mergers to the total growth is of 50 % and 100 % (total). There are many interesting aspects that can be inferred by looking at Figure 6.7.

- 1) First of all, the plot gives the immediate impression about the impact the choice of a scaling relation has in performing the calculation. Starting from exactly the same stellar masses, the scenarios that are depicted can be very different. In particular, it seems that if one opts for a pure linear relation, i.e.  $\alpha = 1.00$  (violet squares), then the contribution of merger becomes predominant (more than a half) already at black hole final masses of  $\sim 10^{7.5} M_{\odot}$  and then grows up in a rather exponential mode. The situation is mitigated when a slight steeper slope is considered (blue points corresponding to  $\alpha = 1.25$ ) and becomes much distant when a slope of the order of 1.50 is adopted. In here I am referring just to the slopes of relations because the normalization is cancelled out in the ratio, hence has no significance in here.

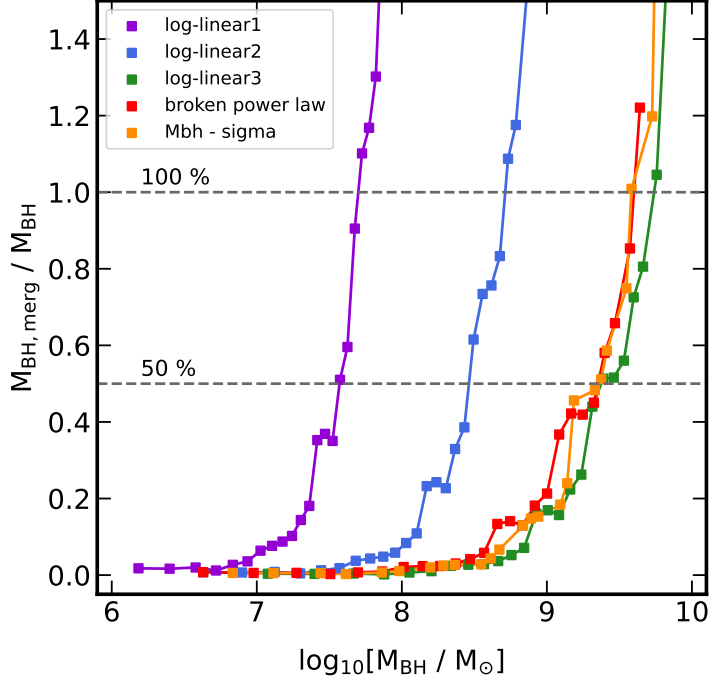


Figure 6.7: Percentage of cumulative merger contribution as a function of final mass of the supermassive black holes. Different color squares are representative of the different scaling relations adopted to evaluate mergers: violet, blue and green ones are related to the log-linear  $M_{\text{BH}} - M_{\star}$  relations with parameters found in Table 4.1 respectively; red points are derived from the application of the reference broken power law relation of Equation 6.1; orange ones are from the chosen modified log-quadratic  $M_{\text{BH}} - \sigma$  relation, Equation 5.10.

Such a behavior produced by a flatter scaling relation has to be attributed to the fact that the difference in mass between the components in a BH - BH merger is not so distant, meaning the mass of the in-falling BH is similar to the one of the progenitor. Actually the trend of the pure linear scaling relation is the same as what is derived by considering the maximal merger contribution for galaxies, because  $M_{\text{BH}}$  is equivalent to  $M_{\star}$  scaled by a constant factor, i.e.  $10^{-3.6}$  in our case. It means that if one selects the broken power law relation as the reference one (red squares), then at most the relative contribution of mergers in the growth of the supermassive black hole is much lower than what is found for the host galaxy, or, put in a different way, the predicted accretion through in-falling gas is on average less efficient in the galaxy (encoded by star formation rate values (SFR)) with respect to the central black hole. In fact, in the case of a galaxy the mean mass assembly through mergers is in a certain way reduced if one includes the actual time needed

for a merger to conclude, i.e. the total mass at  $z = 0$  that has been 'truly' gained by mergers is not as high because some satellites have not yet been incorporated. Hence for a correct evaluation of the contribution of mergers, the merging timescale (see Section 2.2.4) should be included. Since in the case of black hole I have no real indication of the amount of this delay then for the moment I continue to refer to the maximal contribution.

- 2) A second issue to be noted and discussed is the fact that for all considered cases there are some points that stay in a 'forbidden' region, that is above the 100 % line. It would mean that the mass grown by mergers is higher than the total one made by the sum of gas + mergers. It is not physical and solutions of this type should be discarded. This is actually a rather ambiguous passage because few things are interplaying and it is not easy to attribute a cause and an effect. As seen in the previous point, the scaling relation has for sure an important part of responsibility, in the sense that if one changes it (e.g. making the slope even steeper) then possibly the overflow effect is restrained. But is that enough? And has then it significance, i.e. is it coherent with data points and/or S09 reference model? Actually the other relevant aspect has already been introduced in point 1) and concerns the 'real' contribution of mergers. Some of them may have not occurred yet and hence should be not taken in to account in the calculation. Intuitively one can hypothesize that supermassive black holes hosted by galaxies that have not yet completed the merger are themselves still present as individual component (not fallen) and their contribution should be discarded. It is far from easy, the mechanisms involved are not well understood and difficult to reproduce without the help of semi analytic models/simulations. Constraints related to supermassive black hole mergers will be achieved only from future space-based gravitational wave observatories like LISA (Laser Interferometer Space Antenna) and BBO (Big Bang Observer). In here I limit the treatment of mergers and go through the easiest approach that is to introduce in the calculation of BH merger contribution the same merging time-scale as for the galaxies (see Section 6.2.2).
- 3) A last interesting fact is related instead to the  $M_{\text{BH}} - \sigma$  scaling relation, that predicts merger contributions given by orange squares in Figure 6.7. I have decided just to show results derived from the use of the modified log-quadratic relation (Equation 5.10) because essentially considerations made before regarding  $M_{\text{BH}} - M_{\star}$  relation can be repeated also in this case. In my opinion, the positive outcome is that the trend linked to the increase of merger contribution achieved by that particular  $M_{\text{BH}} - \sigma$  relation is similar to the one inferred from the reference  $M_{\text{BH}} - M_{\star}$  relation (in red). This is not for granted especially because the passages and transformations to arrive at Equation 5.10 are performed independently from the shape of the chosen relation with the stellar mass. Only last points (corresponding to the highest values of final  $M_{\star}$ ) are shifted upwards in the case of the relation with velocity dispersion. I think that this is more practical than conceptual, in the sense that it is probable that velocity dispersions calculated in correspondence to that stellar masses (from  $M_{\star}/R_e$ ) are slightly too large at higher redshift, and this leads to total black hole

growing curves with a sort of descending mode (Figure 5.6).

What I am going to do next is to re-calculate merger contributions both for galaxies and for their central black holes (through the reference  $M_{\text{BH}} - M_{\star}$  relation) including merging timescales. These latter are evaluated for single galaxy satellite according to the prescription of [McCavana et al. \(2012\)](#) in the way described in Section 2.2.4 and given as output of DECODE. I repeat again the fact that using them also for black holes means forcing a little bit the situation. But, since I have no indication at disposition about the merging timescales of black holes, I will try and go on with this rough approximation.

### 6.2.2 High mass end: merging timescale

Inserting a time delay in the calculation of cumulative merger histories goes with no particular difficulties. Basically once I have the epochs of the first in-falling,  $z_{\text{inf}}$ , assigned to every sub-halo (sub-galaxy through SMHM conversion), it is enough to add to this latter the corresponding merging timescale, and obtain the final redshift of in-fall,  $z_{\text{fin}}$ . Then at single redshift step considered, the objects that enter in the calculation of mass gained from mergers at that  $z$  are only those with  $z_{\text{fin}} \geq z$ . Final results can be observed in Figure 6.8, where red squares are referred to supermassive black holes while blue ones to their hosting galaxies. Red-dashed segments connect points that represent maximal merger contribution for SMBHs and straight one instead link those in which calculation of mergers has been conducted inserting the merging timescale. Analogous, but concerning galaxies, are the points in blue, that depict a more realistic situation with respect to the maximal merger approach. Despite the reduction of the amount of mass that has actually entered in the central galaxy, mean merger histories predicted at high final masses are still overcoming the mean global growth of the galaxies. Causes of this may be of different typologies: i) the SMHM relation may be not completely appropriate towards high masses, e.g. slightly less evolving relation at high mass end? (see Figure 3.5); ii) there could have been a statistical over-production of sub-halos in that bins of mass; iii) it is possible that not all the mass of a satellite galaxy is accreted, just a part of it (more physical option). Other reasons can be given to describe this peculiar behaviour but it is not the aim here to discuss about them. What is observable is that the problem, at least in this range of masses, is in a certain sense avoided if one makes the conversion  $M_{\star} \rightarrow M_{\text{BH}}$  applying the reference scaling relation defined by Equation 6.1. As already mentioned in the previous Section it seems that with such a resolution the efficiency of gas accretion processes is higher in the case of supermassive black holes. What is even more 'surprising' is the fact that considerable differences between including or not a merging timescale start to appear only towards very massive SMBHs, i.e. at  $M_{\text{BH}} \gtrsim 10^9 M_{\odot}$ . Hence the procedure defined before this point can be considered, if not completely correct, at least sustainable. At this point it is possible to have a feeling of how much the situation improves if inserting a  $t_{\text{merg}}$ , even if it may not be the correct one. Figure 6.9 illustrates the case of a supermassive black hole with final mass of the order of  $M_{\text{BH}}(z=0) \approx 10^{9.5} M_{\odot}$ , for which a maximal merger approach would have led to a non properly physical condition ( $\langle M_{\text{BH,merg}} \rangle > \langle M_{\text{BH,tot}} \rangle$ ). This is well depicted by the blue curve (total - merger) on the left panel, that abruptly falls down up to the moment at

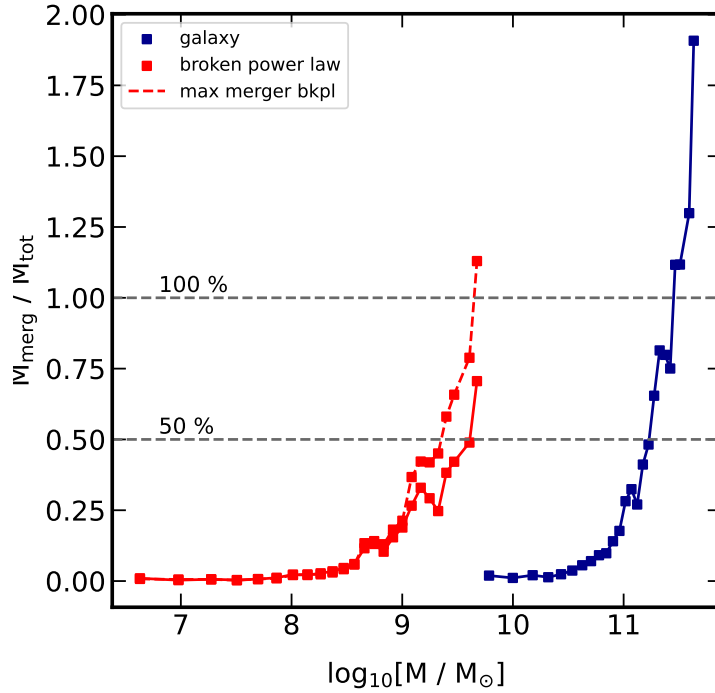


Figure 6.8: Same as Figure 6.7, but illustrating, in red, points pertained to the reference  $M_{\text{BH}} - M_{\star}$  relation and in blue merger contributions of the hosting galaxies. These last and red squares linked through straight segments have been calculated with the inclusion of merging timescales, while red dashed segments unite points for which the maximal merger contribution approach has been followed.

which it is interrupted because it can not be longer defined (negative log). On the right panel, instead, the effect of the merging timescale is immediately noted. The blue curve is significantly flattened but the total merger contribution does not overpass the total growing of the black hole and at the end its amount rises up to  $\sim 70\%$ , which is still important without being prohibitive. That treatment can be optimized in many ways, e.g. retrieving estimates of the proper merging timescales for black holes or confronting the total number of mergers in our case with respect to other semi-analytic and hydrodynamic simulations. Naturally the same passages can be applied for all the scaling relations that have entered at some point in this work and see what changes in one or another case. Here I limit the discussion to the reference  $M_{\text{BH}} - M_{\star}$  scaling relation because it was the one with a better realization in comparison to the model of S09 and it was more directly approachable than the  $M_{\text{BH}} - \sigma$  relation that is derived after some slightly problematic steps.

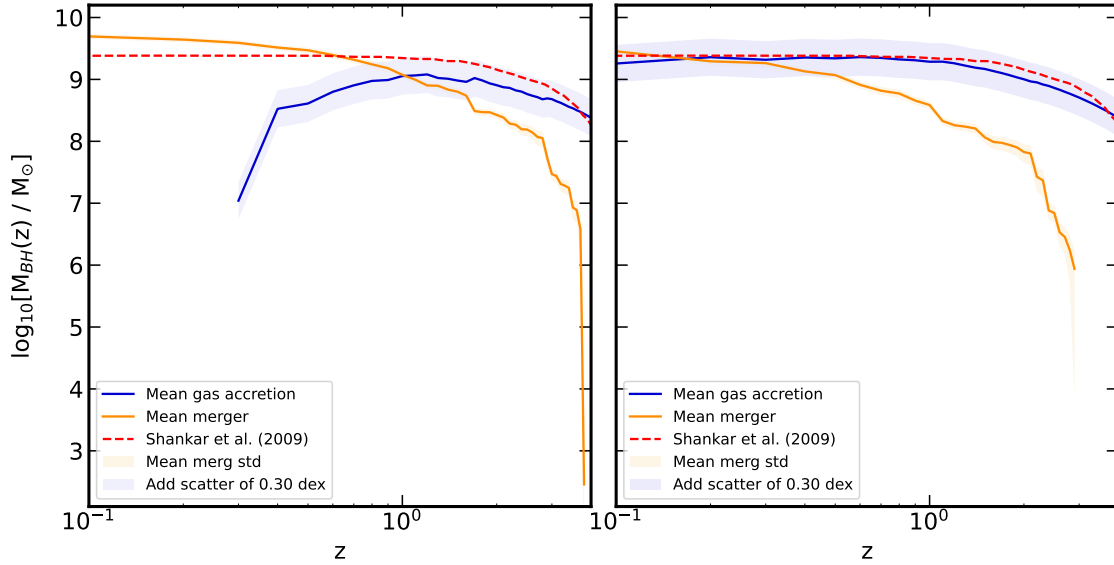


Figure 6.9: Difference in the treatment of mean merger contribution (orange lines) when a SMBH of final mass  $\gtrsim$  is considered. Left: maximal merger contribution approach is followed with a consequent situation in which it overcomes the total growth of BH predicted and the subtracted curve (blue line) is interrupted; Right: merging timescales are included in the calculation leading a reduction of merger contribution and a more suitable aspect of the subtracted blue curve.

### 6.3 Conclusions

I would like to conclude by making some final remarks about the general framework that it is depicted as a consequence of what discussed so far. It is about the mean behaviour of gas accretion processes that happens in supermassive black holes with different final masses. The scenarios may be really diverse and there is the possibility that a global rule will never be found. Nevertheless, common features among macro-groups, i.e. defined by mass ranges, can at least be understood by connecting all information available at the moment. Part of it is provided by SEMs, of which DECODE is a new example. Figure 6.10 is representative of the efficiency of gas accretion processes pertained to different supermassive black hole final masses and predicted through the application of all the procedures illustrated up to now. Growing curves, subtracted from the mean merger contribution, have been normalized to their final values so to have the possibility to compare their trends. The range of mass is the one always considered, e.g. final black hole masses go from  $M_{\text{BH}} \approx 10^{6.5}$  up to  $M_{\text{BH}} \approx 10^{9.5} M_{\odot}$ . Actually the Figure is a picture of what happens when the reference  $M_{\text{BH}} - M_{\star}$  relation is employed and the calculation of mergers performed with the inclusion of the merging timescales. It is a specific example and the one of choice because, as already said, it is the case in which the agreement with

accretion curves of our model of reference, [Shankar et al. \(2009\)](#), is fairly the best among the ones introduced in this work. Anyway other possibilities can be explored without problems and following same passages. In this situation what is immediately perceivable from [Figure 6.10](#) is the fact that gas accretion mechanisms are of particular importance, in the epochs under consideration, just for objects with lower masses (bottom lines in the plot). Indeed in these latter in-falling gas produces an increase of mass that amounts to nearly  $10^4 M_{\odot}$ . Much different is the case of more massive objects in which gas accretion processes, for  $z < 4$ , are almost nearly silenced and their contribution to the growing of the SMBH is of a totality of  $\sim 10 - 100 M_{\odot}$ . This implies a scenario in which the reservoir of gas is almost exhausted and with the most part of accretion probably happened in a more distant past. Any clues about such possibilities will be only given through observational investigations of AGN populations at high redshift, at least  $z > 4$ . The ultimate part of their growth, as discussed in the previous Sections, seems to be dominated by major merger events that are maybe responsible for the un-setting of the linear trend between the mass of the supermassive black hole and the one of the spheroid component  $M_{\star, \text{bulge}}$ , see [Figure 6.6](#). On the other hand, low-mass and probably gas-rich systems have been growing their central SMBHs through in-falling gas for more than 12 Gyr. However the behaviour of them can be only understood if one has the availability of characterizing AGN luminosity functions at high redshift and for faint objects, thing that is far from easy. What is important to underline at this point is that the potentialities of an approach of this type are wide and always improvable along with the results obtained from observational campaigns.

As conclusive notes I would like to briefly sum up what are, in my opinion, the most interesting results of the project. The novel semi-empirical procedure adopted and described in full details in [Chapters 2 and 3](#) has allowed to investigate the growth of supermassive black holes within their host galaxies in a way almost independent on predefined assumptions and parametrizations. The only free quantities that enter are the stellar mass - halo mass relation (see [Sections 2.3.1 and 3.2](#)) and the scaling relations between the black hole mass,  $M_{\text{BH}}$ , and the host galaxy properties,  $M_{\star}$  and  $\sigma_{\star}$  ([Chapters 4 and 5](#)). The ones adopted in this project are repeated here: i) the SMHM relation of reference is the one introduced in [Section 3.2](#) (blue curve and blue shaded area of [Figure 3.5](#)) and evaluated by the redshift-dependent stellar mass function that combines the observational works of [Baldry et al. \(2008\)](#), [Bernardi et al. \(2017\)](#) and [Tomczak et al. \(2014\)](#); ii) the un-evolved  $M_{\text{BH}} - M_{\star}$  relation used to calculate SMBH growing curves in agreement with the model of [Shankar et al. \(2009\)](#) (principal term of comparison in this thesis) is the broken power law type relation expressed by [Equation 6.1](#); iii) the un-evolved  $M_{\text{BH}} - \sigma_{\star}$  relation of choice is a modified log-quadratic relation, defined in [Equation 5.10](#), for analogous reasons as for  $M_{\text{BH}} - M_{\star}$ . Adopting these inputs, the scenario about the growth of supermassive black holes that I retrieved is the following:

- SMBH with final masses up to about  $\sim 10^9 M_{\odot}$ , grow their mass principally through secular processes that involve the in-fall of cold gas present in their surroundings. They reside in the smaller gas-rich galaxies, the ones with less probability of having been subjected to a major merger in their past. Actually the scaling relations that

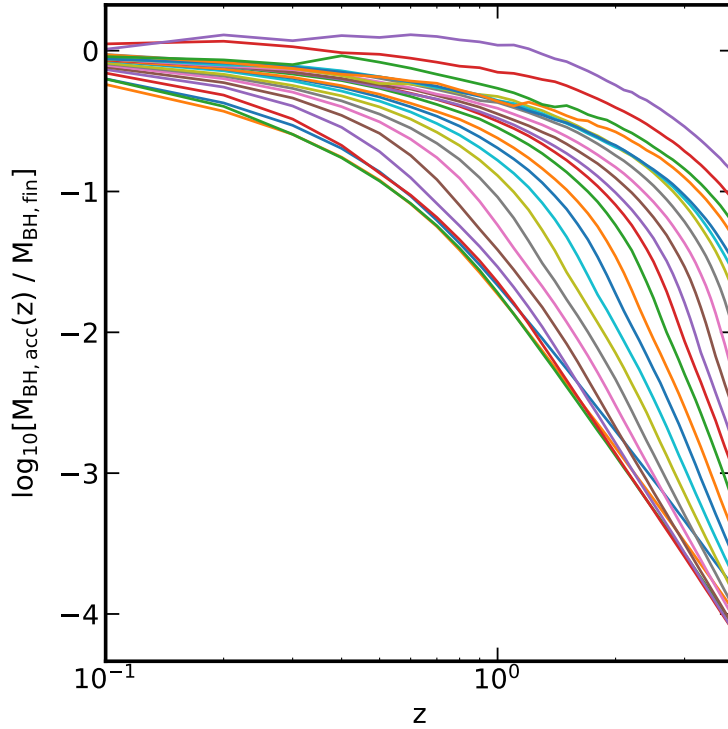


Figure 6.10: Efficiency of gas accretion mechanisms starting from  $z = 4$  up to recent epochs. The curves are obtained from the subtraction of the mean total growth of SMBHs and mean merger contribution evaluated for single mass step and with the inclusion of a  $t_{\text{merg}}$ . They are then normalized to the final mass so to make clearer the differences in the behaviours. The final mass increases from the bottom part of the set to the top, in which lines of high mass objects are illustrated.

connect the smallest black holes to their hosts can not be defined with high accuracy neither by observations (sparse in that range of masses) neither through the comparison of the respective growing curves with our model of reference (Shankar et al. (2009)), which is less reliable in describing the evolution of small SMBHs at high redshift. Therefore results about them should be taken with caution and not considered exact. What is for sure is the fact that for objects of this type the merger contribution in their growth is far more limited with respect to the one of gas-accretion processes (see Figures 6.7 and 6.8).

- Towards the very high mass end, specifically supermassive black holes of final mass  $\gtrsim 10^9 M_{\odot}$ , the resulting situation is slightly diverse. Those objects seem to be characterized by an initial phase of very fast gas-accretion (at  $z < 4$ ) and then this process becomes less and less efficient towards lower redshift. The reasons of such a behaviour are not well known, a possible one involve some AGN feedback mechanisms able to sweep away the reservoir of cold gas; other explanations consider

the effects of major mergers between the host galaxies. Nevertheless, what is found in the context of this project is that the merger contribution to the growth of SMBHs in this range of mass is important, quite predominant, especially at recent epochs (Figures 6.7 and 6.8). Actually it should be treated with some adjustments: adopting a maximal merger approach may not be convenient because it leads to undesired situations in which  $\langle M_{\text{BH,merg}} \rangle > \langle M_{\text{BH,tot}} \rangle$ , and a delay time, accounting for the 'correct' merging timescale, is needed to solve in part this problem.



# Chapter 7

## Future

In this Chapter I am going to suggest some possible developments for the project just outlined. From one side it would be interesting making links with other models and simulations, that may differ in the treatment of physical inputs or in the approach used; on the other side one should always maintain a contact with the 'real' world, that is to consider new available observational data.

### 7.1 Modification of DECODE

A first direction for future steps is surely in the perfecting of the DECODE model. As described in Chapters 2 and 3, presenting the main characteristics and functions of the model, this latter relies on very few input elements, that are basically the halo and sub-halo mass functions (HMF and SHMF), the stellar mass function (SMF, empirical) and the consequent stellar mass - halo mass (SMHM) relation. In Section 2.3 I have introduced the SMHM relation of reference in this work (RM) evaluated from the combination of SMF data of Baldry et al. (2012) + Bernardi et al. (2017) + Tomczak et al. (2014). Also, I have briefly discussed about a possible alternative to the latter, represented by the SMHM relation calculated with the empirical model of Moster et al. (2018), EMERGE. The different behaviours of the two is shown in Figure 3.5 of Chapter 3. The authors of DECODE (Fu et al., personal communication) have found that another SMHM relation could be in better agreement with observational data. In particular such a relation is represented by a low-mass end made of a non-evolving SMF up to  $z \sim 1.5$  and by an high-mass end similar to the one of the RM in this project. Indeed it seems that a  $M_{\text{halo}} - M_{\star}$  relation obtained through a constant SMF towards low masses is more capable of reproducing (mean) star formation rates compared to the ones derived by spectral energy distributions (SEDs). On the other hand, considerations made in (Fu et al., in preparation p.c.) for high-mass objects remain unchanged since all quantities involved depend on major mergers, hence significant for stellar masses of  $M_{\star} \gtrsim 10^{11} M_{\odot}$ . The new relation so built-up is represented in Figure 7.1 along with the reference SMHM relation (in blue). The orange curve traces the new local ( $z = 0$ ) stellar mass - halo mass relation and orange shaded area its evolution across cosmic time up to  $z = 4$ . The same, but in blue, is for the RM relation. As just said, the new relation has an almost

null evolution up to  $M_\star \sim 10^9 M_\odot$ , while at increasing masses the evolution is more significant and tends to overlap with the situation depicted by the RM. At this point it

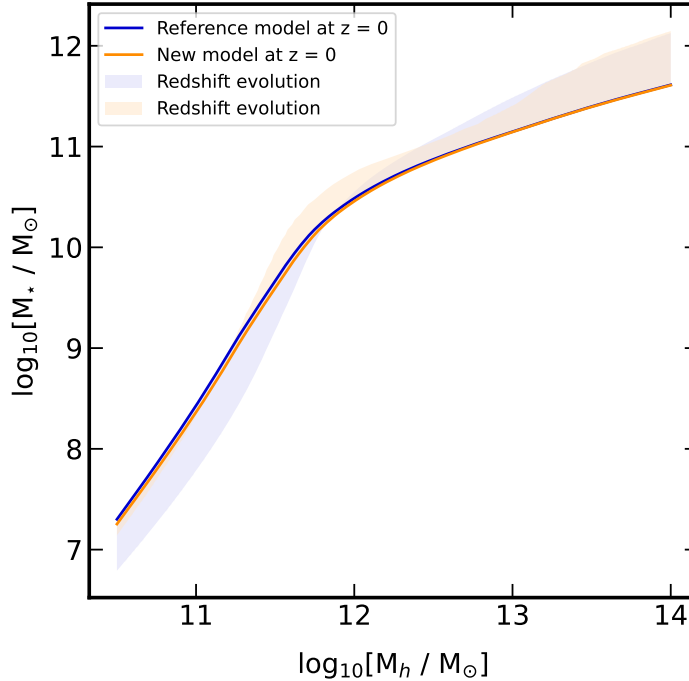


Figure 7.1: Stellar mass - halo mass relations and relative evolution up to  $z = 4$ . The blue curve and respective shaded area represents the reference relation (RM) of this project and obtained through passages described in Section 3.2 of Chapter 3. Orange line and shaded area are referred to a new relation introduced by Fu et al. (in preparation) to have a better agreement with SFRs from SEDs.

would be interesting to adopt this latter SMHM relation and re-evaluate all the quantities described in this thesis, i.e. global SMBH growing curves, merger contributions and so on. An approximated tentative is displayed in Figure 7.2. As usual the blue curves are representative of the global growing of supermassive black holes and to them the mean merger contribution should be subtracted. For the moment it is just to show how the behaviour of the tracks is changed when the new relation is used. The scaling relation I have used to make the plot of Figure 7.2 is again a broken power law type  $M_{\text{BH}} - M_\star$  relation, with a low-mass slope of about  $\alpha_1 \sim 1$  and a much steeper one towards higher masses, of  $\approx 2$ . Actually the stellar mass at which such a change is made to occur is  $M_\star = 10^9 M_\odot$ , hence the flatter trend regards only the very small black hole masses. In the Figure 7.2, it appears that for SMBHs with final masses  $\gtrsim 10^8 M_\odot$  the agreement is not bad and at the highest masses blue curves are much above the red ones (from Shankar et al. (2009), S09) because still the merger contribution has not been taken

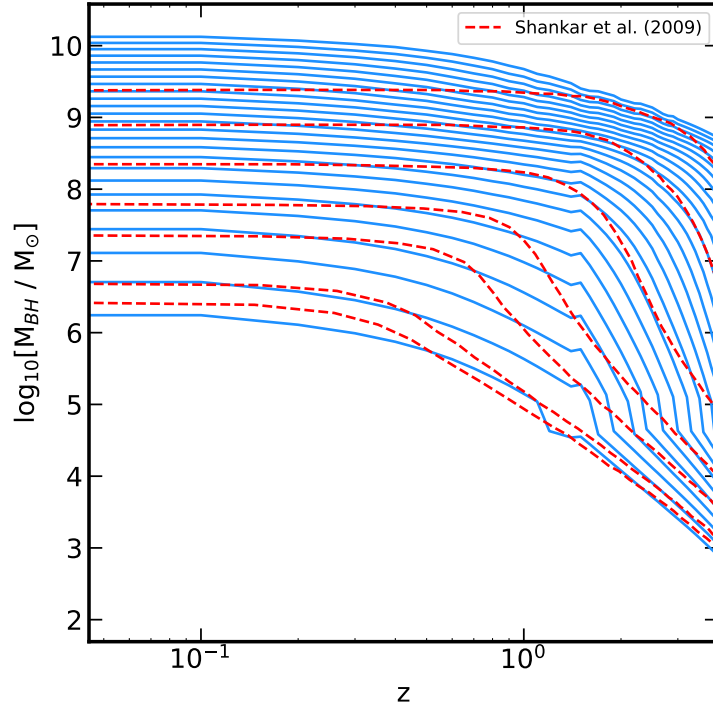


Figure 7.2: Global supermassive black hole growing curves made from the new SMHM relation, introduced in this last Chapter (Figure 7.1, in orange), and through a broken power law  $M_{\text{BH}} - M_{\star}$ . This latter has a low-mass end slope of about 1 and an high-mass end slope nearly 2. Red dashed lines are the accretion curves by Shankar et al. (2009), model of reference for the entire project.

into account (and there should be important). SMBHs with lower final masses do not perfectly match the S09 curves in the range of masses between  $\sim 10^5$  and  $10^7 M_{\odot}$ , that, according to the conversion used, are associated to stellar masses in between  $\sim 10^9 - 10^{10} M_{\odot}$ . By looking at Figure 7.1 this region is nearly in correspondence to the knee of SMHM relation (orange) and in there at higher redshift the new model predicts indeed higher stellar masses. Anyway a deeper analysis should be followed in order to find a coherent and well-motivated solution.

## 7.2 Diffmah: Differentiable Model of Halo Assembly

To the side of models and simulations, a chance is represented by the employment of a different empirical model, Diffmah, that has been implemented by Hearin et al. (2021). In Section 3.1.1 of Chapter 3 a brief comment was made about this when discussing the possible accretion tracks to assign to the parent dark matter halos. The recipe selected in that occasion was to make parent halos evolve according to the formalism of van den Bosch et al. (2014), hence through the use of mean growing tracks. The particularity of Diffmah,

instead, is to model the growth of individual DM halos adopting a functional form so to approximate results taken from merger trees of halos identified in both gravity-only (Klypin et al. (2011) and Klypin et al. (2016)) and hydrodynamic simulations (TNG300-1, Nelson et al. (2017)). Diffmah builds the evolution of *cumulative peak* halo mass,  $M_{\text{peak}}(t)$ , i.e. the largest mass the main progenitor halo has ever attained up until the time  $t$ . This means that  $M_{\text{peak}}(t)$  is a non-decreasing function of time and eventually it remains constant in case of mass loss.  $M_{\text{peak}}$  is modelled as a power-law function of cosmic time given by:

$$M_{\text{peak}}(t) = M_0(t/t_0)^{\alpha(t)}, \quad (7.1)$$

with  $t_0$  the present age of universe,  $M_0 = M_{\text{peak}}(t_0)$  and  $\alpha(t)$  defined as:

$$\alpha(t; \tau_c, k, \alpha_{\text{early}}, \alpha_{\text{late}}) \equiv \alpha_{\text{early}} + \frac{\alpha_{\text{late}} - \alpha_{\text{early}}}{1 + \exp(-k(t - \tau_c))}. \quad (7.2)$$

The parameters  $\alpha_{\text{early}}$  and  $\alpha_{\text{late}}$  are the asymptotic values of the power-law index at early and late times respectively. They are related to two phases of halo growth: a fast (early) phase during which the timescale of mass accretion is shorter than the timescale of Hubble expansion and probably dominated by major merger; a slow (late) phase is instead characterized by a longer timescale accretion and dominated by minor mergers according to (Li et al. (2007)). The term  $\tau_c$  is defined as the transition time between the early- and late-time indices, while  $k$  controls the speed of transition between the two regimes. These parameters essentially describe the mode with which a halo evolve: e.g. assuming small values of  $\tau_c$  would imply having a halo of lower final mass.

What is interesting in this case is the fact that for each object one can retrieve the assigned time of transition,  $\tau_c$ , that should also corresponds to the moment at which a halo reaches its maximum virial velocity (Li et al. (2007)). This is in turn calculated as a function of  $z$  and the halo mass  $M_{\text{halo}}(z)$ :

$$V_{\text{vir}}(z) = \sqrt{\frac{GM_{\text{halo}}}{R_{\text{vir}}}} = \left[ \frac{\Delta_{\text{vir}}(z)}{2} \right]^{1/6} [M_{\text{halo}}(z)H(z)] \quad (7.3)$$

with  $R_{\text{vir}}$  is the virial radius of the halo and  $H(z)$  is the Hubble parameter. The quantity  $\Delta_{\text{vir}}(z)$  is the density contrast between the mean density of the halo and the critical density for closure, for which typically the fitting formula used is the one by Bryan & Norman (1998):  $\Delta(z) = 18\pi^2 + 82[\Omega_{\text{m}}(z) - 1] - 39[\Omega_{\text{m}}(z) - 1]^2$ . At the maximum value of  $V_{\text{vir}}$ , a relation with the central velocity dispersion,  $\sigma$ , is supposed to establish. Some literature works (Ferrarese (2002); Baes et al. (2003); Pizzella et al. (2005)) have tried to characterize this relation, at  $z \sim 0$ , by using the large scale circular velocities of spiral galaxies (flat branch of rotation curves). Hence making a connection between  $M_{\text{halo}}(z) - \sigma(z)$  for specific evolutionary paths and then using the  $M_{\text{BH}} - \sigma$  scaling relation it would be possible to acquire information about i) growing curves of SMBH derived from this particular situation; ii) possible connection between black holes and dark matter halos; iii) clues on the formation and evolution of  $M_{\text{BH}} - \text{velocity dispersion}$  scaling relation (and processes implied).

### 7.3 Question of mergers

As repeated many times the fundamental information provided by DECODE is the mean merger contribution that characterizes the population of halos with different final masses. In turn this is used to calculate the predicted cumulative merger histories related to supermassive black holes, once assuming stellar mass - halo mass and SMBH mass and galaxy properties relations. In Section 6.2.2 I have also discussed about the possibility of including a merging timescale and showed the results obtained with the inclusion of this latter referred to galaxies (see Section 2.2.4). The mean merger contributions, hence mean number of mergers and so on, derived in this framework can be compared to other pieces of information supplied by different models/simulations and by the almost new field of research that regards gravitational waves.

#### Gravitational Wave Background

Supermassive black hole mergers are the principal target for long-wavelength (mHz to nHz) gravitational waves being searched for by pulsar timing arrays (PTAs,  $\mu\text{Hz}$  - nHz) and by upcoming Laser Interferometer Space Antenna, LISA, in the frequency range 0.1 Hz to 0.1 mHz (Amaro-Seoane et al. (2017)). The main difficulty is to disentangle gravitational wave signal (either stochastic background, GWB, or deterministic low-frequency GWs) from other sources of noise in PTA data (Goncharov et al. (2020)). Thorough well calibrated scaling relations, that also accounts for morphological differences (Sahu et al. (2019a)), It would be possible to improve the GWB strain model used to look for long-wavelength GWs in PTA and LISA data. As an example in Mapelli et al. (2012) the use of a quadratic relation instead of a linear  $M_{\text{BH}} - M_{\star, \text{bulge}}$  one changes the predicted event rates by an order of magnitude. Indeed the GWB strain model is evaluated by the integration of the individual characteristic strains over the SMBH Binary (SMBHB). The GWB strain model elaborated by Chen et al. (2017) depends on the SMBH binary merger rate  $\frac{d^2n}{dzd\mathcal{M}}$ , i.e. the number density of merging SMBHBs per unit of  $z$  and unit of chirp mass  $\mathcal{M}(=(m_1m_2)^{3/5}/(m_1+m_2)^{1/5})$ . During a galaxy merger, the hosted SMBHBs are pushed towards the central region of the remnant galaxy through dynamical friction processes. This leads to the formation of a SMBH binary at parsec scales that interacts with the surrounding stars and may enter a binary hardening phase characterized by a binding energy between the two objects higher than the average kinetic energy of stars in the vicinity. From that situation the binary successively enters the so called GW emission phase, that finally drives the merger. Assuming a scenario of this kind, the SMBHB merger rate (that affects the calculation of the GWB strain) naturally depends on the galaxy stellar mass function (SMF), galaxy pair fraction (GPF), SMBH merger time-scale (see next) and the scaling relation between the black hole mass and host galaxy properties (Sesana (2013)). Scaling relations allows to pass from SMF to BH mass function (BHMf) and from GPF into BH pair fraction (as seen in Section 6.2). From the combination of GWB strain models and future detections made available by PTAs and LISA it would be possible to get more stringent information about BH merger rates and scaling relations to be inserted in the present project.

## Merging timescale of SMBH

An issue not completely taken into account in the treatment of merger contribution I made in this thesis is the merging timescale related to SMBHs. In fact, for almost all the passages performed I consider a maximal merger contribution without the inclusion of any delaying timescale. Only in a second moment (Section 6.2.2) I re-do the calculation of mean mergers using galaxy merging timescales (Section 2.2.4), that is often used to approximate the SMBH merger timescale (e.g. Chen et al. (2019)). However, the SMBH merger timescale may be further delayed during the transition from the hardening phase to the GW emission one, and it has been argued (Sesana & Khan (2015)) that such transition phase is where SMBHBs spend most of their lifetime. One could estimate this time-scale for a given binary eccentricity following the model in Sesana & Khan (2015), if density at the black hole influence radius and the stellar velocity dispersion are known. As an example in Biava et al. (2019), authors present a model to derive SMBH merging timescale: through the  $M_{\text{BH}} - M_{\star, \text{bulge}}$ ,  $M_{\star, \text{bulge}} - R_{\text{e, bulge}}$  and  $M_{\text{BH}} - n_{\text{bulge}}$  relations taken from different studies they estimate Sérsic parameters of a remnant bulge hosting a SMBHB and then use Prugniel & Simien (1997) model to calculate the density within the black hole influence radius,  $\rho_i$ . With models and data of these type one can observe how much results, presented in Section 6.2, would be changed and improved.

## 7.4 Future observations and applications

In this final Section I underline the necessity of collecting more and more observational data so to obtain up-dated black hole-galaxy correlations that could also take into account differentiation among populations of objects considered (e.g. morphology-types, active or non active galaxies etc.). New relations may be used as a test for the model described in this work and also for other simulations trying to reproduce realistic galaxies with central SMBHs (e.g. Schaye et al. (2015); Mutlu-Pakdil et al. (2018); Hopkins et al. (2018); Davé et al. (2019); Li et al. (2020)), with the additional possibility that results can be compared to each other.

Steps forward may also be conducted in the study of scaling relations evolution. As repeated many times in this work, first results in terms of SMBH growing curves have been obtained assumed constant scaling relations (hence of the same type along cosmic epochs up to  $z = 4$ ). In a second moment, in Chapter 6, I have discussed about the introduction of an eventual  $z$ -dependent term in the relations adopted (of the form  $\propto (1+z)^\gamma$ ). Some studies have approached this issue (e.g. Park et al. (2015); Sexton et al. (2019); Li et al. (2021)) basing on a sample of active galaxies and have suggested that  $M_{\text{BH}} - \sigma$  and  $M_{\text{BH}} - M_{\star, \text{bulge}}$  relations remain almost the same as the local ones up to  $z \sim 0.6$ . Further investigations extended to higher redshift would improve the situation and also give insights regarding BH mass function, BH merger rates and finally gravitational wave strain models (discussed above), and all of this could help making the procedure on which this project is based more reliable.

Finally the black hole scaling relations need to incorporate low-mass or dwarf galaxies and also be completed with the inclusion of nuclear star clusters and globular clusters, that probably host BHs of masses lower than  $\sim 10^5 M_\odot$ . These objectives would be achieved

in the next few years thanks to new high-resolution observations from telescopes such as the James Webb Space Telescope (JWST, [Gardner et al. \(2006\)](#); [Kalirai \(2018\)](#)), Multi-conjugate adaptive optics Assisted Visible Imager and Spectrograph (MAVIS, [Ellis et al. \(2020\)](#)), Advanced Telescope for High-ENERgy Astrophysics (ATHENA, [Barcons et al. \(2017\)](#)), the next generation Very Large Array (ngVLA, [Di Francesco et al. \(2019\)](#)), Extremely Large Telescope (ELT, [Batcheldor & Koekemoer \(2009\)](#)), and the Square Kilometre Array (SKA, [Cembranos et al. \(2020\)](#)).



# Bibliography

- Abel T., Bryan G. L., Norman M. L., 2000, [ApJ](#), 540, 39
- Aird J., Nandra K., Laird E. S., et al., 2010, [MNRAS](#), 401, 2531
- Amaro-Seoane P., Audley H., Babak S., et al., 2017, Laser Interferometer Space Antenna, [doi:10.48550/ARXIV.1702.00786](https://arxiv.org/abs/1702.00786), <https://arxiv.org/abs/1702.00786>
- Antonucci R., 1993, [ARA&A](#), 31, 473
- Aversa R., Lapi A., de Zotti G., Shankar F., Danese L., 2015, [ApJ](#), 810, 74
- Awaki H., Koyama K., Inoue H., Halpern J. P., 1991, [PASJ](#), 43, 195
- Baes M., Buyle P., Hau G. K. T., Dejonghe H., 2003, [MNRAS](#), 341, L44
- Baldassare V. F., Reines A. E., Gallo E., Greene J. E., 2015, [ApJL](#), 809, L14
- Baldassare V. F., Reines A. E., Gallo E., et al., 2016, [ApJ](#), 829, 57
- Baldassare V. F., Dickey C., Geha M., Reines A. E., 2020, [ApJL](#), 898, L3
- Baldry I. K., Glazebrook K., Driver S. P., 2008, [MNRAS](#), 388, 945
- Baldry I. K., et al., 2012, [MNRAS](#), 421, 621
- Ball W. H., Tout C. A., Żytkow A. N., Eldridge J. J., 2011, [MNRAS](#), 414, 2751
- Barcons X., Barret D., Decourchelle A., et al., 2017, [Astronomische Nachrichten](#), 338, 153
- Barger A. J., Cowie L. L., 2005, [ApJ](#), 635, 115
- Barger A. J., Cowie L. L., Capak P., et al., 2003, [ApJ](#), 584, L61
- Barger A. J., Cowie L. L., Mushotzky R. F., et al., 2005, [AJ](#), 129, 578
- Barkat Z., Rakavy G., Sack N., 1967, [Phys. Rev. Lett.](#), 18, 379
- Barth A. J., Sarzi M., Rix H.-W., et al., 2001, [ApJ](#), 555, 685
- Barth A. J., Ho L. C., Rutledge R. E., Sargent W. L. W., 2004, [ApJ](#), 607, 90

- Barth A. J., Pancoast A., Thorman S. J., et al., 2011, [ApJL](#), 743, L4
- Batcheldor D., Koekemoer A. M., 2009, [PASP](#), 121, 1245
- Baugh C. M., 2006, [ApJ](#), 69, 3101
- Begelman M. C., 2010, [MNRAS](#), 402, 673
- Begelman M. C., Blandford R. D., Rees M. J., 1980, [Nat](#), 287, 307
- Begelman M. C., Volonteri M., Rees M. J., 2006, [MNRAS](#), 370, 289
- Behroozi P. S., Silk J., 2015, [ApJ](#), 799, 32
- Behroozi P. S., Conroy C., Wechsler R. H., 2010, [ApJ](#), 717, 379
- Behroozi P. S., Wechsler R. H., Conroy C., 2013, [ApJ](#), 770, 57
- Behroozi P., et al., 2019, [MNRAS](#), 488, 3143
- Beifiori A., Courteau S., Corsini E. M., Zhu Y., 2012, [MNRAS](#), 419, 2497
- Bell E. F., McIntosh D. H., Katz N., Weinberg M. D., 2003, [ApJ](#), 585, L117
- Bennert V. N., Auger M. W., Treu T., et al., 2011, [ApJ](#), 742, 107
- Benson A. J., Bower R. G., Frenk C. S., et al., 2003, [ApJ](#), 599, 38
- Bentz M. C., Katz S., 2015, [PASP](#), 127, 67
- Bentz M. C., Walsh J. L., Barth A. J., et al., 2009, [ApJ](#), 705, 199
- Bernardi M., et al., 2013, [MNRAS](#), 436, 697
- Bernardi M., et al., 2016, [MNRAS](#), 455, 4122
- Bernardi M., et al., 2017, [MNRAS](#), 467, 2217
- Bernardi M., Sheth R. K., Fischer J.-L., et al., 2018, [MNRAS](#), 475, 757
- Biava N., Colpi M., Capelo P. R., et al., 2019, [MNRAS](#), 487, 4985
- Boizelle B. D., Barth A. J., Walsh J. L., et al., 2019, [ApJ](#), 881, 10
- Bond J. R., Arnett W. D., Carr B. J., 1984, [ApJ](#), 280, 825
- Bongiorno A., Zamorani G., Gavignaud I., et al., 2007, [A&A](#), 472, 443
- Bonoli S., Mayer L., Callegari S., 2013, [MNRAS](#), 437, 1576
- Bournaud, F. Jog, C. J. Combes, F. 2007, [A&A](#), 476, 1179
- Bournaud F., Jog C. J., Combes F., 2007, [A&A](#), 476, 1179

- Bower R. G., Benson A. J., Malbon R., et al., 2006, [MNRAS](#), 370, 645
- Boylan-Kolchin M., Ma C.-P., Quataert E., 2008, [MNRAS](#), 383, 93
- Boyle Terlevich R. J., 1998, [MNRAS](#), 293, L49
- Bromm V., Coppi P. S., Larson R. B., 1999, [ApJ](#), 527, L5
- Bromm V., Coppi P. S., Larson R. B., 2002, [ApJ](#), 564, 23
- Bryan G. L., Norman M. L., 1998, [ApJ](#), 495, 80
- Burkert A., Silk J., 2001, [ApJ](#), 554, L151
- Busarello G., Longo G., Feoli A., 1992, [A&A](#), 262, 52
- Calvi R., Vulcani B., Poggianti B. M., et al., 2018, [MNRAS](#), 481, 3456
- Carr B. J., Bond J. R., Arnett W. D., 1984, [ApJ](#), 277, 445
- Cattaneo, A. Mamon, G. A. Warnick, K. Knebe, A. 2011, [A&A](#), 533, A5
- Cavaliere A., Morrison P., Wood K., 1971, [ApJ](#), 170, 223
- Cembranos J. A., de la Cruz-Dombriz Á., Gammaldi V., Méndez-Isla M., 2020, [Physics of the Dark Universe](#), 27, 100448
- Cen R., 2015, [ApJ](#), 805, L9
- Chabrier G., 2003, [PASP](#), 115, 763
- Chen S., Sesana A., Del Pozzo W., 2017, [MNRAS](#), 470, 1738
- Chen S., Sesana A., Conselice C. J., 2019, [MNRAS](#), 488, 401
- Ciotti L., van Albada T. S., 2001, [ApJ](#), 552, L13
- Clauwens B., Schaye J., Franx M., Bower R. G., 2018, [MNRAS](#), 478, 3994
- Combes F., García-Burillo S., Audibert A., et al., 2019, [A&A](#), 623, A79
- Conselice C. J., Arnold J., 2009, [MNRAS](#), 397, 208
- Cool R. J., Kochanek C. S., Eisenstein D. J., et al., 2006, [AJ](#), 132, 823
- Cowie L. L., Songaila A., Hu E. M., Cohen J. G., 1996, [AJ](#), 112, 839
- Croton D. J., Springel V., White S. D. M., et al., 2006, [MNRAS](#), 365, 11
- Davidzon I., et al., 2017, [A&A](#), 605, A70
- Davis B. L., Graham A. W., Seigar M. S., 2017, [MNRAS](#), 471, 2187
- Davis B. L., Graham A. W., Cameron E., 2018, [ApJ](#), 869, 113

- Davis B. L., Graham A. W., Cameron E., 2019, *ApJ*, 873, 85
- Davison T. A., et al., 2020, *MNRAS*, 497, 81
- Davé R., Anglés-Alcázar D., Narayanan D., et al., 2019, *Monthly Notices of the Royal Astronomical Society*, 486, 2827
- DeGraf C., Di Matteo T., Treu T., et al., 2015, *MNRAS*, 454, 913
- Denney K. D., Peterson B. M., Pogge R. W., et al., 2010, *ApJ*, 721, 715
- Devecchi B., Volonteri M., 2009, *ApJ*, 694, 302
- Di Francesco J., Chalmers D., Denman N., et al., 2019, The Next Generation Very Large Array, [doi:10.5281/zenodo.3765763](https://doi.org/10.5281/zenodo.3765763), <https://doi.org/10.5281/zenodo.3765763>
- Diamond-Stanic A. M., Rieke G. H., 2012, *ApJ*, 746, 168
- Ding X., Silverman J., Treu T., et al., 2020, *ApJ*, 888, 37
- Dressler A., Richstone D. O., 1988, *ApJ*, 324, 701
- Driver S. P., Liske J., Graham A. W., 2007, The Millennium Galaxy Catalogue: Science highlights, [doi:10.48550/ARXIV.ASTRO-PH/0701468](https://arxiv.org/abs/astro-ph/0701468), <https://arxiv.org/abs/astro-ph/0701468>
- Drouart G., De Breuck C., Vernet J., et al., 2014, *A&A*, 566, A53
- Dubois Y., Devriendt J., Slyz A., Teyssier R., 2012, *MNRAS*, 420, 2662
- Ebrero J., Carrera F. J., Page M. J., et al., 2009, *A&A*, 493, 55
- Ellis S., McDermid R., Cresci G., et al., 2020, in Society of Photo-Optical Instrumentation Engineers (SPIE) Conference Series. p. 11447A0, [doi:10.1117/12.2561930](https://doi.org/10.1117/12.2561930)
- Elvis M., Risaliti G., Zamorani G., 2002, *ApJ*, 565, L75
- Enoki M., Ishiyama T., Kobayashi M. A. R., Nagashima M., 2014, *ApJ*, 794, 69
- Fabian A. C., 1999, *MNRAS*, 308, L39
- Fabian A. C., 2012, *ARA&A*, 50, 455
- Fabian A. C., Iwasawa K., 1999, *MNRAS*, 303, L34
- Fan X., Strauss M. A., Schneider D. P., et al., 2001, *AJ*, 121, 54
- Fan X., Hennawi J. F., Richards G. T., et al., 2004, *AJ*, 128, 515
- Fanidakis N., Baugh C. M., Benson A. J., et al., 2012, *MNRAS*, 419, 2797
- Fanidakis N., Georgakakis A., Mountrichas G., et al., 2013, *MNRAS*, 435, 679

- Fender R., Belloni T., 2012, *Science*, 337, 540
- Feng H., Shen Y., Li H., 2014, *ApJ*, 794, 77
- Ferrarese L., 2002, *ApJ*, 578, 90
- Ferrarese L., Ford H., 2005, *Space Sci. Rev.*, 116, 523
- Ferrarese L., Merritt D., 2000, *ApJ*, 539, L9
- Filippenko A. V., Sargent W. L. W., 1989, *ApJL*, 342, L11
- Fontanot F., Monaco P., Cristiani S., Tozzi P., 2006, *MNRAS*, 373, 1173
- Fontanot F., Monaco P., Cristiani S., Tozzi P., 2007, *MNRAS*, 373, 1173
- Fontanot F., Macciò A. V., Hirschmann M., et al., 2015, *MNRAS*, 451, 2968
- Franca F. L., Fiore F., Comastri A., et al., 2005, *ApJ*, 635, 864
- Fryer C. L., Woosley S. E., Heger A., 2001, *ApJ*, 550, 372
- Gao L., Yoshida N., Abel T., et al., 2007, *MNRAS*, 378, 449
- Gardner J. P., Mather J. C., Clampin M., et al., 2006, *Space Sci. Rev.*, 123, 485
- Gaskell C. M., 2009, arXiv: Cosmology and Nongalactic Astrophysics
- Gebhardt K., Bender R., Bower G., et al., 2000, *ApJ*, 539, L13
- Gebhardt K., Adams J., Richstone D., et al., 2011, *ApJ*, 729, 119
- Genel S., et al., 2010, *ApJ*, 719, 229
- Georgakakis A., Coil A. L., Laird E. S., et al., 2009, *MNRAS*, 397, 623
- Ghez A. M., Duchêne G., Matthews K., et al., 2003, *ApJ*, 586, L127
- Giacconi R., Gursky H., Paolini F. R., Rossi B. B., 1962, *Phys. Rev. Lett.*, 9, 439
- Goncharov B., Reardon D. J., Shannon R. M., et al., 2020, *MNRAS*, 502, 478
- González V., et al., 2011, *ApJ*, 735, L34
- Graham A. W., 2012, *ApJ*, 746, 113
- Graham A. W., Driver S. P., 2005, *PASA*, 22, 118–127
- Graham A. W., Driver S. P., 2007, *MNRAS*, 380, L15
- Graham A. W., Scott N., 2013, *ApJ*, 764, 151
- Graham A. W., Scott N., 2015, *ApJ*, 798, 54

- Graham A. W., Erwin P., Trujillo I., et al., 2003, [AJ](#), 125, 2951
- Graham A. W., Driver S. P., Allen P. D., Liske J., 2007, [MNRAS](#), 378, 198
- Graham A. W., Onken C. A., Athanassoula E., Combes F., 2011, [MNRAS](#), 412, 2211
- Granato G. L., Zotti G. D., Silva L., et al., 2004, [ApJ](#), 600, 580
- Green S. B., van den Bosch F. C., Jiang F., 2021, [MNRAS](#), 503, 4075
- Greene J. E., Ho L. C., 2005, [ApJL](#), 630, 122
- Greene J. E., Ho L. C., 2006, [ApJ](#), 641, L21
- Greene J. E., Ho L. C., 2007a, [ApJ](#), 667, 131
- Greene J. E., Ho L. C., 2007b, [ApJ](#), 670, 92
- Grylls P. J., Shankar F., Zanisi L., Bernardi M., 2019, [MNRAS](#), 483, 2506
- Grylls P. J., et al., 2020, [MNRAS](#), 491, 634
- Gultekin K., Richstone D. O., Gebhardt K., et al., 2009, [ApJ](#), 698, 198
- Gultekin K., Gebhardt K., Kormendy J., et al., 2014, [ApJ](#), 781, 112
- Guo Q., White S. D. M., 2008, [MNRAS](#), 384, 2
- Haring N., Rix H.-W., 2004, [ApJ](#), 604, L89
- Hasinger G., Miyaji T., Schmidt M., 2005, [A&A](#), 441, 417
- Hearin A. P., et al., 2021, [The Open Journal of Astrophysics](#), 4
- Heckman T. M., Best P. N., 2014, [ARA&A](#), 52, 589
- Heckman T. M., Kauffmann G., Brinchmann J., et al., 2004, [ApJ](#), 613, 109
- Henriques B. M. B., et al., 2019, [MNRAS](#), 491, 5795
- Henriques B. M. B., Yates R. M., Fu J., et al., 2020, [MNRAS](#), 491, 5795
- Hirschmann M., Khochfar S., Burkert A., et al., 2010, [MNRAS](#), 407, 1016
- Hirschmann M., et al., 2012a, [MNRAS](#), 419, 3200
- Hirschmann M., Somerville R. S., Naab T., et al., 2012b, [MNRAS](#), 426, 237
- Hirschmann M., Dolag K., Saro A., et al., 2014, [MNRAS](#), 442, 2304
- Ho L. C., 1999, in Chakrabarti S. K., ed., *Observational Evidence for Black Holes in the Universe*. Springer Netherlands, Dordrecht, pp 157–186, [doi:10.1007/978-94-011-4750-7\\_11](https://doi.org/10.1007/978-94-011-4750-7_11)

- Hopkins P. F., Quataert E., 2010, [MNRAS](#), 407, 1529
- Hopkins P. F., Richards G. T., Hernquist L., 2007a, [ApJ](#), 654, 731
- Hopkins P. F., Hernquist L., Cox T. J., Robertson B., Krause E., 2007b, [ApJ](#), 669, 67
- Hopkins P. F., Hernquist L., Cox T. J., Kereš D., 2008, [ApJS](#), 175, 356
- Hopkins P. F., et al., 2009a, [MNRAS](#), 397, 802
- Hopkins P. F., Somerville R. S., Cox T. J., et al., 2009b, [MNRAS](#), 397, 802
- Hopkins P. F., Younger J. D., Hayward C. C., et al., 2010, [MNRAS](#), 402, 1693
- Hopkins P. F., Wetzel A., Kereš D., et al., 2018, [MNRAS](#), 480, 800
- Hosokawa T., Yoshida N., Omukai K., Yorke H. W., 2012, [ApJ](#), 760, L37
- Hu J., 2008, [MNRAS](#), 386, 2242
- Hunt M. P., Steidel C. C., Adelberger K. L., Shapley A. E., 2004, [ApJ](#), 605, 625
- Huré J.-M., Hersant F., Surville C., et al., 2011, [A&A](#), 530, A145
- Hyde J. B., Bernardi M., 2009, [MNRAS](#), 394, 1978
- Ichimaru S., 1977, [ApJ](#), 214, 840
- Ilbert O., et al., 2013, [A&A](#), 556, A55
- Jahnke K., Macciò A. V., 2011, [ApJ](#), 734, 92
- Jahnke K., Bongiorno A., Brusa M., et al., 2009, [ApJ](#), 706, L215
- Jarrett T. H., Chester T., Cutri R., et al., 2003, [AJ](#), 125, 525
- Jiang F., van den Bosch F. C., 2014, [MNRAS](#), 440, 193
- Jiang F., van den Bosch F. C., 2016, [MNRAS](#), 458, 2848
- Jiang L., Fan X., Cool R. J., et al., 2006, [AJ](#), 131, 2788
- Jiang F., et al., 2021, [MNRAS](#), 502, 621
- Johnson J. L., Whalen D. J., Fryer C. L., Li H., 2012, [ApJ](#), 750, 66
- Kalirai J., 2018, [Contemporary Physics](#), 59, 251
- Kennefick J. D., Djorgovski S. G., de Carvalho R., 1995, [AJ](#), 110, 2553
- Khochfar S., Burkert A., 2006, [A&A](#), 445, 403
- King A. R., 2010, [MNRAS](#), 402, 1516

- King A., 2019, *Supermassive Black Hole Accretion and Feedback*. Springer Berlin Heidelberg, Berlin, Heidelberg, pp 95–157, [doi:10.1007/978-3-662-59799-6\\_2](https://doi.org/10.1007/978-3-662-59799-6_2), [https://doi.org/10.1007/978-3-662-59799-6\\_2](https://doi.org/10.1007/978-3-662-59799-6_2)
- King I. R., Minkowski R., 1966, *ApJ*, **143**, 1002
- King A., Nealon R., 2019, *MNRAS*, **487**, 4827
- King A., Pounds K., 2015, *ARA&A*, **53**, 115
- Kiuchi G., Ohta K., Akiyama M., et al., 2006, *ApJ*, **647**, 892
- Klypin A. A., Trujillo-Gomez S., Primack J., 2011, *ApJ*, **740**, 102
- Klypin A., Yepes G., Gottlöber S., et al., 2016, *MNRAS*, **457**, 4340
- Kodama T., Yamada T., Akiyama M., et al., 2004, *MNRAS*, **350**, 1005
- Kormendy J., Ho L. C., 2013, *ARA&A*, **51**, 511
- Kormendy J., Richstone D., 1995, *ARA&A*, **33**, 581
- Kormendy J., Bender R., Cornell M. E., 2011, *Nat*, **469**, 374
- Krajnović D., Cappellari M., McDermid R. M., et al., 2018, *MNRAS*, **477**, 3030
- Kravtsov A. V., et al., 2004, *ApJ*, **609**, 35
- Kuo C. Y., Braatz J. A., Condon J. J., et al., 2010, *ApJ*, **727**, 20
- L’Huillier, B. Combes, F. Semelin, B. 2012, *A&A*, **544**, A68
- LaMassa S. M., Heckman T. M., Ptak A., Urry C. M., 2013, *ApJ*, **765**, L33
- Lacey C. G., et al., 2016a, *MNRAS*, **462**, 3854
- Lacey C. G., Baugh C. M., Frenk C. S., et al., 2016b, *MNRAS*, **462**, 3854
- Lackner C. N., Cen R., Ostriker J. P., Joung M. R., 2012, *MNRAS*, **425**, 641
- Laor A., 1998, *ApJ*, **505**, L83
- Laor A., 2001, *ApJ*, **553**, 677
- Lapi A., Cavaliere A., 2011, *Advances in Astronomy*, 2011
- Lauer T. R., Faber S. M., Richstone D., et al., 2007a, *ApJ*, **662**, 808
- Lauer T. R., Tremaine S., Richstone D., Faber S. M., 2007b, *ApJ*, **670**, 249
- Lee J., Yi S. K., 2013, *ApJ*, **766**, 38
- Leja J., Speagle J. S., Johnson B. D., et al., 2020, *ApJ*, **893**, 111

- Li Y., Mo H. J., van den Bosch F. C., Lin W. P., 2007, *MNRAS*, **379**, 689
- Li Y., Habouzit M., Genel S., et al., 2020, *ApJ*, 895, 102
- Li J. I.-H., Shen Y., Ho L. C., et al., 2021, *ApJ*, 906, 103
- Lodato G., Natarajan P., 2006, *MNRAS*, 371, 1813
- Lynden-Bell D., 1969, *Nat*, 223, 5207
- Läscher R., Ferrarese L., van de Ven G., Shankar F., 2014, *ApJ*, 780, 70
- Madau P., Dickinson M., 2014, *ARA&A*, 52, 415
- Madau P., Rees M. J., 2001, *ApJ*, 551, L27
- Magorrian J., Tremaine S., Richstone D., et al., 1998, *ApJ*, 115, 2285
- Mapelli M., Ripamonti E., Vecchio A., et al., 2012, *A&A*, 542, A102
- Marconi A., Hunt L. K., 2003, *ApJ*, 589, L21
- Marconi A., Risaliti G., Gilli R., et al., 2004, *MNRAS*, 351, 169
- Marconi A., Axon D. J., Maiolino R., et al., 2008, *ApJ*, 678, 693
- Marsden C., Shankar F., Ginolfi M., Zubovas K., 2020, *Front. Phys.*, 8
- Marsden C., Shankar F., Bernardi M., et al., 2022, *MNRAS*, **510**, 5639
- Marulli F., Bonoli S., Branchini E., et al., 2008, *MNRAS*, **385**, 1846
- Matteo T. D., Colberg J., Springel V., et al., 2008, *ApJ*, 676, 33
- McCavana T., et al., 2012, *MNRAS*, 424, 361
- McConnell N. J., Ma C.-P., 2013, *ApJ*, 764, 184
- McLure R. J., Dunlop J. S., 2002, *MNRAS*, 331, 795
- Meidt S. E., Schinnerer E., van de Ven G., et al., 2014, *ApJ*, 788, 144
- Menci N., Fiore F., Bongiorno A., Lamastra A., 2016, *A&A*, 594, A99
- Merritt D., Ferrarese L., 2001, *ApJ*, 547, 140
- Miyaji T., Hasinger G., Schmidt M., 2000, *A&A*, **353**, 25
- Miyaji T., Hasinger G., Salvato M., et al., 2015, *ApJ*, 804, 104
- Monaco P., Fontanot F., Taffoni G., 2007, *MNRAS*, 375, 1189
- Moster B. P., et al., 2010, *ApJ*, 710, 903

- Moster B. P., Naab T., White S. D. M., 2013, [MNRAS](#), 428, 3121
- Moster B. P., Naab T., White S. D. M., 2018, [MNRAS](#), 477, 1822
- Moustakas J., et al., 2013, [ApJ](#), 767, 50
- Murali C., Katz N., Hernquist L., Weinberg D. H., Dave R., 2002, [ApJ](#), 571, 1
- Mutlu-Pakdil B., Seigar M. S., Hewitt I. B., Treuthardt P., Berrier J. C., Koval L. E., 2018, [MNRAS](#), 474, 2594
- Muzzin A., et al., 2013, [ApJ](#), 777, 18
- Nakamura O., Fukugita M., Yasuda N., et al., 2003, [AJ](#), 125, 1682
- Nandra K., Laird E. S., Steidel C. C., 2005, [MNRASL](#), 360, L39
- Neistein E., Netzer H., 2014, [MNRAS](#), 437, 3373
- Nelson D., Pillepich A., Springel V., et al., 2017, [MNRAS](#), 475, 624
- Nguyen D. D., Seth A. C., Neumayer N., et al., 2018, [ApJ](#), 858, 118
- Nguyen D. D., Seth A. C., Neumayer N., et al., 2019, [ApJ](#), 872, 104
- Nguyen D. D., den Brok M., Seth A. C., et al., 2020, [ApJ](#), 892, 68
- Nowak N., Saglia R. P., Thomas J., et al., 2007, [MNRAS](#), 379, 909
- Oklopčić A., Hopkins P. F., Feldmann R., et al., 2017, [MNRAS](#), 465, 952
- Omukai K., Schneider R., Haiman Z., 2008, [ApJ](#), 686, 801
- Oser L., et al., 2010, [ApJ](#), 725, 2312
- Page M. J., Symeonidis M., Vieira J. D., Altieri B., et al., 2012, [Nature](#), 485, 213
- Park D., Woo J.-H., Bennert V. N., et al., 2015, [ApJ](#), 799, 164
- Paturel G., Petit C., Prugniel P., et al., 2003, [A&A](#), 412, 45
- Pei Y. C., 1995, [ApJ](#), 438, 623
- Peterson B. M., 1993, [PASP](#), 105, 247
- Peterson B. M., Ferrarese L., Gilbert K. M., et al., 2004, [ApJ](#), 613, 682
- Peterson B. M., Bentz M. C., Desroches L.-B., et al., 2005, [ApJ](#), 632, 799
- Pillepich A., et al., 2014, [MNRAS](#), 444, 237
- Pillepich A., et al., 2018a, [MNRAS](#), 473, 4077
- Pillepich A., et al., 2018b, [MNRAS](#), 475, 648

- Pizzella A., Corsini E. M., Dalla Bontà E., et al., 2005, *ApJ*, 631, 785
- Planck Collaboration et al., 2020, *A&A*, 641, A6
- Prugniel P., Simien F., 1997, *A&A*, 321, 111
- Qu Y., et al., 2016, *MNRAS*, 464, 1659
- Rees M. J., 1984, *ARA&A*, 22, 471
- Reines A. E., Volonteri M., 2015, *ApJ*, 813, 82
- Reines A. E., Sivakoff G. R., Johnson K. E., Brogan C. L., 2011, *Nat*, 470, 66
- Reines A. E., Greene J. E., Geha M., 2013, *ApJ*, 775, 116
- Ricarte A., Natarajan P., 2018, *MNRAS*, 474, 1995
- Richards G. T., Croom S. M., Anderson S. F., et al., 2005, *MNRAS*, 360, 839
- Richards G. T., Strauss M. A., Fan X., et al., 2006, *AJ*, 131, 2766
- Richstone D., Ajhar E. A., Bender R., et al., 1998, *Nat*, 385, A14
- Rigby J. R., Rieke G. H., Donley J. L., et al., 2006, *ApJ*, 645, 115
- Rodriguez-Gomez V., et al., 2016, *MNRAS*, 458, 2371
- Saglia R. P., Opitsch M., Erwin P., et al., 2016, *ApJ*, 818, 47
- Sahu N., Graham A. W., Davis B. L., 2019a, *ApJ*, 876, 155
- Sahu N., Graham A. W., Davis B. L., 2019b, *ApJ*, 887, 10
- Sahu N., Graham A. W., Davis B. L., 2020, *ApJ*, 903, 97
- Salpeter E. E., 1964, *ApJ*, 140, 796
- Salucci P., Szuszkiewicz E., Monaco P., Danese L., 1999, *MNRAS*, 307, 637
- Salucci P., Ratnam C., Monaco P., Danese L., 2000, *MNRAS*, 317, 488
- Salviander S., Shields G. A., 2013, *ApJ*, 764, 80
- Sani E., Marconi A., Hunt L. K., Risaliti G., 2011, *MNRAS*, 413, 1479
- Santini P., et al., 2012, *A&A*, 538, A33
- Satyapal S., Secret N. J., McAlpine W., Ellison S. L., et al., 2014, *ApJ*, 784, 113
- Savorgnan G. A. D., Graham A. W., 2016a, *ApJS*, 222, 10
- Savorgnan G. A. D., Graham A. W., 2016b, *ApJS*, 222, 10

- Schaye J., et al., 2014, [MNRAS](#), 446, 521
- Schaye J., Crain R. A., Bower R. G., et al., 2015, [MNRAS](#), 446, 521
- Schechter P., 1976, [ApJ](#), 203, 297
- Schmidt M., 1963, [Nat](#), 197, 1040
- Schodel R., Ott T., Genzel R., et al., 2003, [ApJ](#), 596, 1015
- Schramm M., Silverman J. D., 2013, [ApJ](#), 767, 13
- Schramm M., Silverman J. D., Greene J. E., et al., 2013, [ApJ](#), 773, 150
- Schulze A., Wisotzki L., 2010, [A&A](#), 516, A87
- Scott N., Graham A. W., Schombert J., 2013, [ApJ](#), 768, 76
- Secrest N. J., Satyapal S., Gliozzi M., Cheung C. C., et al., 2012, [ApJ](#), 753, 38
- Sérsic J. L., 1963, [BAAA](#), 6, 41
- Sesana A., 2013, [MNRAS](#), 433, L1
- Sesana A., Khan F. M., 2015, [MNRAS](#), 454, L66
- Sexton R. O., Canalizo G., Hiner K. D., et al., 2019, [ApJ](#), 878, 101
- Seymour N., Altieri B., Breuck C. D., et al., 2012, [ApJ](#), 755, 146
- Shakura N. I., Sunyaev R. A., 1973, [Astron. Astrophys.](#), 24, 337
- Shankar F., Mathur S., 2007, [ApJ](#), 660, 1051
- Shankar F., Salucci P., Granato G. L., et al., 2004, [MNRAS](#), 354, 1020
- Shankar F., Lapi A., Salucci P., Zotti G. D., Danese L., 2006, [ApJ](#), 643, 14
- Shankar F., Weinberg D. H., Miralda-Escudé J., 2009, [ApJ](#), 690, 20
- Shankar F., Weinberg D. H., Shen Y., 2010, [MNRAS](#), 406, 1959
- Shankar F., et al., 2012, [MNRAS](#), 428, 109
- Shankar F., Marulli F., Bernardi M., et al., 2013, [MNRAS](#), 428, 109
- Shankar F., et al., 2014, [MNRAS](#), 439, 3189
- Shankar F., Bernardi M., Sheth R. K., et al., 2016, [MNRAS](#), 460, 3119
- Shen Y., Kelly B. C., 2012, [ApJ](#), 746, 169
- Shen Y., Greene J. E., Ho L. C., et al., 2015, [ApJ](#), 805, 96

- Sheth R. K., Bernardi M., Schechter P. L., et al., 2003, *ApJ*, 594, 225
- Sheth K., Regan M., Hinz J. L., et al., 2010, *PASP*, 122, 1397
- Shields G. A., Gebhardt K., Salviander S., et al., 2003, *ApJ*, 583, 124
- Silk J., Rees M. J., 1998, *A&A*, 331, L1
- Silverman J. D., Green P. J., Barkhouse W. A., et al., 2008, *ApJ*, 679, 118
- Simmons B. D., Lintott C., Schawinski K., et al., 2013, *MNRAS*, 429, 2199
- Small T. A., Blandford R. D., 1992, *MNRAS*, 259, 725
- Soltan A., 1982, *MNRAS*, 200, 115
- Sun M., Trump J. R., Brandt W. N., et al., 2015, *ApJ*, 802, 14
- Thater S., Krajnovic D., Cappellari M., et al., 2019, *A&A*, 625, A62
- Thornton C. E., Barth A. J., and L. C. H., 2008, *ApJ*, 686, 892
- Tinker J., et al., 2008, *ApJ*, 688, 709
- Tomczak A. R., et al., 2014, *ApJ*, 783, 85
- Treu T., Woo J.-H., Malkan M. A., et al., 2007, *ApJ*, 667, 117
- Tundo E., Bernardi M., Hyde J. B., et al., 2007, *ApJ*, 663, 53
- Ueda Y., 2015, *Proc. Jpn. Acad., Ser. B*, 91, 175
- Ueda Y., Akiyama M., Ohta K., Miyaji T., 2003, *ApJ*, 598, 886
- Ueda Y., Akiyama M., Hasinger G., et al., 2014, *ApJ*, 786, 104
- Vale A., Ostriker J. P., 2004, *MNRAS*, 353, 189
- Vestergaard M., Osmer P. S., 2009, *ApJ*, 699, 800
- Vogelsberger M., et al., 2014, *MNRAS*, 444, 1518
- Volonteri M., 2010, *Astron. Astrophys. Rev.*, 18, 279
- Volonteri M., Ciotti L., 2013, *ApJ*, 768, 29
- Wandel A., 1999, *ApJ*, 519, L39
- White S. D. M., Rees M. J., 1978, *MNRAS*, 183, 341
- White M., Martini P., Cohn J. D., 2008, *MNRAS*, 390, 1179
- Wisotzki L., 1999, *A&A*, 353, 853

- Wolf C., Wisotzki L., Borch A., et al., 2003, [A&A](#), 408, 499
- Woo J.-H., Treu T., Malkan M. A., Blandford R. D., 2008, [ApJ](#), 681, 925
- Woosley S. E., Weaver T. A., 1986, [ARA&A](#), 24, 205
- Wurster J., Thacker R. J., 2013, [MNRAS](#), 431, 2513
- Wyithe J. S. B., 2006, [MNRAS](#), 365, 1082
- Xiao T., Barth A. J., Greene J. E., et al., 2011, [ApJ](#), 739, 28
- Yenko B., Barger A. J., Trouille L., Winter L. M., 2009, [ApJ](#), 698, 380
- York D. G., Adelman J., Anderson J. E., 2000, [AJ](#), 120, 1579
- Yoshida N., Omukai K., Hernquist L., Abel T., 2006, [ApJ](#), 652, 6
- Yu Q., Tremaine S., 2002, [MNRAS](#), 335, 965
- Yu L.-M., Bian W.-H., Wang C., et al., 2019, [MNRAS](#), 488, 1519
- Zavala J., et al., 2012, [MNRAS](#), 427, 1503
- Zhang W., Woosley S. E., Heger A., 2008, [ApJ](#), 679, 639
- Zibetti S., Charlot S., Rix H.-W., 2009, [MNRAS](#), 400, 1181
- de Nicola S., Marconi A., Longo G., 2019, [MNRAS](#), 490, 600
- van den Bosch R. C. E., 2016, [ApJ](#), 831, 134
- van den Bosch R. C. E., Tim de Zeeuw P., 2010, [MNRAS](#), 401, 1770
- van den Bosch R. C. E., Gebhardt K., Gültekin K., et al., 2012, [Nature](#), 491, 729
- van den Bosch F. C., et al., 2014, [MNRAS](#), 445, 1713